New robust control schemes linking linear and sliding mode approaches

Elias Tahoumi

THESE DE DOCTORAT DE

L'ÉCOLE CENTRALE DE NANTES
COMUE UNIVERSITE BRETAGNE LOIRE

ECOLE DOCTORALE N° 601
Mathématiques et Sciences et Technologies de l'Information et de la Communication
Spécialité : *Automatique, productique et robotique*

Par

« Elias TAHOUMI»

« New robust control schemes linking linear and sliding mode approaches»

Thèse présentée et soutenue à Nantes, le 9 décembre 2019
Unité de recherche : Laboratoire des Sciences du Numérique de Nantes

Rapporteurs avant soutenance :

Jaime Alberto MORENO PEREZ	Professeur, Universidad Nacional Autónoma de México, Mexique
Noureddine MANAMANNI	Professeur des Universités, Université de Reims Champagne Ardenne,

Composition du Jury :

Président : Noureddine MANAMANNI	Professeur des Universités, Université de Reims Champagne Ardenne, Reims
Examinateurs :	
Jaime Alberto MORENO PEREZ	Professeur, Universidad Nacional Autónoma de México, Mexique
Florentina NICOLAU	Maitre de conférence, ENSEA, Cergy-Pontoise
Dir. de thèse : Franck PLESTAN	Professeur des Universités, École Centrale de Nantes, Nantes
Co-dir. de thèse: Malek GHANES	Professeur des Universités, École Centrale de Nantes, Nantes
Co-encadrant de thèse:	Jean-Pierre BARBOT Professeur des Universités, ENSEA, Cergy-Pontoise

Contents

List of Figures

List of Tables

Acknowledgments

First of all, I would like to thank my supervisors Franck Plestan, Malek Ghanes and Jean-Pierre Barbot for the guidance, encouragement and advice provided throughout this journey. I learned from you how to work with clarity, conviction and integrity.

Throughout my thesis, I was lucky to collaborate with other fellow doctoral students and for that, Cheng Zhang, Susana Gutierrez and Etienne Picard, I say thank you. Our discussions were always very interesting and we overcame numerous obstacles together.

I would also like to thank Antoine, Christian, Jack, Jose and Gustavo for their crucial role during the writing of this thesis. Thank you for the stimulating discussions, for the sleepless nights we were working together before deadlines, and for all the fun we have had in the last three years.

Last but not least, I would like to express my deepest gratitude to my family and friends. Thank you for the moral support and most of all for accepting nothing less than excellence from me.

"don't go up to a scientist and say 'how does that [your research] relate to me today', the only right answer is 'I have no idea', but evidence of the history of this exercise tells us that one day it will [...] all that matters, if you're curious, is that you're exploring something that you do not yet know"

Neil deGrasse Tyson

1

Introduction to Sliding Mode Control

Contents

1.1 Principle of standard sliding mode Control

Automatic control systems were first developed over two thousand years ago. The first feedback control device on record is thought to be the ancient Ktesibios's water clock in Alexandria, Egypt around the third century B.C. [5]. It kept time by regulating the water level in a vessel and, therefore, the water flow from that vessel. Control theory made significant strides since then, boosted by new mathematical techniques, as well as advancements in electronics and computer technologies which made it possible to control significantly more complex dynamical systems. Applications of control methodology have helped to make possible space travel and communication satellites, safer and more efficient aircraft and cleaner automotive engines. As systems become more and more complex, one needs suitable tools to control them. In fact, it is in general a delicate

task to mathematically model physical systems as well as the perturbations acting on them. Robust control solutions such as the backstepping technique [6] and robust LMI switched controllers [7] [8] have been designed to control such systems. Another control solution for nonlinear uncertain systems is (SMC) [9, 10]. Indeed, SMC is well known for its robustness against matching perturbations/uncertainties. It is also known for its finite time convergence and relative simplicity for application.
The principle of SMC is to force the system trajectory to reach a domain, called sliding surface, in a finite time. Once the system trajectory reaches the sliding surface, it will remain confined to it in spite of perturbations/uncertainties and needs only be viewed as sliding along that surface. SMC design is performed in 2 steps:

- Defining the sliding variable: this step is based on the control objective. The sliding variable is in general expressed as a function of the system output and eventually a finite number of its consecutive time derivatives. The sliding variable is defined such that, once it is equal to zero, the control objective will be reached, *i.e.* the output goes towards the objective.
- Designing a discontinuous control law: the control law forces the system trajectory to reach the sliding surface in finite time and to remain on it in spite of the uncertainties and perturbations.

In the sequel, these two steps are detailed.

1.1.1 Sliding variable design

First of all, consider the following system

$$\begin{aligned} \dot{x} &= f(x,t) + g(x,t)u \\ y &= h(x,t) \end{aligned} \tag{1.1}$$

where $x \in \mathcal{X} \subset \mathbb{R}^n$ is the state vector, $u \in \mathcal{U} \subset \mathbb{R}$ the control input ($\mathcal{X}$ and $\mathcal{U}$ being bounded subsets of $\mathbb{R}^n$ and $\mathbb{R}$ respectively), f and g uncertain sufficiently smooth functions, and y the output function (sufficiently smooth). The control objective is to constrain the output y to track a sufficiently differentiable reference trajectory $y_{ref}(t)$, *i.e.* to force the tracking error $e_y = y - y_{ref}(t)$ to 0 in spite of uncertainties/perturbations.

Assumption 1.1. *The relative degree*[1] *m of (1.1) with respect to the tracking error e_y is constant and known i.e.*[2]

$$e_y^{(m)} = a(x,t) + b(x,t)u \tag{1.2}$$

with $b(x,t) \neq 0$ for $x \in \mathcal{X}$ and $t \geq 0$.

■

Now, consider $\sigma(x,t)$ a sufficiently smooth function that can be viewed as a virtual output for system (1.1) and called "sliding variable". The sliding surface $\mathcal{S}$ is defined as

$$\mathcal{S} = \{x \in \mathcal{X}, t \geq 0 \mid \sigma(x,t) = 0\} \tag{1.3}$$

1. The relative degree is an integer equal to the minimum number of times that e_y should be differentiated with respect to time in order to make u appearing explicitly [11].

2. $e_y^{(m)}$ denotes the m^{th} time derivative of e_y. This notation is used throughout the thesis for all the variables/functions.

Definition 1.1. *[10]. There exists an ideal sliding mode (or called sliding motion) on $\mathcal{S}$ if, after a finite time t_F, the solution of system (1.1) satisfies $\sigma(x,t) = 0$ for all $t \geq t_F$.*

The sliding surface can be considered as a hypersurface in the state space. Once the system (1.1) trajectories are evolving on $\mathcal{S}$, the dynamics of the system are determined by the definition of σ. Furthermore, the choice of $\mathcal{S}$ (and then choice of σ) must lead to the convergence of the system output y towards the control objective. This is why σ must be defined such that, when $\sigma = 0$, then $e_y \to 0$. Then, a usual relationship between σ and e_y is given as follows

$$\sigma(x,t) = e_y^{(m-1)} + \cdots + c_1 \dot{e}_y + c_0 e_y \tag{1.4}$$

where the coefficients $c_i > 0$ $(1 \leq i \leq m-2)$ are chosen such that the polynomial

$$\Pi(\lambda) = \lambda^{m-1} + \sum_{i=0}^{m-2} c_i \lambda^i \tag{1.5}$$

is Hurwitz. Moreover, given (1.2) and Assumption 1.1, the sliding variable has a relative degree equal to 1; it yields

$$\dot{\sigma} = \bar{a}(x,t) + \bar{b}(x,t)u. \tag{1.6}$$

Assumption 1.2. *$\bar{a}(x,t)$ and $\bar{b}(x,t)$ are unknown but bounded functions such that there exist positive constants a_M, b_m and b_M such that $\forall x \in \mathcal{X}, t \geq 0$*

$$|\bar{a}(x,t)| \leq a_M, \quad 0 < b_m \leq \bar{b}(x,t) \leq b_M. \tag{1.7}$$

■

Once the sliding variable defined, the second step consists in designing the control input u stabilizing system (1.6) in a finite time, and in spite of uncertainties and perturbations.

1.1.2 First order sliding mode control design

The standard SMC firstly proposed by [12] can be applied to systems with relative degree equal to 1 with respect to the sliding variable as (1.6). Then, this controller can also be referred as first order SMC (FOSMC).
Recall that the control input u must be designed in order to force the system trajectories to reach and evolve on the sliding surface $\mathcal{S}$ in spite of the uncertainties and perturbations. In other words, it should render the sliding surface locally attractive. Then, the control law design should verify a condition that ensures the stability of $\sigma(x,t) = 0$. A solution is the use of Lyapunov approach in order to get stabilizing controller.
The Lyapunov function technique [13] is a very popular approach to study the stability of an equilibrium point $(\sigma(x,t) = 0)$ and therefore will be used in the sequel.

Definition 1.2. *A function $V : \mathbb{R}^n \to \mathbb{R}$ is a Lyapunov function candidate if*

- *$V(0) = 0$;*
- *$\forall x \in \mathcal{X} - \{0\}$, one has $V(x) > 0$.*

Given the above definition and that 0 is the equilibrium point, then the sign of the time derivative of the Lyapunov function candidate gives the information about the system

stability. Considering the sliding variable σ (1.4), a Lyapunov function candidate satisfying Definition 1.2 takes the following form

$$V(\sigma) = \frac{1}{2}\sigma^2. \tag{1.8}$$

In order to ensure the asymptotic convergence of the sliding variable σ, the time derivative of V has to be negative definite *i.e.*

$$\dot{V}(\sigma) = \sigma\dot{\sigma} < 0. \tag{1.9}$$

In the context of SMC, the inequality (1.9) is called the sliding condition; it ensures that the sliding surface σ is attractive *i.e.* once the trajectories of the system reach σ, they remain on it despite the perturbations and uncertainties. Remark that in order to achieve the finite time convergence of σ towards 0, a more strict condition called η-attractive condition [10] must be satisfied and reads as

$$\sigma\dot{\sigma} \leq -\eta|\sigma|, \quad \eta > 0. \tag{1.10}$$

It means that

$$\dot{V} \leq -\eta\sqrt{2V}. \tag{1.11}$$

Integrating (1.11) gives

$$\sqrt{2V(t)} - \sqrt{2V(0)} \leq -\eta t. \tag{1.12}$$

Then,

$$\eta t \leq |\sigma(0)| - |\sigma(t)|. \tag{1.13}$$

Consequently, σ reaches zero in a finite time t_F with

$$t_F \leq \frac{|\sigma(0)|}{\eta}. \tag{1.14}$$

Hence, a control u satisfying (1.10) drives the sliding variable σ to 0 in finite time. Such control u takes the form

$$u = -ksign(\sigma) \tag{1.15}$$

The control gain k must be chosen large enough to ensure the η-attractive condition (1.10). It is the case if the gain k verifies

$$k \geq \frac{|\bar{a}(x,t)| + \eta}{\bar{b}(x,t)}. \tag{1.16}$$

From Assumption 1.2, a sufficient condition reads as

$$k \geq \frac{a_M + \eta}{b_m}. \tag{1.17}$$

Then, with the control input (1.15) and the gain k verifying (1.17), the convergence of σ to zero is ensured in a finite time t_F verifying (1.14). Once the system trajectory is evolving on the sliding surface, the dynamics of the system is determined by the parameters in the definition of the sliding variable (1.4) *i.e.*

$$e_y^{(m-1)} + \cdots + c_1\dot{e}_y + c_0 e_y = 0. \tag{1.18}$$

Then, given the feature (1.5), the tracking error will asymptotically converge to zero in spite of the perturbations/uncertainties.

1.1.3 To summarize

The closed-loop behavior of system (1.1) controlled by (1.15) with k satisfying (1.17) can be divided into 2 phases:

- **Reaching phase:** this phase corresponds to the time interval $[0, t_F[$ where the trajectories are not evolving on the sliding surface; nevertheless, they are converging towards it. Note that during this phase the system is still sensitive to uncertainties and perturbations. Following (1.14), the duration of this phase, t_F, can be reduced by increasing η; this corresponds to increase the gain k.
- **Sliding phase:** this phase corresponds to the time interval $[t_F, +\infty[$ during which the trajectories are evolving on the sliding surface $\mathcal{S}$. If the gain k is well tuned (1.17), the system is insensitive to uncertainties and perturbations, and the tracking error e_y converges to 0.

1.1.4 Example

In order to clarify the FOSMC design, an academic example is treated in the sequel. Consider the following system

$$\begin{aligned} \dot{x}_1 &= x_2 \\ \dot{x}_2 &= 3sin(t) + u \\ y &= x_1 \end{aligned} \tag{1.19}$$

Suppose that the control objective is to force the output y towards a reference trajectory y_{ref}. Notice that the term $3sin(t)$ represents the perturbation. The relative degree with respect to the error $e_y = y - y_{ref}$ is equal to 2, satisfying Assumption 1.1. Then, following (1.4), define the sliding variable as

$$\sigma = \dot{e}_y + c_0 e_y \tag{1.20}$$

with $c_0 > 0$. Then, the sliding surface is given by

$$\mathcal{S} = \{x \in \mathcal{X} \mid \sigma = \dot{e}_y + c_0 e_y = 0\}. \tag{1.21}$$

The relative degree of system (1.19) with respect to σ is equal to 1 and has the following dynamics

$$\begin{aligned} \dot{\sigma} &= 3sin(t) + c_0 x_2 - \ddot{y}_{ref} - c_0 \dot{y}_{ref} + u \\ &= \bar{a}(x,t) + \bar{b}(x,t)u \end{aligned} \tag{1.22}$$

with $\bar{a}(x,t) = 3sin(t) + c_0 x_2 - \ddot{y}_{ref} - c_0 \dot{y}_{ref}$, $\bar{b}(x,t) = 1$. $\bar{a}(x,t)$ can be divided into a nominal term $\bar{a}_{Nom}(x,t)$ and an unknown term $\Delta\bar{a}(x,t)$ as follows

$$\bar{a}_{Nom}(x,t) = c_0 x_2 - \ddot{y}_{ref} - c_0 \dot{y}_{ref}, \quad \Delta\bar{a}(x,t) = 3sin(t). \tag{1.23}$$

Hence, define the control input u as

$$u = -\bar{a}_{Nom}(x,t) + \bar{u} \tag{1.24}$$

Then, $\sigma-$dynamics reads as

$$\dot{\sigma} = \Delta\bar{a}(x,t) + \bar{u} \tag{1.25}$$

which is of the form of (1.6) satisfying Assumption 1.2. Then, design the control input as

$$\bar{u} = -ksign(\sigma). \tag{1.26}$$

According to (1.16), the gain k must be large enough such that

$$k \geq \eta + 3|sin(y)|. \tag{1.27}$$

With such a choice for k, the controller forces the system trajectories to the sliding surface $\mathcal{S}$ in a finite time (see trajectory $L - M$ in Figure 1.1). Once the system trajectories are evolving on the sliding surface (see trajectory $M - N$ in Figure 1.1), one has $x_2 = \dot{x}_1 = -c_0 x_1$. It yields that $x_1(t) = x_1(0)e^{-c_0 t}$. Then, the system output $y = x_1$ exponentially converges to zero, with a convergence rate defined by c_0.

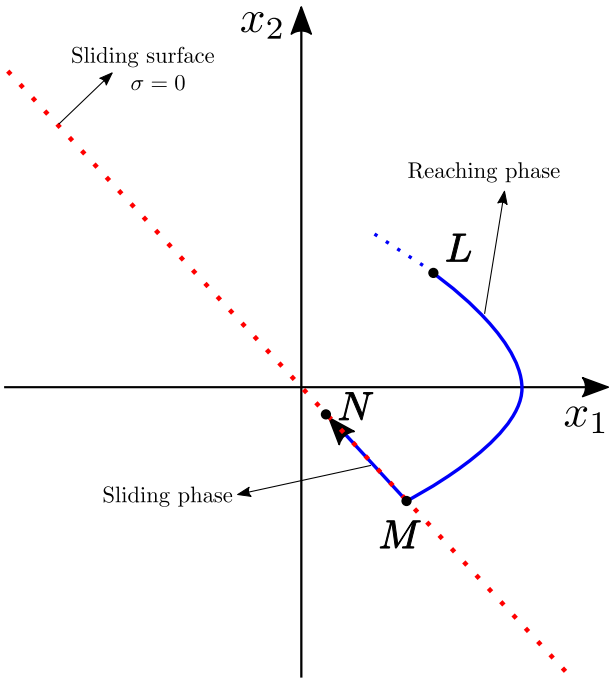

Figure 1.1 – Example of system (1.19) trajectory (blue curve) in the phase plane (x_1, x_2).

1.2 Chattering

In practical applications of SMC, an undesirable phenomenon known as chattering can appear: high frequency oscillations that may lead to low control accuracy, high wear of moving mechanical parts, and high heat losses in power circuits [14]. There are two main reasons which can cause the chattering:

- neglected dynamics in the model of the system [15];
- the use of digital controllers with finite sampling rate [16]. Indeed, the "ideal" sliding motion $\sigma = 0$ requires the switching of the control input at an infinite frequency.

A simulation of system (1.19) controller by the standard SMC is made with a limited sampling period value ($T_e = 0.1\ ms$) and $k = 12$, and results are presented in Figure 1.2. Once the system trajectories have converged to the sliding surface ($t \simeq 0.7\ s$), the chattering phenomena appears: high frequency switching of the control input u as well as high frequency oscillations of σ around the sliding surface ($\sigma = 0$).

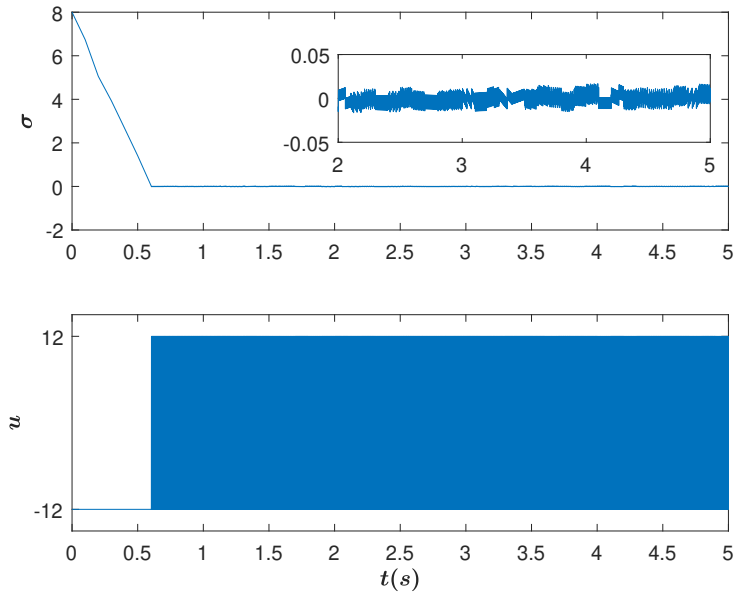

Figure 1.2 – **Top.** Sliding variable σ versus time (s); **Bottom.** control input u versus time (sec).

Several methods have been proposed for the reduction of the chattering effect. Notably, the boundary layer SMC method consists in replacing the sign function by an approximate continuous one, in a vicinity of the sliding surface $\mathcal{S}$ [17]. The sliding mode is no longer confined to $\mathcal{S}$, but to a vicinity of it. Then, the system is said to have a "pseudo" sliding motion [18]. Among the used continuous functions, one can cite

The saturation function. The function $sign(\sigma)$ (Figure 1.5 (a)) is replaced by a straight line with slope equal to $1/\delta$ $(0 < \delta < 1)$ at a vicinity of the origin whose width is 2δ (see Figure 1.5 (b)). Its expression is given by

$$sat(\sigma, \delta) = \begin{cases} sign(\sigma) & \text{if} \quad |\sigma| > \delta \\ \frac{\sigma}{\delta} & \text{if} \quad |\sigma| \leq \delta \end{cases} \tag{1.28}$$

The *atan* function. It is given by

$$v(\sigma, \delta) = \frac{2}{\pi} atan(\frac{\sigma}{\delta}) \tag{1.29}$$

This function (see Figure 1.5 (c)) gives a good approximation of the sign function for sufficiently small δ.

The *tanh* function. Another solution is to use the hyperbolic tangent function (see Figure 1.5 (d))

$$v(\sigma, \delta) = tanh(\frac{\sigma}{\delta}) \tag{1.30}$$

with $0 < \delta < 1$.

Notice that, in the previous approximation approaches, δ strongly influences the slope of the function at a vicinity of $\mathcal{S}$: the smaller the value of δ, the greater the slope. Notice that replacing the sign function by its continuous approximation reduces the chattering, but also reduces the robustness of the controller.
Another solution to reduce the chattering phenomenon is higher order SMC (HOSMC) which will be detailed in the sequel. This is performed by introducing the discontinuous control on a higher order time derivative of the sliding variable giving a smoother output.

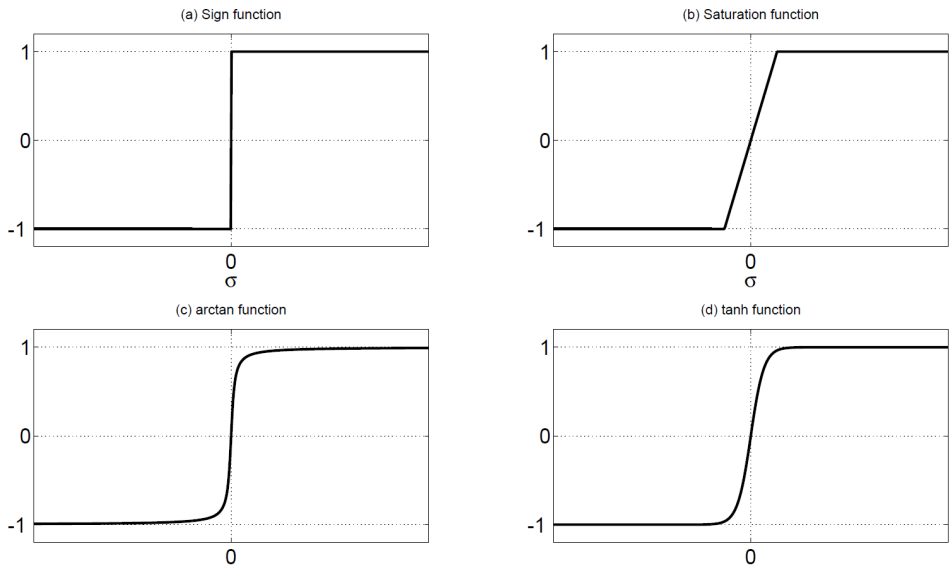

Figure 1.3 – Sign function and some approximate functions.

1.3 Higher order sliding mode control

HOSMC is a generalization of FOSMC where not only σ is stabilized to 0 in finite time, but also a finite number of its consecutive time derivatives. In fact, in the case of FOSMC, the discontinuous control acts on the first derivative of the sliding variable. In HOSMC, the discontinuous control acts on a higher derivative of σ (depending on the sliding mode order).
Recall that it is mainly the high frequency switching of the control input that induces chattering. Then, applying a discontinuous control on a higher order time derivative of the sliding variable leads to the attenuation of chattering on the system output. In this section, the principle of HOSMC as well as a few algorithms are presented.

Definition 1.3. *[9] Consider system (1.1) with the sliding variable σ, let $r \geq m$ be an integer. Then, if*

1. *the successive time derivatives $\sigma, \dot{\sigma}, \cdots \sigma^{(r-1)}$ are continuous functions of x,*
2. *the set*

$$\mathcal{S}^r = \{x \in \mathcal{X} \mid \sigma = \dot{\sigma} = \cdots \sigma^{(r-1)} = 0\} \tag{1.31}$$

   is a nonempty integral set,

3. *the Filippov set of admissible velocities at the $r-$sliding points (1.31) contains more than one vector,*

the motion on the set (1.31) is said to exist in an $r^{th}-$order sliding mode. The set (1.31) is called the $r^{th}-$order sliding mode set.

As for FOSMC, the establishment of HOSM requires a controller with infinite switching frequency which is not possible to get in practice. Therefore, the sliding motion can only take place in a vicinity of the $r^{th}-$order sliding mode set. This behavior is called "real" $r^{th}-$order sliding mode.

Definition 1.4. *[19] Consider the nonlinear system (1.1) and the sliding variable σ; let $r \geq m$ be an integer. Assume that the successive time derivatives $\sigma, \dot{\sigma}, \cdots \sigma^{(r-1)}$ are*

continuous functions. The manifold defined as (T_e being the sampling period of the control law)

$$\mathcal{S}^r_{real} = \{x \in \mathcal{X} \mid |\sigma| \leq \mu_0 T_e^r, \cdots, |\sigma^{(r-1)}| \leq \mu_{r-1} T_e\} \tag{1.32}$$

with $\mu_i \geq 0$ (with $0 \leq i \leq r-1$), is called "real $r^{th}-$order sliding mode set", which is nonempty and is locally an integral set in the Fillipov sense. The motion on this manifold is called "real $r^{th}-$ order sliding mode" with respect to the sliding variable σ.

The development of HOSMCs has attracted a lot of attention in the last two decades and one can cite works as

- [1, 20, 21, 22] on second order SMC;
- [23, 24, 25, 26, 27, 28, 29] on HOSMC.

In the sequel, only some algorithms, that are used in the thesis work, are presented.

1.3.1 Twisting control [1]

Consider the system (1.1) and the sliding variable $\sigma(x,t)$, the objective of the second order SMC being to drive σ and its first time derivative to zero in a finite time *i.e.*

$$\sigma = \dot{\sigma} = 0. \tag{1.33}$$

The twisting controller (TWC) [1] is a discontinuous control that can be applied to a class of systems with a relative degree equal to 1 or 2 [3] with respect to the sliding variable. Consider system (1.1), and without loss of generality, define, from the control objective, the sliding variable $\sigma(x,t)$ with a relative degree equal to 2. One gets

$$\ddot{\sigma} = \bar{a}(x,t) + \bar{b}(x,t)u \tag{1.34}$$

with functions $\bar{a}(x,t)$ and $\bar{b}(x,t)$ supposed to be bounded such that there exist positive constants a_M, b_m, b_M such that

$$\begin{aligned} &|\bar{a}(x,t)| \leq a_M \\ &0 < b_m \leq \bar{b}(x,t) \leq b_M \end{aligned} \tag{1.35}$$

for $x \in \mathcal{X}$ and $t > 0$. The TWC [1] reads as

$$u = -k_1 sign(\sigma) - k_2 sign(\dot{\sigma}). \tag{1.36}$$

If k_1 and k_2 satisfy the conditions

$$\begin{aligned} &k_1 > k_2 > 0, (k_1 - k_2)b_m > a_M \\ &(k_1 + k_2)b_m - a_M > (k_1 - k_2)b_M + a_M, \end{aligned} \tag{1.37}$$

the controller guarantees the establishment of a second order sliding mode with respect to σ in a finite time.

3. If the sliding variable is defined such the system admits a relative degree equal to 1, the TWC is applied on $\dot{u}$.

1.3.2 Switching gain strategy [2]

The switching gain control strategy proposed in [2] is an original formalism that allowed to rewrite the TWC. As a consequence of this formalism, the TWC can be viewed as a relay control. It has also allowed to determine the convergence domain of an uncertain nonlinear system controlled by a sampled TWC which is one of the contributions of this thesis (see Section 3.7). Consider system (1.1) and sliding variable $\sigma(x,t)$ as defined in Section 1.3.1. Suppose that

Assumption 1.3. *The system trajectories are supposed to be infinitely extendible in time for any bounded Lebesgue measurable inputs.* ■

Assumption 1.4. *The controller is updated in discrete-time with the sampling period T_e. The control input u is constant between two successive sampling steps, i.e*

$$\forall t \in [\varsigma T_e,\ (\varsigma+1)T_e[\ \ u(t) = u(\varsigma T_e). \tag{1.38}$$

with $\varsigma \in \mathbb{N}$. ■

The so-called "switching gain" strategy [22], [2] means that the control input u can switch between two levels: a low level $u = u_L$, and a high level $u = u_H$, with $|u_L| < |u_H|$. More precisely, the switching gain control strategy can be described as follows

$$u(\varsigma T_e) = \begin{cases} u_L(\varsigma T_e) = U(\varsigma T_e) & \text{if } \varsigma T_e \notin \mathcal{T}_{\mathcal{H}} \\ u_H(\varsigma T_e) = \varpi U(\varsigma T_e) & \text{if } \varsigma T_e \in \mathcal{T}_{\mathcal{H}} \end{cases} \tag{1.39}$$

with $\varpi > 1$, $\varsigma \in \mathbb{N}$ and $\mathcal{T}_{\mathcal{H}}$ defining the time interval during which u_H is applied. Define U as

$$U(\varsigma T_e) = -K_m sign(\sigma(\varsigma T_e)) \tag{1.40}$$

with $K_m > 0$. Notice that the large gain u_H is applied on a time interval and the small gain u_L is applied on another. The strategy consists of knowing when to switch between u_H and u_L. This latter is defined by $\mathcal{T}_{\mathcal{H}}$. This class of controllers is composed of three parts:

- the general control form (1.39)-(1.40);
- two gain parameters: K_m and ϖ;
- a switching gain condition $\mathcal{T}_{\mathcal{H}}$.

Notice that the control input u switches between four values $\pm K_m$ and $\pm\varpi K_m$. Recall $\sigma-$dynamics as defined in (1.34). Define $u^*(t)$ as

$$u^*(t) = \begin{cases} -K_m^*(t) \cdot \text{sign}(\sigma(kT_e)) \text{ if } \varsigma T_e \notin \mathcal{T}_{\mathcal{H}} \\ -K_M^*(t) \cdot \text{sign}(\sigma(kT_e)) \text{ if } \varsigma T_e \in \mathcal{T}_{\mathcal{H}} \end{cases} \tag{1.41}$$

with K_m^* and K_M^* defined by

$$\begin{aligned} K_m^*(t) &= b(x,t)K_m - a(x,t)\text{sign}(\sigma(kT_e)) \\ K_M^*(t) &= b(x,t)\varpi K_m - a(x,t)\text{sign}(\sigma(kT_e)) \end{aligned} \tag{1.42}$$

Then, system $\sigma-$dynamics can be rewritten as

$$\ddot{\sigma} = u^* \tag{1.43}$$

Define t_i (see Figure 1.4) the instant at which the system trajectory crosses $\dot{\sigma}$-axis in the phase plane for the i^{th} time (with $\sigma(t_i) = 0$), T_s^i the time at which the i^{th} σ-sign switching is *detected* and τ_i^d the duration of the detection

$$\text{sign}(\sigma(T_s^i)) \neq \text{sign}(\sigma(T_s^i - T_e)) \tag{1.44}$$

and

$$\tau_i^d = T_s^i - t_i. \tag{1.45}$$

$$\tau_i^d = T_s^i - t_i.$$

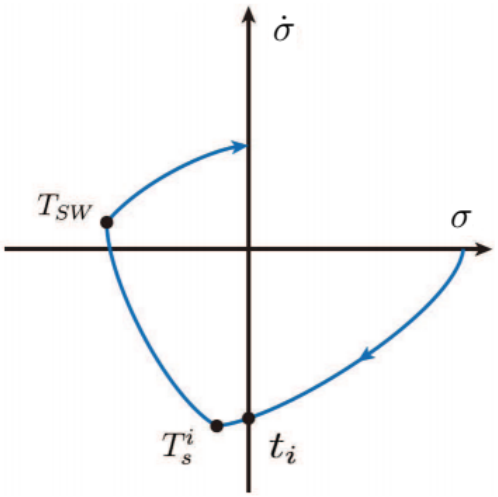

Figure 1.4 – Example of system trajectory in the $(\sigma, \dot{\sigma})$-phase plane.

Theorem 1.1. *[2] Consider system (1.1) with $\sigma-$dynamics reading as (1.43), controlled by the switching gain form controller (1.39)-(1.40) and fulfilling Assumptions 1.1-1.4. Then, the system trajectory tends to be closer from the origin if the following conditions hold*

- $K_m > \dfrac{a_M}{b_m}$
- $\varpi > 2 + \dfrac{b_M}{b_m}$
- *The duration of the large magnitude control τ_i satisfies*

$$\int_{T_s^i}^{T_s^i+\tau_i} K_M^*(t)dt \geq |\dot{\sigma}(t_i)| + K_m^{max}\tau_i^d - \Delta \int_{T_s^i}^{T_s^i+\tau_i} K_M^*(t)dt \leq |\dot{\sigma}(t_i)| + K_m^{max}\tau_i^d + \Delta' \tag{1.46}$$

with Δ the positive root of

$$(\frac{1}{K_m^{min}} - \frac{1}{K_M^{min}})\Delta^2 = (\frac{\dot{\sigma}^2(t_i)}{K_m^{max}} - \frac{\dot{\sigma}_0^2}{K_M^{min}}), \tag{1.47}$$

Δ' the positive root of

$$(\frac{1}{K_m^{max}} - \frac{1}{K_M^{max}})\Delta'^2 = (\frac{\dot{\sigma}^2(t_i)}{K_m^{max}} - \frac{\dot{\sigma}_0^2}{K_M^{min}}) \tag{1.48}$$

and

$$\dot{\sigma}_0^2 = (|\dot{\sigma}(t_i)| + K_m^{max}\tau_i^d)^2 + 2K_M^{min}(|\dot{\sigma}(t_i)|\tau_i^d + \frac{1}{2}K_m^{max}(\tau_i^d)^2)\ . \tag{1.49}$$

with

$$\begin{aligned} K_m^{max} &= \max(K_m^*) = b_M K_m + a_M \\ K_m^{min} &= \min(K_m^*) = b_m K_m - a_M \\ K_M^{max} &= \max(K_M^*) = \varpi b_M K_m + a_M \\ K_M^{min} &= \min(K_M^*) = \varpi b_m K_m - a_M. \end{aligned} \tag{1.50}$$

■

TWC under switching gain form. Consider system (1.1) with $\sigma-$dynamics reading as (1.34); the sampled TWC reads as

$$u(\varsigma Te) = -k_1 sign(\sigma(\varsigma Te)) - k_2 sign(\dot{\sigma}(\varsigma Te)). \tag{1.51}$$

This controller ensures the establishment of a real second order sliding mode in finite time if gains k_1 and k_2 are tuned as (1.37). Under this control law, the amplitude of the

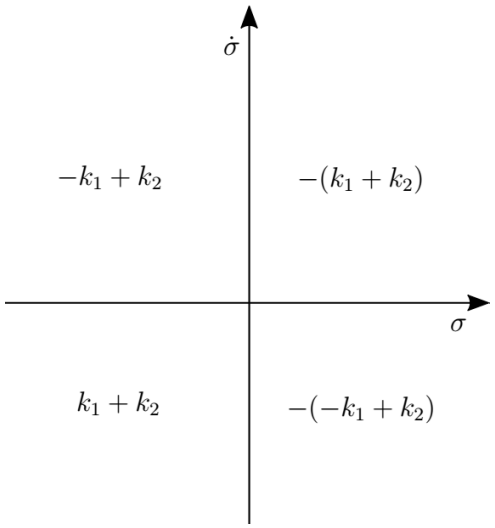

Figure 1.5 – TWC: values of the control input in $(\sigma, \dot{\sigma})-$phase plane.

input switches between four values $\pm(k_1 + k_2)$ and $\pm(k_1 - k_2)$. This property offers the possibility to revisit TWC with the switching gain form. If one defines K_m and ϖ as

$$K_m = (k_1 - k_2), \qquad \varpi = \frac{(k_1 + k_2)}{(k_1 - k_2)} \tag{1.52}$$

the TWC can be written as

$$u = \begin{cases} -K_m \text{sign}(\sigma) & \text{if } \sigma\dot{\sigma} \leq 0 \\ -\varpi K_m \text{sign}(\sigma) & \text{if } \sigma\dot{\sigma} > 0 \end{cases}. \tag{1.53}$$

Then, the TWC (1.51) can be written in the switching gain control form (1.39)-(1.40), with $\mathcal{T}_\mathcal{H}$ defined as

$$\mathcal{T}_\mathcal{H} = \{\varsigma T_e \mid \sigma\dot{\sigma} > 0\}\,. \tag{1.54}$$

Theorem 1.2. *[2] Consider system (1.1) with $\sigma-$dynamics reading as (1.34), under Assumptions 1.1-1.4 and controlled by (1.39)-(1.40) with K_M and ϖ defined as (1.52) with $\mathcal{T}_\mathcal{H}$ defined as (1.54). Then, if $K_m > a_M/b_m$ and $\varpi > 2 + b_M/b_m$, a real second order sliding mode with respect to σ is established after a finite time.*

■

1.3.3 Higher order sliding mode controllers

Preserving the main advantages of the standard FOSMC, HOSMC has been proposed in order to reduce the chattering phenomenon. Instead of influencing the first sliding variable time derivative, the sign function acts on its higher order time derivative. This method can also achieve a better accuracy with respect to FOSMC. Some HOSMCs have been designed using homogeneity tools [23], [24] and more recently using a Lyapunov framework [26], [27], [28], [29]. However, only the controller from [29] is presented in the sequel given that it be used later in the thesis (see Chapter 4). Consider the system (1.1), and suppose that the sliding variable σ is defined such that the relative degree of (1.1) with respect to σ equals r with $r \geq m$. It means that

$$\sigma^{(r)} = \bar{a}(x,t) + \bar{b}(x,t)u \tag{1.55}$$

with functions $\bar{a}(x,t)$ and $\bar{b}(x,t)$ bounded such that

$$|\bar{a}(x,t)|, \leq a_M \quad 0 < b_m \leq \bar{b}(x,t) \leq b_M \tag{1.56}$$

for $x \in \mathcal{X}$ and $t > 0$ with a_M, b_m, b_M positive constants.

In [29], a family of HOSMCs is designed to control (1.1) with $\sigma-$dynamics reading as (1.55) and is based on control Lyapunov functions (CLFs). In this paper, the focus is made on a particular set of these HOSMCs where the control law u reads as [4]

$$\begin{aligned} u =& -k_r \lceil \xi_r \rfloor^0, \\ \xi_i =& \lceil \sigma^{(i-1)} \rfloor^{\frac{\epsilon_1}{\epsilon_i}} + k_{i-1}^{\frac{\epsilon_1}{\epsilon_i}} \xi_{i-1} \end{aligned} \tag{1.57}$$

with $2 \leq i \leq r$, $\epsilon = (\epsilon_1, \cdots, \epsilon_r) = (r, r-1, \cdots, 1)$ and $\xi_1 = \sigma$. $(k_1, \cdots, k_r)$ are the controller gains where $(k_2, \cdots, k_r)$ can be written as a function of k_1 such that

$$\begin{aligned} & k_i = ß_{i-1} k_1^{\frac{r}{r-(i-1)}} \qquad \forall i = 2, \cdots, r-1 \\ & b_m k_r - a_M \geq ß_{r-1} k_1^r \end{aligned} \tag{1.58}$$

with the parameters $ß_{i-1}$ $(2 \leq i \leq r-1)$ calculated by evaluating homogeneous functions [30] and numerically finding their maxima on a homogeneous sphere. Proposed values of $ß_{i-1}$ for $r = 2, 3, 4$ in [29] are given in Table 1.1. The form of u for $r = 2, 3, 4$ is given in Table 1.2. For the tuning of the control gain k_r, the redundantly large estimation of a_M, b_m and b_M may lead to an over-sized gain, then enhances the chattering phenomenon.

r	Parameters
2	$ß_1 = 1.26$
3	$ß_2 = 9.62,\ ß_1 = 1.5$
4	$ß_3 = 739.5,\ ß_2 = 8.1,\ ß_1 = 2$

Table 1.1 – Parameters $ß_{i-1}$ for $2 \leq i \leq r-1$

4. $\lceil \cdot \rfloor^\alpha = |\cdot|^\alpha \text{sign}(\cdot)$

r	ξ_r
2	$u = -k_2 \left\lceil \lceil \dot{\sigma} \rfloor^2 + k_1^2 \sigma \right\rfloor^0$
3	$u = -k_3 \left\lceil \lceil \ddot{\sigma} \rfloor^3 + k_2^3 (\lceil \dot{\sigma} \rfloor^{\frac{3}{2}} + k_1^{\frac{3}{2}} \sigma) \right\rfloor^0$
4	$u = -k_4 \left\lceil \lceil \sigma^{(3)} \rfloor^4 + k_3^4 \Big(\lceil \ddot{\sigma} \rfloor^2 + k_2^2 (\lceil \dot{\sigma} \rfloor^{\frac{4}{3}} + k_1^{\frac{4}{3}}) \sigma \Big) \right\rfloor^0$

Table 1.2 – Control form, u, for $2 \leq i \leq r-1$

1.4 Sliding mode control with gain adaptation

As viewed previously, for all controllers the gain is depending on the bounds of uncertainties and perturbations. The determination of these bounds can require tedious process of identification, and usually induces overestimation of the gains. Then, the gain adaptation offers a solution to the control problem for which the bounds of uncertainties and perturbations are unknown or not well-known. The gain adaptation allows a gain adjustment with respect to a predefined criterion and then simplifies the tuning process. The gain adaptation is based on the following principle: if the system trajectories are not evolving on the sliding surface, it could be caused by a insufficiently large gain or a too long convergence time. In this case, the control gain must be increased in order to reduce the convergence time and ensure the establishment of the sliding mode; on the other hand, if the system trajectories are evolving on the sliding surface, it means that the control gain is large enough to reject the perturbations and to guarantee the sliding mode: therefore it has to be reduced.
These techniques have been designed for systems with relative degree 1 in [31], [32], [33], [34], [35] and 2 in [36], [37]. A generalized algorithm for arbitrary relative degree is given in [38]. For a sake of clarity, only the adaptive controller presented in [32] is presented in the sequel; indeed, it is one of the most cited papers on adaptive SMC and it has initialized a solution for first order SMC.
Consider system (1.1) with $\sigma-$dynamics reading as

$$\dot{\sigma} = \bar{a}(x,t) + \bar{b}(x,t)u \tag{1.59}$$

where function $\bar{a}(x,t)$ is a bounded uncertain function and $\bar{b}(x,t)$ is positive and bounded. Thus, there exist *unknown* positive constants a_M, b_m and b_M such that

$$\begin{aligned} &|\bar{a}(x,t)| \leq a_M \\ &0 < b_m \leq \bar{b}(x,t) \leq b_M \end{aligned} \tag{1.60}$$

In [32], an adaptive gain algorithm is designed for a FOSMC

$$u = -k(t)sign(\sigma) \tag{1.61}$$

with $k(t)$ the time varying gain. The design of the adaptation gain law is usually composed of two parts: the design of a sliding mode detector and the design of a gain adaptation law.

Sliding mode detector. Through the parameter $\hbar$, the real sliding mode surface is defined in accordance with (1.32)

$$\mathcal{S}^1_{real} = \{x \in \mathcal{X} \mid |\sigma| < \hbar\}. \tag{1.62}$$

It means that, when the sliding variable reaches the vicinity of zero with accuracy $\hbar$, one considers that a real first order sliding mode is established.

Gain adaptation law. The time varying gain $k(t)$ is defined through the following dynamics

$$\dot{k} = \begin{cases} \bar{k}|\sigma|\text{sign}(|\sigma| - \hbar) & \text{if } k > \digamma \\ \digamma & \text{if } k \leq \digamma \end{cases} \tag{1.63}$$

with $k(0) > 0, \digamma > 0, \bar{k} > 0$ and $\hbar > 0$ very small. The parameter $\digamma$ is introduced to ensure a positive gain k. Given (1.63), if $|\sigma| > \hbar$, then real sliding mode is not established and the gain increases. On the other hand, if $|\sigma| < \hbar$, then real sliding mode is established and the gain decreases. Then, there is adaptation.

1.5 Motivation

The standard FOSMC engenders the chattering phenomenon, *i.e.* high frequency oscillations that may lead to low control accuracy, high wear of moving mechanical parts, and high heat losses in power circuits [14]. This is especially due to neglected dynamics such as the fast dynamics of the servodistributors in an electro-pneumatic system. This class of controllers is made for systems with relative degree equal to 1 with respe ct to the sliding variable. Higher order sliding mode controllers [39], [23], [24] have relieved the relative degree restriction. In fact, they bring the sliding variable and its consecutive derivatives to zero in a finite time. The main disadvantage of these control strategies is the use of higher order time derivatives that inject noise into the control, depleting the accuracy. Moreover, due to the tuning process of the gain (that can be said "made in the worst-case") the gain is often overestimated. Then, sliding mode control induces a large control effort, in other words, it is high energy consuming. A way reducing the chattering effect as well as the energy consumption has been proposed thanks to adaptive gain sliding mode techniques. The idea consists of dynamically adapting the gain amplitude with respect to the effect of perturbations/uncertainties. However, accuracy can be affected due to the loss of sliding mode: indeed, the controller gain can temporarily become too small with respect to perturbations/uncertainties.
By another point of view, a control solution that is smooth and has low energy consumption is the linear state feedback. In fact, it has good closed loop performances in the absence of perturbations/uncertainties (high accuracy) but the accuracy is degraded in their presence. The objective of this thesis is twofold:

- the development of controllers that have the advantages of both sliding mode control (robustness and high accuracy) and linear state feedback (low energy consumption). This is performed by introducing a parameter that makes the control more or less smooth. In the sequel, control laws for systems with relative degree 1 and 2 with respect to the sliding variable are developed as well as an algorithm for systems with arbitrary relative degree. They allow high accuracy tracking and robustness with reduced energy consumption and chattering.

- the proof of the applicability of the proposed control laws to real systems. Control laws are designed and implemented on the LS2N electro-pneumatic actuator. Applications are also performed on a wind system.

The control methods developed in this thesis are intrinsically new given that it is not the gain that is time-varying as in adaptive sliding mode techniques. In the proposed controllers, the time-varying parameter corresponds to the exponent term of the controllers.

1.6 Organization and contribution of the thesis

This thesis is divided into two parts:

- Part I is dedicated to the presentation of accurate and robust control laws with reduced energy consumption.
  - In Chapter 2, a controller presenting an efficient trade-off between first order sliding mode control (FOSMC) (high accuracy and robustness) and first order linear state feedback (FOLSF) (low energy consumption) is proposed. It can be applied to systems with relative degree equal to 1 with respect to the sliding variable. An academic example is treated showing the effectiveness of the proposed controller versus FOSMC and FOLSF.
  - In Chapter 3, by a similar logic, controllers are proposed with the advantages of the twisting controller (TWC) (high accuracy and robustness) and the second order linear state feedback (SOLSF) (low energy consumption). They can be applied to systems with relative degree equal to 1 or 2. Three controllers having the same structure but different time varying approaches for α are presented: switching, dynamic, and algebraic. In the context of real physical applications, the knowledge of the convergence domain of the TWC could give a more efficient trade-off between accuracy and energy consumption. Then, in the second part of this chapter, the convergence domain of the TWC is calculated by writing the TWC in the switching form. An academic example is treated comparing the three methods to TWC and SOLSF. The simulations also show that when the TWC is applied, the trajectories of the system converge to the theoretically calculated domain.
  - In Chapter 4, a robust, accurate and with reduced energy consumption algorithm for systems of arbitrary relative degree is presented. It is based on a high order sliding mode controller recently presented [29]. An academic example is treated showing its effectiveness.
- Part II presents the applications of these new control laws on real systems.
  - Chapter 5 deals with the position control problem of an electropneumatic system. This is a typical nonlinear system with uncertainties and perturbations. The proposed methods show their advantages for the control of such systems. The first order controller presented in Chapter 2 and a second order controller presented in Chapter 3 are applied to the electropneumatic system, and their performances are compared to standard controllers (sliding mode control and linear state feedback). The interest for the use of such controllers is highlighted from the experimental results.
  - In Chapter 6, the generalized algorithm presented in Chapter 4 is applied to a twin wind turbine which belongs to the family of perturbed and uncertain systems. The system includes two identical wind turbines mounted on the

same tower. The main control objective is to force the structure face the wind while keeping maximal power production. The performances of the proposed approach are compared to higher order sliding mode control via simulations.

Some of the results presented in this thesis have been published or are under revision process for publication in international journals and international conferences.

Journal Papers

- Elias Tahoumi, Malek Ghanes, Franck Plestan, and Jean-Pierre Barbot, "New robust schemes based on both linear and sliding mode approaches: design and application to an electropneumatic setup," *IEEE Transactions on Control System Technology.* [40]
  Accepted.
- Elias Tahoumi, Carolina Evangelista, Malek Ghanes, Franck Plestan, Jean-Pierre Barbot, Paul Puleston "Energy efficient control with time varying parameters derived from homogeneous algorithm - application to a wind system," *Control Engineering Practice.* [41]
  under second round of revision.

International Conference Papers

- Elias Tahoumi, Malek Ghanes, Franck Plestan, and Jean-Pierre Barbot, "A new controller switching between linear and twisting algorithms," in *American Control Conference (ACC)*, Milwaukee, Wisconsin, USA, 2018. [42]
- Elias Tahoumi, Franck Plestan, Malek Ghanes, and Jean-Pierre Barbot, "A Controller Switching between Twisting and Linear Algorithms for an Electropneumatic Actuator," in *European Control Conference (ECC)*, Limasol, Cyrpus, 2018. [43]
- Elias Tahoumi, Franck Plestan, Malek Ghanes, and Jean-Pierre Barbot, "Adaptive exponent parameter: a robust control solution balancing between linear and twisting controllers," in *15th International Workshop on Variable Structure Systems (VSS)*, Gratz, Austria, 2018. [44]
- Muriel Primot, Elias Tahoumi, Xinming Yan, and Franck Plestan, "Determination of the convergence domain of the twisting algorithm thanks to a switching gain approach," in *IEEE Conference on Decision and Control (CDC)*, Miami, Florida, USA, 2018. [45]
- Elias Tahoumi, Franck Plestan, Malek Ghanes, and Jean-Pierre Barbot, "Robust and energy efficient control schemes based on higher order sliding mode," in *European Control Conference (ECC)*, Naples, Italy, 2019. [46]
- Cheng Zhang, Elias Tahoumi, Susana Gutierrez, Franck Plestan, Jesus De Leon Morales "Adaptive Robust Control of Floating Offshore Wind Turbine Based on Sliding Mode," in *IEEE Conference on Decision and Control (CDC)*, Nice, France, 2019. [47]

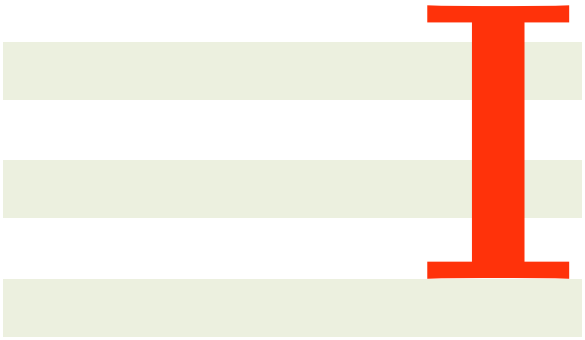

Energy efficient controllers based on Sliding Mode Control

2

Controller balancing between FOSMC and FOLSF

Contents

2.1 Introduction

This chapter presents a new control strategy for systems with relative degree 1 with respect to the sliding variable. The standard first order sliding mode controller (FOSMC) [10] is designed for such systems and is known for its robustness to matched uncertainties/perturbations. However, it induces the so-called chattering phenomenon [14] that increases the energy consumption of the controller (from a control effort point of view). A way to attenuate the chattering phenomenon is to replace the *sign* function in the control by the saturation function. Another control solution that stabilizes a system of relative degree equal to 1 is the first order linear state feedback (FOLSF) which is known for being a smooth controller with low energy consumption. However, its accuracy can be degraded in the presence of uncertainties/perturbations.
The objective in this chapter is the design of a controller that gives rise to an efficient tradeoff between the standard FOSMC (high accuracy and robustness) and the FOLSF (low energy consumption). This is made possible by introducing a parameter α and by varying it with respect to efficient (or not) tracking of the control objectives.

In the sequel, simulations show the effectiveness of the proposed controller and its performances are mainly compared to those of the FOSMC and FOLSF.

2.2 Problem statement

Consider the following system

$$\begin{aligned} \dot{x} &= f(x,t) + g(x,t)u \\ \sigma &= \sigma(x,t) \end{aligned} \tag{2.1}$$

where $x \in \mathcal{X}^n \subset \mathbb{R}^n$ is the state space, f and g uncertain sufficiently smooth functions, $u \in \mathcal{U} \subset \mathbb{R}$ the control input and σ the sliding variable. The control objective is to constrain σ to a vicinity of the origin in a finite time in spite of uncertainties/perturbations. Suppose that

Assumption 2.1. *The relative degree of (2.1) is equal to 1, i.e.*

$$\dot{\sigma} = \bar{a}(x,t) + \bar{b}(x,t)u. \tag{2.2}$$

■

Assumption 2.2. *$\bar{a}(x,t)$ and $\bar{b}(x,t)$ are unknown but bounded functions such that there exist positive known constants a_M, b_m and b_M such that $\forall x \in \mathcal{X}, t \geq 0$ one has*

$$|\bar{a}(x,t)| \leq a_M, \quad 0 < b_m \leq \bar{b}(x,t) \leq b_M. \tag{2.3}$$

■

Assumption 2.3. *The internal dynamics of system (2.1) are bounded.*

■

A control solution stabilizing (2.1) to a vicinity of the origin reads as [1] [48], [49]

$$u = -k\lceil\sigma\rfloor^{\alpha} \tag{2.4}$$

where k and α are positive constants with $\alpha \in [0,1]$. Remark that, when $\alpha = 1$, FOLSF is obtained

$$u = -k\ \sigma \tag{2.5}$$

where, in the steady state, σ is bounded if $k > 0$. When $\alpha = 0$, a FOSMC is obtained [10]

$$u = -k\ \text{sign}(\sigma). \tag{2.6}$$

It has been proven [10] that, if this controller is tuned such that

$$k > \frac{a_M}{b_m}, \tag{2.7}$$

1. $\lceil\sigma\rfloor^{\alpha} = |\sigma|^{\alpha} sign(\sigma)$

it allows the establishment of a first order sliding mode, *i.e.* the system trajectory converges in a finite time to $\mathcal{S}^1$ defined as [10]

$$\mathcal{S}^1 = \{x \in \mathcal{X} \,|\, \sigma = 0\}. \tag{2.8}$$

In case of a sampled sliding mode controller, the system trajectory converges to

$$\mathcal{S}^1_{real} = \{x \in \mathcal{X} \,|\, |\sigma| \leq \mu T_e\} \tag{2.9}$$

with μ a positive constant and T_e the controller sampling period. Recall that this behavior of (2.1) on $\mathcal{S}^1$ (*resp.* $\mathcal{S}^1_{real}$) is called ideal (*resp.* real) sliding mode [19]. Notice that, with controller (2.4), parameter α is not restricted to 0 and 1 and can take any value between 0 and 1. In the sequel, a discussion on the accuracy (that is an image of the robustness) and energy consumption obtained in the steady state thanks to the controller (2.4) is made for several values of α.

2.2.1 Accuracy and energy consumption

For a sake of clarity, in this section, no uncertainty on the control term is considered: one supposes $b_m = b_M = 1$. Furthermore, $\bar{a}(x,t)$ is taken constant and positive and denoted $\bar{a}(x,t) = \mathcal{A}$[2]. Recall that, in this subsection, the objective is to evaluate accuracy and energy consumption for several values of α in (2.4) and for specific systems (2.1) with $\sigma-$dynamics defined as (2.2).
When controller (2.4) is applied to system (2.1), the equilibrium point is calculated by setting $\dot{\sigma} = 0$ and one has

$$\sigma \to \left(\frac{\mathcal{A}}{k}\right)^{\frac{1}{\alpha}} \tag{2.10}$$

in the steady state. Suppose that k is tuned as (2.7), then $\frac{\mathcal{A}}{k} < 1$. Hence, as α decreases, the accuracy of the closed-loop system increases. In fact, $\sigma \to 0$ when $\alpha \to 0$ *i.e.*

$$\lim_{\alpha \to 0} \left(\frac{\mathcal{A}}{k}\right)^{\frac{1}{\alpha}} = 0. \tag{2.11}$$

That is consistent with the fact that, for $\alpha = 0$, *i.e.* when FOSMC is applied, σ converges to 0 in a finite time (see (2.8)). It means that the worst accuracy, in the steady state, is obtained when the FOLSF is applied ($\alpha = 1$) for which one gets

$$\sigma \to \frac{\mathcal{A}}{k}. \tag{2.12}$$

Define now the following indicator for the energy consumption [50]

$$\mathcal{E} = \int_{t_0}^{t_f} u^2(t)dt \tag{2.13}$$

with t_0 and t_f the initial and final instants respectively of the time interval over which the energy is evaluated. Consider the controller (2.4) applied to system (2.1) and suppose that $|\sigma| < 1$[3]. Then $\forall \alpha_1, \alpha_2 \in [0,1]$, if $\alpha_1 < \alpha_2$, one has

$$k|\sigma|^{\alpha_1} > k|\sigma|^{\alpha_2} \tag{2.14}$$

2. Of course, $a(x,t)$ is practically never constant for real systems. The purpose here is to present the effect of the value of α in the clearest manner.

3. Given that k is tuned as (2.7), then following (2.10), it is not restrictive to consider $|\sigma| < 1$ in the steady state.

where the left hand side (*resp.* the right hand side) of the previous inequality is the control input u (2.4) in absolute value for $\alpha = \alpha_1$ (*resp.* $\alpha = \alpha_2$). Hence, for same values of σ, the control effort increases when α decreases. However, due to the nonlinearity of the system, it is not guaranteed that the system follows the same trajectory for different values of α and then, it is not guaranteed that (2.14) holds. Nevertheless, the trend is visible via simulations: Consider system (2.2) and control law (2.4) such that

$$a_M = 10,\ b_m = 0.98,\ b_M = 1.02 \text{ and } k = 12$$

for different values of $\alpha \in [0, 1]$. It can be seen in Figure 2.1 that as α is increasing, the energy consumption $\mathcal{E}$ and the accuracy $mean(|\sigma|)$ are decreasing.

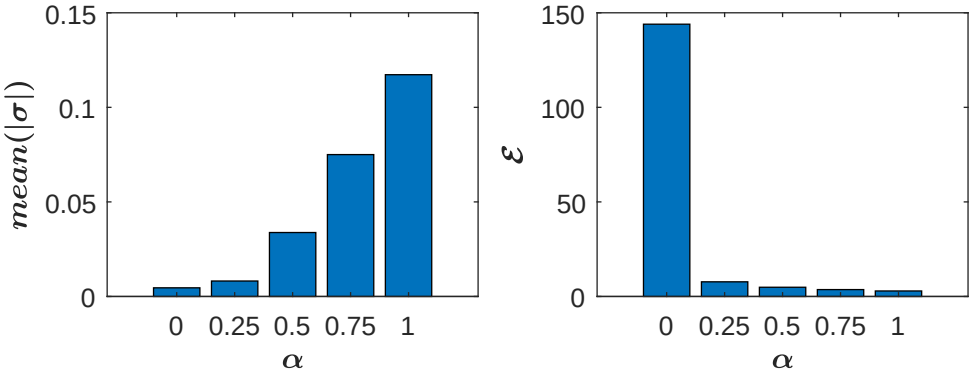

Figure 2.1 – **Left:** evolution of $mean(|\sigma|)$ with respect to α. **Right:** evolution of $\mathcal{E}$ with respect to α.

Note that more detailed simulations illustrating this fact are given in Section 2.5.

2.2.2 To summarize

As discussed in the previous section, it is noticed that when controller (2.4) is applied, decreasing α improves the accuracy of the closed loop system and increases the energy consumption whereas increasing α has opposite effects. This conclusion is the basis of what follows. First, a new controller based on (2.4) stabilizing system (2.1) and having a time-varying parameter α is proposed with the advantages of the FOLSF (low energy consumption) and those of the FOSMC (robustness and accuracy). This is achieved thanks to a variation law of α in (2.4), this variation law being based on the accuracy of σ. In the sequel, a formalization of the variation process of parameter α and the stability of the closed loop system are detailed.

2.3 Proposed controller

The proposed controller reads as

$$u = -k\lceil\sigma\rfloor^{\alpha} \tag{2.15}$$

with k tuned as (2.7) and $\alpha \in [0, 1]$. This latter varies according to the following variation law

$$\alpha = \max(-\beta\frac{|\sigma|}{|\sigma| + \varepsilon} + 1\,,\, 0) \tag{2.16}$$

with $\beta > 1$ and $\varepsilon > 0$.

The logic of this variation law can be summarized as follows: when $|\sigma|$ increases, it means that the accuracy of the closed loop system is degraded. As a consequence of (2.16), the value of α automatically decreases in order to increase the robustness of the system and then to increase the accuracy. On the other hand, when the accuracy of the system is improving, the value of α automatically increases in order to reduce the energy consumption.

Parameters tuning

- Closed loop stability should be ensured $\forall \alpha \in [0, 1]$, then the gain k should be tuned as (2.7). Note that the closed loop stability is ensured for $\alpha \neq 0$ when $k > 0$ which is satisfied in (2.7).
- Parameters ε and β act on the accuracy of the controller (see (2.18) in the sequel). Therefore, if β is increased or ε is decreased, the accuracy of the closed-loop system is improved;
- however, increasing β or decreasing ε leads to lower average value of α since a greater accuracy is required; as a consequence, one gets higher energy consumption. Then, these two parameters have to be wisely tuned to achieve the required trade-off between accuracy and energy consumption. This tuning depends on the objectives of the control problem.
- A key point of this adaptive strategy is that it engenders a reduced energy consumption lower than that of the FOSMC. Then, ε and β should be tuned such that when $|\sigma| > 1$, $\alpha = 0$. Hence, following (2.16), this is ensured by the following condition

$$\frac{\varepsilon}{\beta - 1} < 1. \tag{2.17}$$

The following theorem states the first result of this work *i.e* the closed loop system trajectories reach in a finite time a domain that is precisely defined.

Theorem 2.1. *[40] Consider system (2.1) with $\sigma-$dynamics defined as (2.2) and Assumptions 2.1, 2.2 and 2.3 fulfilled. Suppose that the system is controlled by (2.15)-(2.16) with gain k tuned as (2.7). Then, there exist positive parameters ε and β ($\beta > 1$) satisfying (2.17) such that, $\forall x(0) \in \mathcal{X}$, the trajectories of system (2.1) converge in finite time to $\mathcal{B}_1$ defined as*

$$\mathcal{B}_1 = \{x \in \mathcal{X} \mid |\sigma| \leq \frac{\varepsilon}{\beta - 1}\} \tag{2.18}$$

Proof. Consider the case such that $x \notin \mathcal{B}_1$, *i.e.* $|\sigma| > \frac{\varepsilon}{\beta-1}$. Therefore, according to (2.16), $\alpha = 0$ and FOSMC is applied. Hence, with gain k tuned as (2.7) and thanks to the features of sliding mode control, the trajectory of the system will converge to $\mathcal{B}_1$ in finite time (see (2.9)).
Once system trajectory has reached $\mathcal{B}_1$, the variation of α begins: α is evolving between 0 and 1 following (2.16) and the system trajectories are evolving in $\mathcal{B}_1$. Since $\alpha \neq 0$, the controller is smooth, chattering is reduced, but robustness and accuracy can be lower. Suppose that the trajectories reach the boundary of $\mathcal{B}_1$, *i.e.* $|\sigma| = \frac{\varepsilon}{\beta-1}$: in this case, from (2.16), $\alpha = 0$. Then, $\dot{\sigma}$-dynamics reads as

$$\dot{\sigma} = \bar{a}(x, t) - \bar{b}(x, t)k \text{ sign}(\sigma). \tag{2.19}$$

As k is tuned as (2.7), one has $\dot{\sigma}\ \text{sign}(\sigma) < 0\ \forall \bar{a}(x,t),\ \bar{b}(x,t)$ satisfying Assumption 2.2. Thus, as long as $\alpha = 0$, $|\sigma|$ decreases; then, the trajectory is kept in $\mathcal{B}_1$. ■

Remark: Note that by a practical point of view, the FOSMC forces the trajectories to reach $\mathcal{S}^1_{real}$ (2.9). It means that, if one wants to get an efficient trade-off, one has to tune ε and β such that $\mathcal{S}^1_{real} \subset B_1$. Otherwise, a risk is to have the FOSMC ($\alpha = 0$) all the time. In such case, the interest of the control strategy is limited.

2.4 Discussion on similarity (or not) with saturation function

The controller presented in the previous section is a continuous one around the vicinity of the origin (defined by ε and β). Hence, similarities can be drawn to the saturation function. Then, the objective of this section is to compare both controllers. Recall the FOSMC that uses the saturation function [17]

$$u = -k\ \text{sat}(\sigma, \delta) = \begin{cases} -k\ \text{sign}(\sigma) & \text{if} \quad |\sigma| > \delta \\ -k\ \dfrac{\sigma}{\delta} & \text{if} \quad |\sigma| \leq \delta \end{cases} \tag{2.20}$$

It replaces the sign function in the FOSMC by a straight line with slope equal to $\dfrac{1}{\delta}$ $(0 < \delta < 1)$ at the vicinity of the origin. Now, consider controller (2.15) with a new law for α *i.e.* α switches between 0 and 1 as follows

$$\alpha = \begin{cases} 0 & \text{if} \quad |\sigma| > \delta \\ 1 & \text{if} \quad |\sigma| \leq \delta \end{cases} \tag{2.21}$$

The controller obtained from (2.15) and (2.21) is

$$u = \begin{cases} -k\ \text{sign}(\sigma) & \text{if} \quad |\sigma| > \delta \\ -k\ \sigma & \text{if} \quad |\sigma| \leq \delta \end{cases} \tag{2.22}$$

Hence, one concludes that the behavior of both controllers is similar. They behave as FOLSF in the vicinity of the origin ($|\sigma| \leq \delta$) and FOSMC elsewhere. When control law (2.20) (or (2.22)) is applied to system (2.1), the trajectories of the system converge to

$$\{x \in \mathcal{X} \mid |\sigma| \leq \delta\} \tag{2.23}$$

However, the gains for which the controllers are behaving as a FOLSF, are different: k/δ for saturation function and k for controller (2.22).

The behavior similarity can be extended to the saturation function and controller (2.15)-(2.16). The saturation function is identical to controller (2.15)-(2.16) when trajectories are far from the origin *i.e.* $|\sigma| \geq \delta$ or $|\sigma| \geq \frac{\varepsilon}{\beta - 1}$. The saturation function can be seen as a controller that simply has a different value of α than controller (2.15)-(2.16) at a vicinity of the origin: $\alpha = 1$ for the saturation function and $\alpha \in]0, 1]$ for controller (2.15)-(2.16). Recall from Section 2.2.1 that the smaller the value of α the greater the controller's robustness to uncertainties and perturbations. Then, controller (2.15)-(2.16) is more robust to uncertainties and perturbations at the vicinity of the origin. This fact allows to obtain a more efficient trade-off between energy consumption and accuracy as it will be shown in the next section.

2.5 Simulations

2.5.1 Context

Simulations have as objective to show the effectiveness of the proposed controller (2.15)-(2.16). Its performances are compared to the performances of the FOSMC, FOLSF and FOSMC with saturation function (2.20). The software used is Matlab/Simulink; the controller sampling period is taken as $T_e = 1\,ms$ with Euler integration solver (integration step 0.01 ms). The simulations time is $10\,s$.
The functions $\bar{a}(x,t)$ and $\bar{b}(x,t)$ are generated for $5\,s$ using the Matlab function 'rand' and are the same for all controllers. For the second part of the simulations ($5\,s \leq t \leq 10\,s$), the sequences for $\bar{a}(x,t)$ and $\bar{b}(x,t)$ are repeated but with a different amplitude for $\bar{a}(x,t)$ such that $\forall t \in [0,5]$

$$\bar{a}(x,t+5) = 2 \cdot \bar{a}(x,t), \qquad \bar{b}(x,t+5) = \bar{b}(x,t). \tag{2.24}$$

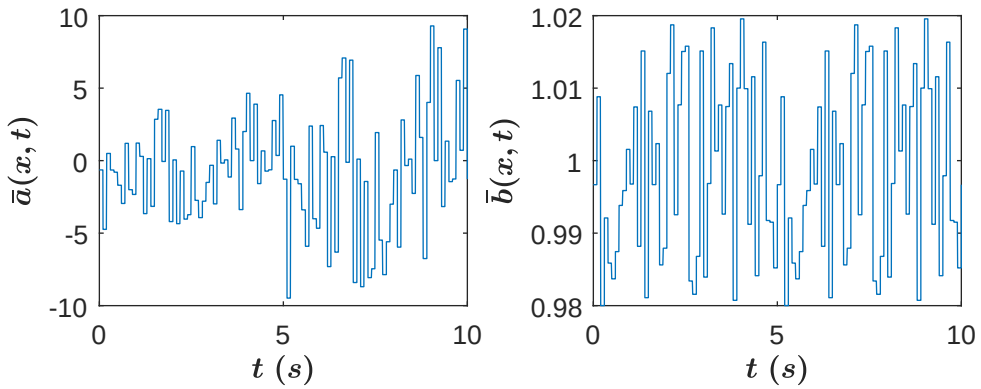

Figure 2.2 – **Left:** $\bar{a}(x,t)$ versus time (s); **Right:** $\bar{b}(x,t)$ versus time (s) versus time (s).

This choice for $\bar{a}(x,t)$ and $\bar{b}(x,t)$ is done in order to show the effect of the amplitude of the perturbation ($\bar{a}(x,t)$) on the controller on the system accuracy and the average value of α. The bounds of these functions are (see Figure 2.2)

$$a_M = 10, \quad b_m = 0.98 \text{ and } b_M = 1.02$$

■

The gain of the controllers is stated as $k = 12$: condition (2.7) is satisfied. The parameters for the proposed controller (2.15)-(2.16) are set as follows

$$\beta = 2 \text{ and } \varepsilon = 5 \cdot 10^{-3}$$

whereas the parameter δ for the saturation function is taken equal to $5 \cdot 10^{-3}$. The choice of δ, ε and β is made such that the saturation function and the proposed controller (2.15)-(2.16) have the same theoretical domain of convergence (see (2.18) and (2.23)). This choice also ensures good performances for both controllers.

2.5.2 Results

The results are shown in Figures 2.3, 2.4, 2.5, and some indicators are presented in Table 2.1.

For controller (2.15)-(2.16), ($\alpha = 0$) is initially applied. When the system converges ($t \simeq 0.08\,s$), the variation of α starts (see Figures 2.3 and 2.5). The phase after the convergence of σ to a vicinity of the origin will be called the steady state. Effective analysis of the performances is achieved on the intervals $t \in [1, 5]$ and $t \in [6, 10]$, when the shape of $\bar{a}(x, t)$ is the same but with a different amplitude (see (2.24)).

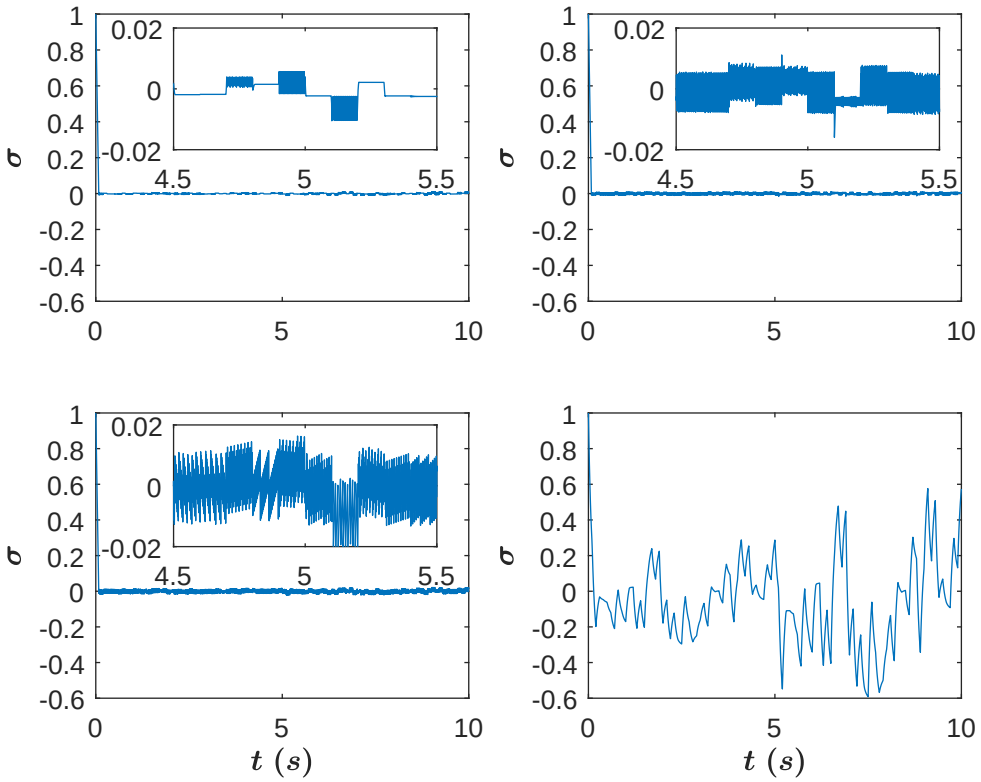

Figure 2.3 – σ versus time (s) **Top-left:** controller (2.15)-(2.16); **Top-right:** saturation function; **Bottom-left:** FOSMC; **Bottom-right:** FOLST.

The energy consumed is much less with controller (2.15)-(2.16) than with the FOSMC (see Table 2.1). Note also that the energy consumed by controller (2.15)-(2.16) and FOLSF are of the same order (see $\mathcal{E}$ in Table 2.1). The average accuracy of $|\sigma|$ (see $mean(|\sigma|)$ in Table 2.1) with controller (2.15)-(2.16) is better than that of all controllers. This better accuracy with respect to the FOSMC is mainly due to the attenuation of the chattering effect.
The indicator used to quantify the chattering effect is the function var defined as

$$var_{[\zeta_1,\zeta_2]}(h) = \sum_{i=0}^{N-1} |h(t_{i+1}) - h(t_i)| \tag{2.25}$$

where h is a real valued function and the set of instants $\{t_0, t_1, \cdots, t_N\}$ is a partition of $[\zeta_1, \zeta_2]$. $var(u)$ of controller (2.15)-(2.16) is significantly less than that of the FOSMC and saturation function but greater than that of the FOLSF (see Table 2.1). This means that controller (2.15)-(2.16) induces significantly less chattering than the FOSMC and saturation function but more than the FOLSF (see Figure 2.4). Less oscillations for controller (2.15)-(2.16) with respect to FOSMC and saturation function are also manifested in Figure 2.3.
When the amplitude of the perturbation/uncertainty $\bar{a}(x, t)$ is high ($5\,s < t < 10\,s$) the average value of α with the proposed controller is lower than when $\bar{a}(x, t)$ is low

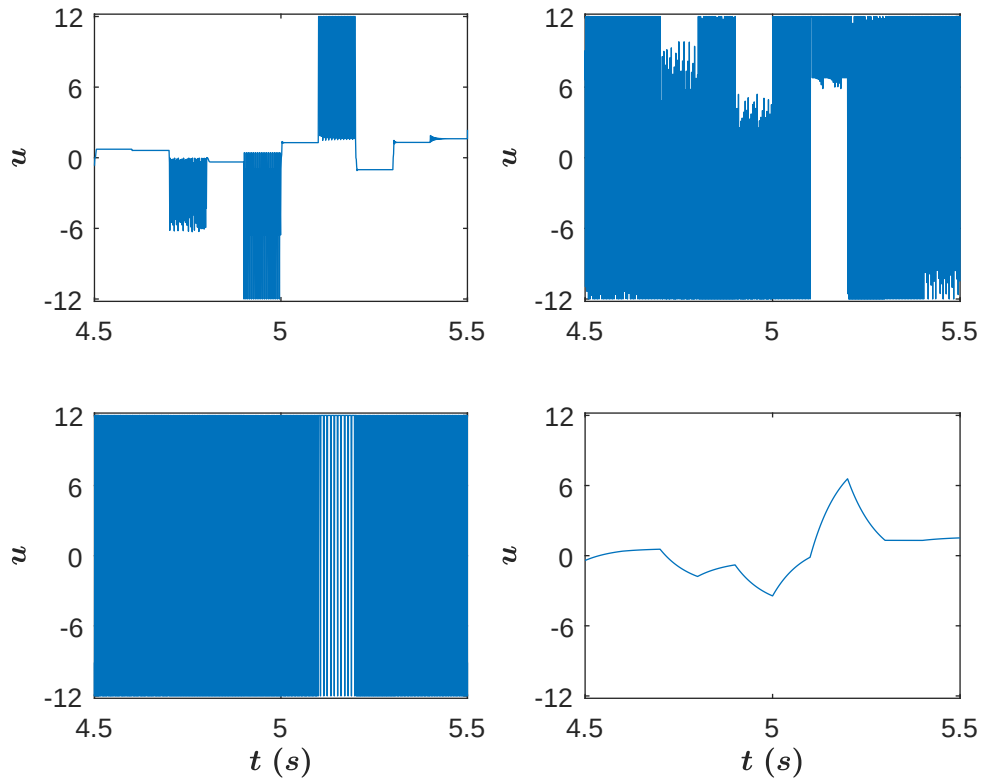

Figure 2.4 – Control input u versus time (s) $(4.5 < t < 5.5)$ **Top-left:** controller (2.15)-(2.16); **Top-right:** saturation function; **Bottom-left:** FOSMC; **Bottom-right:** FOLST.

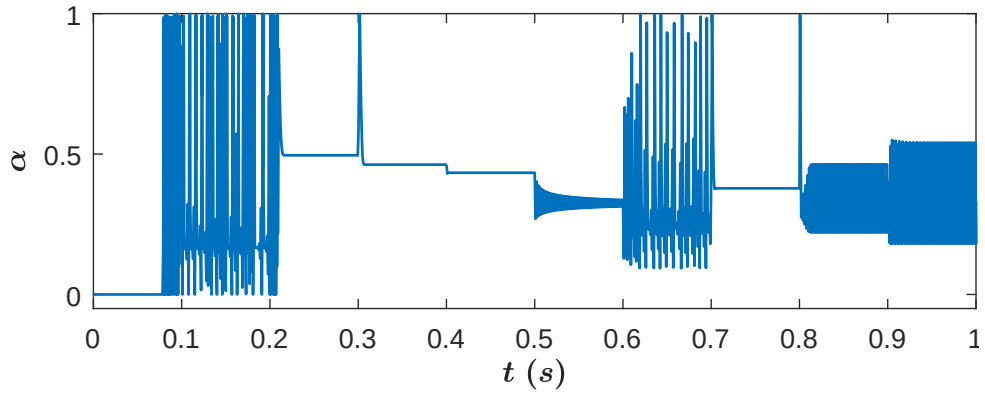

Figure 2.5 – Variable α versus time $(s)(0 < t < 1)$.

$(0\,s < t < 5\,s)$ (see α in Table 2.1). This is due to the fact that a stronger robustness is required to constrain the trajectories to a vicinity of the origin. Notice also the increase in the energy consumption as a result (see $\mathcal{E}$ in Table 2.1): a greater control effort is needed to constrain the trajectories to a vicinity of the origin when the perturbations/uncertainties increase.

As for the comparison between controller (2.15)-(2.16) and the saturation function, it is seen that a more efficient trade-off between accuracy and energy consumption is obtained with the proposed controller. When $\bar{a}(x,t)$ is low $(0\,s < t < 5\,s)$, controller (2.15)-(2.16) has better accuracy with less energy consumption; when $\bar{a}(x,t)$ is high $(5\,s < t < 10\,s)$, both controllers have similar accuracy whereas the proposed controller is less energy consuming and with less chattering (see Table 2.1).

		Controller (2.15)-(2.16)	Saturation function	FOSMC ($\alpha = 0$)	FOLSF ($\alpha = 1$)
$1s < t < 5s$	Energy $\mathcal{E}$	50.28	424.52	576	12.28
	$mean(\lvert\sigma\rvert)$	$2.08 \cdot 10^{-3}$	$2.82 \cdot 10^{-3}$	$4.48 \cdot 10^{-3}$	$1.21 \cdot 10^{-1}$
	$var(u)$	$1.10 \cdot 10^{4}$	$7.76 \cdot 10^{4}$	$7.95 \cdot 10^{4}$	72.18
	$mean(\alpha)$	0.44			
$6s < t < 10s$	Energy $\mathcal{E}$	164.44	388.96	576	49.24
	$mean(\lvert\sigma\rvert)$	$3.09 \cdot 10^{-3}$	$3.12 \cdot 10^{-3}$	$5.80 \cdot 10^{-3}$	$2.41 \cdot 10^{-1}$
	$var(u)$	$2.10 \cdot 10^{4}$	$6.13 \cdot 10^{4}$	$6.3 \cdot 10^{4}$	144.37
	$mean(\alpha)$	0.33			

Table 2.1 – Energy consumption, average accuracy on σ, $var(u)$ and average value of α in steady state with controller Controller (2.15)-(2.16), Saturation function, FOSMC and FOLSF for $1s < t < 5s$ and $6s < t < 10s$.

2.6 Conclusion

The main contributions of this chapter can be summarized as follows:

- a new controller for system whose relative degree is equal to 1 is proposed: it allows high accuracy and low energy consumption. This is done by varying a parameter α.
- The stability of the system controlled by the later is proved and the convergence domain size is given.
- The effectiveness of the proposed controller is shown via simulations and its performances in controlling an uncertain/perturbed system are compared to those of the FOSMC, FOLSF and saturation function. It allows high accuracy tracking with reduced chattering and energy consumption.

3

Controller balancing between TWC and SOLSF

Contents

3.1 Introduction

In the previous chapter, a controller for systems with relative degree 1 balancing between the FOSMC and FOLSF has been presented. In this chapter, this result is extended to systems with relative degree 2. [1]
Therefore, the main objective of this chapter is to control a second order system under unknown but bounded matching uncertainties/perturbations. The twisting controller (TWC) [1] is one of the most popular second order sliding mode controller designed to control such systems and known for its accuracy and robustness. However, the chattering

1. If the sliding variable is defined such the system admits a relative degree equal to 1, the results developed in the sequel can be used by considering that the developed controllers in this chapter are applied on $\dot{u}$.

phenomenon makes the controller high energy consuming. Another control solution consists in using a second order linear state feedback (SOLSF). This controller is smooth and low energy consuming; however, the closed loop system accuracy can be low in the presence of uncertainties/perturbations.
The proposed controllers in this chapter have the advantages of both the TWC and the SOLSF. Similarly to the controller proposed in the previous chapter, the proposed solutions are made possible by varying an exponent term of a well known controller proposed in [51],[52]. This parameter α evolves between 0 and 1, this evolution being based on the accuracy of the closed loop system. Three adaptation approaches are proposed:

- switching approach: α switches between 0 and 1, the switching being based on the closed loop system accuracy;
- dynamic approach: the accuracy of the closed loop system acts on the dynamics of α;
- algebraic approach: the accuracy of the closed loop system directly acts on the value of α.

In the ideal case (infinite sampling frequency of controllers), the TWC allows the establishment of an "ideal" second order sliding mode *i.e.* the sliding variable and its first time derivative converge to 0 in finite time. However, application of control law to a real system is made thanks to a finite sampling frequency and no result is nowadays existing on the convergence domain of the closed-loop system controlled by TWC. It has been established that, in case of non-zero sampling period, "real" second order sliding mode [1] is established but no accurate definition of the convergence domain has been already given. In the sequel, a convergence domain size of the sampled TWC controller is formally determined. This is performed thanks to the original formalism which rewrites the TWC in a so-called switching gain form [2].
A second motivation for this work is that it allows a more efficient parameter tuning of the proposed controllers in this chapter for experimental applications. In fact, as it will be seen in the sequel, if the proposed controllers' parameters are set very small with respect to the TWC convergence domain, one risks to obtain the TWC all the time and no variation of α occurs.

3.2 Problem Statement

Consider the following system

$$\begin{aligned} \dot{x} &= f(x,t) + g(x,t)u \\ \sigma &= \sigma(x,t) \end{aligned} \tag{3.1}$$

with $x \in \mathcal{X} \subset \mathbb{R}^n$ the state vector, $u \in \mathcal{U} \subset \mathbb{R}$ the control input (with $\mathcal{X}$ and $\mathcal{U}$ being bounded open subsets of $\mathbb{R}^n$ and $\mathbb{R}$ respectively), f and g sufficiently differentiable uncertain functions and σ the sliding variable. The control objective is to constrain the trajectories of system (3.1) such that, in spite of the perturbations and uncertainties, σ is evolving in a vicinity of the origin in a finite time. Assume that

Assumption 3.1. *The relative degree of (3.1) is equal to 2, i.e.*

$$\ddot{\sigma} = \bar{a}(x,t) + \bar{b}(x,t)u \tag{3.2}$$

■

Assumption 3.2. *$\bar{a}(x,t)$ and $\bar{b}(x,t)$ are unknown but bounded functions such that there exist positive constants a_M, b_m and b_M such that $\forall x \in \mathcal{X}, t \geq 0$ one has*

$$|\bar{a}(x,t)| \leq a_M, \quad 0 < b_m \leq \bar{b}(x,t) \leq b_M. \tag{3.3}$$

■

Assumption 3.3. *The internal dynamics of the system (3.1) are bounded.*

■

Then, the control problem of system (3.1) with respect to σ is equivalent to the stabilization in a finite time of the system

$$\begin{aligned} \dot{z}_1 &= z_2 \\ \dot{z}_2 &= \bar{a}(x,t) + \bar{b}(x,t)u \end{aligned} \tag{3.4}$$

with $z_1 = \sigma$ and $z_2 = \dot{\sigma}$. A control solution stabilizing (3.4) to a vicinity of the origin reads as [51][52]

$$u = -k_1 \lceil z_1 \rfloor^{\frac{\alpha}{2-\alpha}} - k_2 \lceil z_2 \rfloor^{\alpha} \tag{3.5}$$

where k_1, k_2 are positive gains fulfilling some condition given in the sequel and α is a constant such that $\alpha \in [0,1]$. When $\alpha = 1$, a SOLSF is obtained , *i.e.*

$$u = -k_1 z_1 - k_2 z_2 \tag{3.6}$$

where z_1 and z_2 are bounded for $k_1, k_2 > 0$. When $\alpha = 0$, the TWC is obtained [1], *i.e.*

$$u = -k_1 \text{ sign}(z_1) - k_2 \text{ sign}(z_2). \tag{3.7}$$

With this latter controller, a second order sliding mode versus z_1 is established *i.e.* the system trajectory converges in a finite to $\mathcal{S}^2$ defined as

$$\mathcal{S}^2 = \{x \in \mathcal{X} \,|\, z_1 = z_2 = 0\} \tag{3.8}$$

if the gains k_1 and k_2 are tuned such that [1]

$$\begin{aligned} k_1 > k_2 > 0, \quad (k_1 - k_2)b_m > a_M, \\ (k_1 + k_2)b_m - a_M > (k_1 - k_2)b_M + a_M. \end{aligned} \tag{3.9}$$

In case of a sampled controller (with T_e the sampling period), the system trajectory converges to

$$\mathcal{S}^2_{real} = \{x \in \mathcal{X} \,|\, |z_1| \leq \mu_1 T_e^2, |z_2| < \mu_2 T_e\} \tag{3.10}$$

where μ_1 and μ_2 are positive constants. The behavior of (3.4) on $\mathcal{S}^2_{real}$ is called real second order sliding mode [1].

The parameter α in (3.5) can take any value between 0 and 1. Note that, for a value of α, the stability of (3.4) to a vicinity of the origin is ensured when $k_1, k_2 > 0$. In the sequel, a discussion on the accuracy (that is an image of the robustness) and energy consumption obtained for different constant values of α, is made.

3.3 Accuracy and energy consumption

Similarly to Section 2.2.1, for a sake of clarity, no uncertainty on the control term is considered ($b_m = b_M = 1$) and $\bar{a}(x,t)$ is taken constant and positive, $\bar{a}(x,t) = \mathcal{A}$. When controller (3.5) is applied to system (3.4), the equilibrium point is calculated by setting $\dot{z}_1 = \dot{z}_2 = 0$ that gives

$$z_1 \to \left(\frac{\mathcal{A}}{k_1}\right)^{\frac{2-\alpha}{\alpha}}. \tag{3.11}$$

Suppose that k_1 and k_2 are tuned as (3.9), therefore $\frac{\mathcal{A}}{k_1} < 1$. Hence, as α decreases, the accuracy of the closed loop system increases tending towards zero when $\alpha \to 0$; that is consistent with the fact that, when the TWC is applied ($\alpha = 0$), z_1 and z_2 converge to 0 in a finite time, the worst accuracy being when the SOLSF is applied ($\alpha = 1$)

$$z_1 \to \frac{\mathcal{A}}{k_1}. \tag{3.12}$$

Consider controller (3.5) applied to system (3.4) and suppose that $|z_1| < 1$ and $|z_2| < 1$ [2]. Then, $\forall \alpha_1, \alpha_2 \in]0,1[$ if $\alpha_1 < \alpha_2$, one has

$$\begin{aligned} &\left| -k_1|z_1|^{\frac{\alpha_1}{2-\alpha_1}}\text{sign}(z_1) - k_2|z_2|^{\alpha_1}\text{sign}(z_2)\right| > \\ &\qquad \left| -k_1|z_1|^{\frac{\alpha_2}{2-\alpha_2}}\text{sign}(z_1) - k_2|z_2|^{\alpha_2}\text{sign}(z_2)\right| \end{aligned} \tag{3.13}$$

where the right hand side (*resp.* the left hand side) of the inequality is the control input u of (3.5) in absolute value for $\alpha = \alpha_1$ (*resp.* $\alpha = \alpha_2$). Hence, for same values of z_1 and z_2, the control effort increases when α decreases.
However, due to the nonlinearity of the system, one cannot be sure that the system follows the same trajectory for different values of α; then, it is not guaranteed that (3.13) holds. Nevertheless, the trend is visible via simulations where the linear state feedback has the lowest energy consumption in the steady state.

Based on this discussion, three new controllers based on (3.5) stabilizing system (3.4) and having a time-varying parameter α are proposed with both the advantages of the SOLSF (low energy consumption) and the TWC (robustness and accuracy). This is achieved by making the exponent parameter α of controller (3.5) varying with respect to z_1 and z_2. Three different variation laws of α are considered: switching, dynamic and algebraic. In the sequel, a formalization of these variation laws are detailed and the stability of the closed loop system for each case is proved.

3.4 Switching approach for α

Based on the two controllers explored above, a new control strategy is proposed in the sequel that is a trade-off between the SOLSF and the TWC. The objective is to get a reduced energy consuming controller with high accuracy.

2. Given that k_1 and k_2 are tuned as (3.9), then following (3.11), it is not restrictive to consider $|z_1| < 1$ and $|z_2| < 1$ in the steady state.

The proposed controller is written in the form of the controller proposed in [51] [52]

$$u = -k_1 \lceil z_1 \rfloor^{\frac{\alpha}{2-\alpha}} - k_2 \lceil z_2 \rfloor^{\alpha} \tag{3.14}$$

with k_1 and k_2 tuned as (3.9); the exponent $\alpha \in \{0, 1\}$ is switching between 0 and 1 thanks to the following switching law (the notation $\wedge$ is used for the logical AND operator)

$$\alpha = \begin{cases} 1 & \text{if } |z_1| < \varepsilon_{s,z_1} \wedge |z_2| < \varepsilon_{s,z_2} \\ 0 & \text{otherwise} \end{cases} \tag{3.15}$$

where ε_{s,z_1} and ε_{s,z_2} are positive constants set by the user.

If the trajectories of the system are inside $\mathcal{D}_s$ defined as

$$\mathcal{D}_s = \{(z_1, z_2) \in \mathcal{Z} \mid |z_1| < \varepsilon_{s,z_1} \wedge |z_2| < \varepsilon_{s,z_2}\}, \tag{3.16}$$

the desired accuracy of the system is reached; therefore, the SOLSF ($\alpha = 1$) is applied to decrease the energy consumption. If the trajectories of the system are outside $\mathcal{D}_s$, it means that the desired accuracy is not reached probably due to perturbations and uncertainties. Hence, the TWC ($\alpha = 0$) is applied in order to force the trajectories back to $\mathcal{D}_s$.

Parameters tuning

- Since the proposed controller switches between the SOLSF and the TWC, the gains k_1 and k_2 have to be tuned to converge for both algorithms. Hence, the gains should satisfy (3.9).
- ε_{s,z_1} and ε_{s,z_2} influence the accuracy of the controller. Decreasing them increases the accuracy of the closed loop system.
- However, the remark of the previous item means that the TWC is applied for longer and therefore the energy consumption of the controller is increased.
- Hence, ε_{s,z_1} and ε_{s,z_2} should be chosen wisely as to give a trade-off between accuracy and energy consumption. This trade-off can depend on the specifications expected for the closed-loop system.
- A key point of this new control strategy is that its energy consumption is less than that of the TWC. Therefore, when the proposed controller behaves as a SOLSF, its maximal energy consumption should be less than the minimum energy consumption of the TWC algorithm. Hence, ε_{s,z_1} and ε_{s,z_2} should satisfy the following condition:

  $$k_1 \varepsilon_{s,z_1} + k_2 \varepsilon_{s,z_2} < k_1 - k_2 \tag{3.17}$$

  Note that the left hand side of the inequality is the maximal control effort (in absolute value) of the SOLSF (knowing that the linear state feedback is only applied in $\mathcal{D}_s$) and the right hand side of the inequality is the minimal control effort (in absolute value) of the TWC.
- Note that by a practical point of view, the TWC forces the trajectories to reach $\mathcal{S}_r^2$ (3.10). Hence, the tuning of ε_{s,z_1}, ε_{s,z_2} and β should take this fact into account in order to obtain an efficient trade-off between TWC and SOLSF. It will be further analyzed in Section 3.7.

■

Theorem 3.1. *[42] Consider system (3.1) where $\sigma-$dynamics read as (3.2) with Assumptions 3.1-3.3 satisfied and controlled by (3.14)-(3.15). If k_1 and k_2 are tuned as in (3.9), then there exist positive parameters ε_{s,z_1} and ε_{s,z_2} satisfying (3.17) such that the trajectories of system (3.1) converge, in a finite time, to*

$$\mathcal{B}_s = \{x \in \mathcal{X} || z_1| < \frac{\varepsilon_{s,z_2}^2}{2K_M^{min}} + \varepsilon_{s,z_1}, \quad |z_2| < \sqrt{\varepsilon_{s,z_2}^2 + 2K_m^{max}\varepsilon_{s,z_1}}\} \tag{3.18}$$

with

$$\begin{aligned} K_m^{max} &= b_M(k_1 - k_2) + a_M, \\ K_M^{min} &= b_m(k_1 + k_2) - a_M. \end{aligned} \tag{3.19}$$

Proof: First-of-all, suppose that the trajectory of the system in the phase plan (z_1, z_2) is initially outside $\mathcal{D}_s$: therefore, the TWC is applied. As mentioned in Section 3.2, given that k_1 and k_2 fulfill (3.9), the system trajectory converges in a finite time towards the origin (3.8). Therefore, it is guaranteed that the system trajectory converges to $\mathcal{D}_s$ in a finite time (see curve $O - P$ in Figure 3.1).
Once that occurs, given switching law (3.15) the SOLSF is applied; as a consequence, the trajectory of the system may potentially leave $\mathcal{D}_s$ due to perturbations and uncertainties. This case can be divided into 4 potential cases (see Figure 3.1)

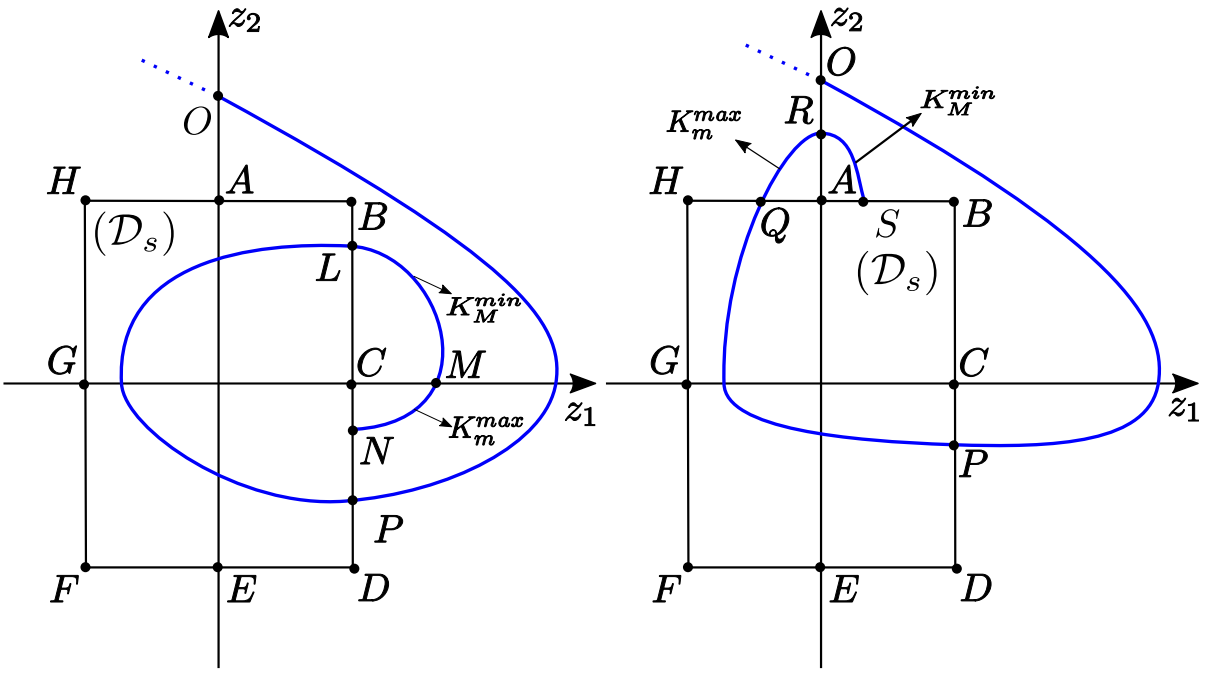

(a) Case 3 (b) Case 4

Figure 3.1 – Description of the system trajectory in the phase plan (z_1, z_2) when controller (3.14)-(3.15) is applied to system (3.4).

Case 1. the trajectory of the system leaves $\mathcal{D}_s$ through $[AB]$ or $[FE]$;
Case 2. the trajectory of the system leaves $\mathcal{D}_s$ through $[CD]$ or $[GH]$;
Case 3. the trajectory of the system leaves $\mathcal{D}_s$ through $[BC]$ or $[FG]$;

Case 4. the trajectory of the system leaves $\mathcal{D}_s$ through $[HA]$ or $[ED]$.

In the sequel, for each case, the convergence boundaries of z_1 and z_2 are given.

Case 1. The trajectory of the system cannot leave $\mathcal{D}_s$ crossing $[AB]$ (*resp.* $[FE]$, see Figure 3.1) since the TWC guarantees that $\dot{z}_2 < 0$ (*resp.* $\dot{z}_2 > 0$); therefore z_2 cannot increase (*resp.* decrease). ■

Case 2. Since $z_2 < 0$ (*resp.* $z_2 > 0$) along $[CD]$ (*resp.* $[GH]$, see Figure 3.1), then z_1 is decreasing (*resp.* z_1 is increasing). Hence, the trajectories of the system cannot leave $\mathcal{D}_s$ crossing $[CD]$ (*resp.* $[GH]$). ■

Case 3. Considering the worst case, $\dot{z}_2 = -K_M^{min}$: it gives the most external trajectory obtained from a point L on $[BC]$ (see L in Figure 3.1a) where K_M^{min} is the minimal possible variation of z_2 in absolute value when the large gain of the TWC is applied. The expression of $z_1(M)$ [3], with $z_2(M) = 0$, is given by

$$z_1(M) = \frac{z_2^2(L)}{2K_M^{min}} + \varepsilon_{s,z_1}. \tag{3.20}$$

Therefore, the worst case is when $z_2(L)$ is maximal, *i.e.* point L coincides with B. So, equation (3.20) becomes

$$z_1(M) = \frac{\varepsilon_{z_2}^2}{2K_M^{min}} + \varepsilon_{s,z_1} \tag{3.21}$$

The objective is now to prove that the trajectory enters $\mathcal{D}_s$ crossing $[CD]$. This is done by calculating $z_2(N)$, with the point N such that $z_1(N) = \varepsilon_{s,z_1}$. Now, the worst case is $\dot{z}_2 = -K_m^{max}$ giving the farthest trajectory from the origin. K_m^{max} is the maximal variation of z_2 in absolute value when the small gain of the TWC is applied. The expression of $z_2(N)$ is given by

$$z_2(N) = -\varepsilon_{s,z_2}\sqrt{\frac{K_m^{max}}{K_M^{min}}}. \tag{3.22}$$

From (3.9), it is obvious that $\frac{K_m^{max}}{K_M^{min}} < 1$; therefore, $z_2(N) < -\varepsilon_{s,z_2}$. Hence, the trajectory of the system enters $\mathcal{D}_s$ through $[CD]$.
Finally, one concludes that if the trajectories of the system leave $\mathcal{D}_s$ through $[BC]$, then

$$\begin{aligned} |z_1| &< \frac{\varepsilon_{s,z_2}^2}{2K_M^{min}} + \varepsilon_{s,z_1} \\ |z_2| &< \varepsilon_{s,z_2} \end{aligned} \tag{3.23}$$

and the trajectory reaches again the domain $\mathcal{D}_s$. Due to symmetry, the same bounds are obtained if the trajectory leaves $\mathcal{D}_s$ through $[FG]$. ■

Case 4. Considering the worst case, $\dot{z}_2 = K_m^{max}$ gives the most external trajectory obtained from a random point Q on $[HA]$ (see Q in Figure 3.1b). The expression of $z_2(R)$, R being such that $z_1(R) = 0$, is given by

$$z_2(R) = \sqrt{\varepsilon_{s,z_2}^2 + 2K_m^{max} z_1(Q)}. \tag{3.24}$$

3. With abuse of notation, $z_1(M)$ is the z_1-coordinate of point M. The notation will be used for other points and z_2 in the sequel.

Therefore, the worst case is obtained when $z_1(Q)$ is maximal and hence point Q coincides with H. Therefore, equation (3.24) becomes

$$z_2(R) = \sqrt{\varepsilon_{s,z_2}^2 + 2K_m^{max}\varepsilon_{s,z_1}}. \tag{3.25}$$

The objective is now to prove that the trajectory enters $\mathcal{D}_s$ crossing $[EF]$. This is done by calculating $z_1(S)$, S being such that $z_2(S) = \varepsilon_{s,z_2}$. Now, the worst case is $\dot{z}_2 = -K_M^{min}$ giving the farthest trajectory from the origin. The expression of $z_1(S)$ is given by

$$z_1(S) = \varepsilon_{s,z_1}\sqrt{\frac{K_m^{max}}{K_M^{min}}}. \tag{3.26}$$

From (3.9), one deduces that $z_1(S) < \varepsilon_{s,z_1}$. Hence the trajectory of the system enters $\mathcal{D}_s$ through $[AB]$.
Finally, one concludes that, if the trajectories of the system leave $\mathcal{D}_s$ through $[HA]$ or $[ED]$ (due to symmetry), then one gets

$$\begin{aligned} |z_1| &< \varepsilon_{s,z_1} \\ |z_2| &< \sqrt{\varepsilon_{s,z_2}^2 + 2K_m^{max}\varepsilon_{s,z_1}}. \end{aligned} \tag{3.27}$$

■

Therefore, by combining the 4 latter cases, the ultimate convergence boundary of the trajectories of the system is given by

$$\begin{aligned} |z_1| &< \frac{\varepsilon_{s,z_2}^2}{2K_M^{min}} + \varepsilon_{s,z_1} \\ |z_2| &< \sqrt{\varepsilon_{s,z_2}^2 + 2K_m^{max}\varepsilon_{s,z_1}} \end{aligned}$$

This concludes the proof. ■

3.5 Dynamic approach for α

In the case of a switching approach for α, the potential of the α-variation process is not fully exploited. With a switching$-\alpha$ approach, when the required accuracy is lost, the TWC ($\alpha = 0$) is applied to increase the robustness again. However, the worst case for the uncertainties/perturbation is not always present: therefore, $\alpha = 0$ is not always required to obtain the required accuracy. Intermediate values of α (between 0 and 1) could provide both required robustness and accuracy. As discussed in Section 3.2, $\alpha \neq 0$ leads to a lower energy consumption and a smoother controller. This discussion is the motivation of the controller described in the sequel.

The proposed controller reads as

$$u = -k_1 \lceil z_1 \rfloor^{\frac{\alpha}{2-\alpha}} - k_2 \lceil z_2 \rfloor^{\alpha} \tag{3.28}$$

with k_1 and k_2 tuned as in (3.9) and $\alpha \in [0, 1]$. Define γ as

$$\gamma = \kappa(-1 + \text{sign}(\varepsilon_{d,z_1} - |z_1|) + \text{sign}(\varepsilon_{d,z_2} - |z_2|)). \tag{3.29}$$

and the dynamic adaptation law of α as

$$\dot{\alpha} = \begin{cases} -1 & \text{if } \gamma > 0 \wedge \alpha \geq 1 \quad (3.30a) \\ 1 & \text{if } \gamma < 0 \wedge \alpha \leq 0 \quad (3.30b) \\ \gamma & \text{otherwise} \quad (3.30c) \end{cases}$$

with $\alpha(0) = 0$, κ, ε_{d,z_1} and ε_{d,z_2} being positive constants.

Then, the adaptation law of α is defined via three equations

(3.30a) the objective is to avoid α increasing beyond 1;

(3.30b) the objective is to avoid α decreasing below 0;

(3.30c) the adaptation is effective and detailed in the sequel.

Note that in (3.30a) and (3.30b) there is formally no adaptation. Both cases imply that conditions are fulfilled to continuously apply either TWC or SOLSF.

In this adaptation algorithm, z_1 and z_2 act on the dynamics of α and the logic of (3.30c) reads as follows. When the trajectory of the system is inside $\mathcal{D}_d$ defined by

$$\mathcal{D}_d = \{(z_1, z_2) \mid |z_1| \leq \varepsilon_{d,z_1} \wedge |z_2| \leq \varepsilon_{d,z_2}\}, \tag{3.31}$$

then the required accuracy of the closed-loop system is reached: $\gamma = k$ and the value of α is increasing in order to reduce the energy consumption. If z_1 or z_2 is outside $]-\varepsilon_{d,z_1}, \varepsilon_{d,z_1}[$ or $]-\varepsilon_{d,z_2}, \varepsilon_{d,z_2}[$ respectively, it means that the desired accuracy is not reached: $\gamma = -\kappa$ and α is decreasing towards zero in order to increase the accuracy of the system. If both z_1 and z_2 are outside of their target intervals, therefore the rate by which α decreases towards zero is three times faster ($\gamma = -3k$) in order to improve the accuracy faster.
Notice that α does not necessarily have to go to 0 to get the required robustness. Consider the case where the trajectory is outside $\mathcal{D}_d$. Then, α decreases following (3.30). However, the trajectory could enter $\mathcal{D}_d$ again before α reaches 0. Indeed, it depends on the uncertainties/perturbations acting on the system. Given that the uncertainties/perturbations are not always in the so-called worst case, then $\alpha \in]0, 1[$ could provide the required robustness to bring the trajectory back to $\mathcal{D}_d$.

Parameters tuning.

- The gains k_1 and k_2 have to be tuned to ensure the stability of the closed loop system $\forall \alpha \in [0, 1]$. Therefore, the gains must satisfy (3.9).
- As in the switching approach (Section 3.4), ε_{d,z_1} and ε_{d,z_2} are also linked to the obtained accuracy by the controller. They are tuned to get the required trade-off between the TWC and SOLSF.

- κ defines the rate by which α increases or decreases. Increasing κ leads to a faster reactivity of the controller to uncertainties/perturbations and vise-versa. Note that if $\kappa \to \infty$, then this controller has the same behavior than controller (3.14)-(3.15) (switching$-\alpha$ approach).

■

Theorem 3.2. *[44] Consider system (3.1) where $\sigma-$dynamics reads as (3.2) with Assumptions 3.1-3.3 fulfilled and controlled by (3.28)-(3.30). If k_1 and k_2 are tuned as in (3.9), then there exist positive parameters κ, ε_{d,z_1} and ε_{d,z_2} satisfying (3.17) such that the trajectories of system (3.1) converge, in a finite time, to a vicinity of the origin.*

Proof: Initially, the TWC is applied ($\alpha(0) = 0$). As mentioned in Section 3.2, the system trajectories converge in a finite time towards the origin (see (3.8)). Therefore, it is guaranteed that the system trajectories converge to $\mathcal{D}_d$ in a finite time (trajectory between L and M in Fig. 3.2). Then, following the adaptation law (3.30), the value of α increases in order to reduce the energy consumption; unfortunately, it makes the controller less robust. By a general point-of-view, uncertainties/perturbations could make the trajectory of the system leave $\mathcal{D}_d$ (point M to point N). Therefore, α decreases again making the controller more robust: as a consequence, the trajectory comes back to $\mathcal{D}_d$ (point N to point O) and so on.
When the trajectory of the system potentially goes out from $\mathcal{D}_d$ due to uncertainties/perturbations, one can be sure that it will converge back to it in finite time. Consider the system under the worst case of uncertainties/perturbations (see Assumption 3.2). Then, α should decrease to 0 to provide the required robustness, bringing the trajectory of the system back to $\mathcal{D}_d$. This happens in finite time ($\leq \frac{1}{\kappa}\, sec$): the worst case is when α should decrease from 1 to 0. When the TWC is applied ($\alpha = 0$), the trajectory converges to $\mathcal{D}_d$ in finite time too. ■
Notice also that the greater the value of κ, the faster the trajectory convergence.

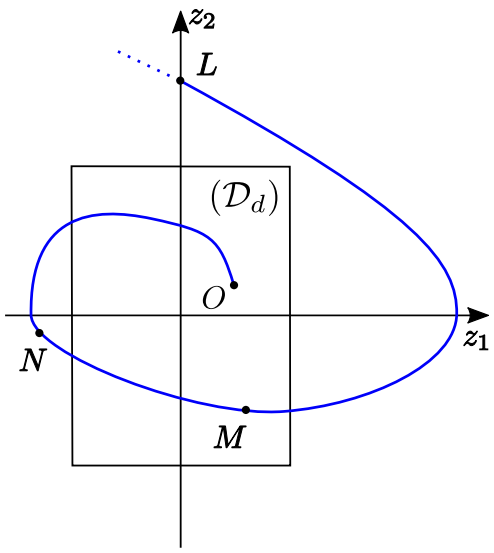

Figure 3.2 – Example of a trajectory of the system in the phase plan (z_1, z_2) when controller (3.28)-(3.30) is applied to system (3.1).

3.6 Algebraic approach for α

In order to get a better performance and a smoother control, a controller with α dynamically varying has been proposed in the previous section. However, it has not been possible to formally determine the convergence domain and the variation of α depends on its initial condition. In this section, the variation law of α is modified by proposing a controller for which α algebraically varies between 0 and 1 with respect to z_1 and z_2. This fact means that α has similar dynamics to the system. Unlike controller (3.28)-(3.30), the convergence domain can be determined; furthermore, given the algebraic nature of the controller, no initial condition for α is required.

The proposed controller reads as

$$u = -k_1 \lceil z_1 \rfloor^{\frac{\alpha}{2-\alpha}} - k_2 \lceil z_2 \rfloor^{\alpha} \tag{3.32}$$

with k_1 and k_2 tuned as (3.9) and $\alpha \in [0, 1]$. The exponent parameter α is defined by the algebraic law

$$\alpha = \max(-\beta(\frac{|z_1|}{|z_1| + \varepsilon_{a,z_1}} + \frac{|z_2|}{|z_2| + \varepsilon_{a,z_2}}) + 1\,,\, 0) \tag{3.33}$$

with $\beta > 1$ and $\varepsilon_{a,z_1}, \varepsilon_{a,z_2} > 0$.

The logic of the algebraic law can be summarized as follows: when $|z_1|$ or $|z_2|$ increase, it means that the accuracy of the closed loop system is reduced. Therefore, the value of α automatically decreases in order to improve the robustness of the system and then, the accuracy again. On the other hand, when the accuracy of the system is improved ($|z_1|$ and $|z_2|$ decrease), the value of α automatically increases in order to reduce the energy consumption.

Parameters tuning.

- Notice that α is restricted to the interval [0,1]. Therefore, the gains k_1 and k_2 should be tuned as (3.9) to ensure the closed loop stability $\forall \alpha \in [0, 1]$;

- the accuracy of the controller depends on ε_{a,z_1}, ε_{a,z_2} and β. If β is increased or ε_{a,z_1} and ε_{a,z_2} are decreased, the accuracy of the closed loop system is improved;

- however, increasing β or decreasing ε_{a,z_1} and ε_{a,z_2} leads to lower average values of α, that induces a higher energy consumption. Then, these three parameters have to be wisely tuned to achieve the required trade-off between accuracy and energy consumption.

- in order to obtain a controller with a lower energy consumption than the TWC, $\varepsilon_{a,z_1}, \varepsilon_{a,z_2}$ and β should be tuned such that, if $z_1 > 1$ or $z_2 > 1$, α should be equal to 0. This is ensured by introducing the following condition on the parameters of α in (3.33)

$$k_1 \frac{\varepsilon_{a,z_1}}{\beta - 1} + k_2 \frac{\varepsilon_{a,z_2}}{\beta - 1} < k_1 + k_2 \tag{3.34}$$

Theorem 3.3. *[40] Consider system (3.1) where $\sigma-$dynamics read as (3.2) with Assumptions 3.1-3.3 satisfied and controlled by (3.32)-(3.33). With k_1 and k_2 tuned as (3.9), then there exist positive parameters ε_{a,z_1}, ε_{a,z_2} and β ($\beta > 1$) satisfying (3.34) such that $\forall x(0) \in \mathcal{X}$, the trajectories of system (3.1) converge in finite time to $\mathcal{B}_a$ defined as*

$$\begin{aligned}\mathcal{B}_a = \{x \in \mathcal{X} \mid |z_1| \leq \max(\frac{\varepsilon_{a,z_1}}{\beta-1}, \frac{\varepsilon_{a,z_2}^2}{2(\beta-1)^2 K_M^{min}}) \\ |z_2| \leq \max(\frac{\varepsilon_{a,z_2}}{\beta-1}, \sqrt{\frac{2K_m^{max}\varepsilon_{a,z_1}}{\beta-1}})\}\end{aligned} \tag{3.35}$$

The proof of Theorem 3.3 is detailed in Appendix A.

3.7 TWC convergence domain

By a practical point-of-view *i.e.* in the case of a sampled controller, the TWC ($\alpha = 0$) forces the trajectories to reach $\mathcal{S}^2_{real}$ (3.10). It means that, if one wants to get an efficient trade-off between accuracy and energy consumption, β, $\varepsilon_{\star,z_1}$ and $\varepsilon_{\star,z_2}$ with $\star = \{s, a\}$ must be tuned such that the convergence domain of the proposed controllers is greater than that of the TWC *i.e.* $\mathcal{S}^2_{real} \subset \mathcal{B}_\star$ [4] (see (3.18) and (3.35)). Otherwise, a risk is to have the TWC all the time and chattering is not reduced.
Hence, the purpose of this section is firstly to evaluate the convergence domain of the system trajectory when system (3.4) is controlled by a sampled TWC. This will be performed by considering the TWC written in its switching form [2]. Consequently, this result will be used to tune β, $\varepsilon_{\star,z_1}$ and $\varepsilon_{\star,z_2}$ such that $\mathcal{S}^2_{real} \subset \mathcal{B}_\star$.

Consider the following assumptions

Assumption 3.4. *The system trajectories are supposed to be infinitely extendible in time for any bounded Lebesgue measurable inputs.* ■

Assumption 3.5. *The controller is updated in discrete-time with a sampling period T_e. The control input u is constant between two successive sampling steps, i.e*

$$\forall t \in [\varsigma T_e,\ (\varsigma+1)T_e[\ \ u(t) = u(\varsigma T_e). \tag{3.36}$$

with $\varsigma \in \mathbb{N}$. ■

Then, the sampled TWC is written as

$$u(\varsigma T_e) = -k_1 \text{sign}\left(z_1(\varsigma T_e)\right) - k_2 \text{sign}\left(z_2(\varsigma T_e)\right). \tag{3.37}$$

3.7.1 Twisting control under switching gain form

Recall the switching gain control

$$u(\varsigma T_e) = \begin{cases} u_L(\varsigma T_e) = U(\varsigma T_e) & \text{if} \varsigma T_e \notin \mathcal{T}_\mathcal{H} \\ u_H(\varsigma T_e) = \varpi U(\varsigma T_e) & \text{if} \varsigma T_e \in \mathcal{T}_\mathcal{H} \end{cases} \tag{3.38}$$

4. Notice that the controller with the dynamic$-\alpha$ approach is not concerned in this discussion since its convergence domain has not been determined.

with $\varpi > 1$, $\varsigma \in \mathbb{N}$ and $\mathcal{T}_{\mathcal{H}}$ defining the time interval during which u_H is applied. In fact, the control input u can switch between two levels: a low level u_L and a high level u_H such that $|u_L| < |u_H|$.

The TWC can be reformulated by U defined as

$$U(\varsigma T_e) = -K_m \text{sign}(z_1(\varsigma T_e)) \tag{3.39}$$

with $K_m > 0$ and ϖ defined as

$$\begin{aligned} K_m &= k_1 - k_2 \\ \varpi &= (k_1 + k_2)/(k_1 - k_2), \end{aligned} \tag{3.40}$$

and with $\mathcal{T}_{\mathcal{H}}$ such that

$$\mathcal{T}_{\mathcal{H}} = \{\varsigma T_e \mid z_1 z_2 > 0\}. \tag{3.41}$$

The latter means that the high gain u_H is applied when $\text{sign}(z_1(\varsigma T_e)) = \text{sign}(z_2(\varsigma T_e))$. Then, the TWC written under the switching gain form is obtained and can be written as

$$u = \begin{cases} -K_m \text{sign}(z_1) & \text{if} z_1 z_2 \leq 0 \\ -\varpi K_m \text{sign}(z_1) & \text{if} z_1 z_2 > 0 \end{cases}. \tag{3.42}$$

Written under this form, it is clear that the amplitude of the input switches between four values $\pm(k_1 + k_2)$ and $\pm(k_1 - k_2)$ ($\pm K_m$ and $\pm\varpi K_m$) [5]. Following (3.9), K_m and ϖ are tuned as follows

$$K_m > \frac{a_M}{b_m}, \quad \varpi > 2 + \frac{b_M}{b_m}. \tag{3.43}$$

As discussed in Chapter 1, if system (3.4) is controlled by (3.38)-(3.39) with $\mathcal{T}_{\mathcal{H}}$ defined as (3.41) and K_m and ϖ tuned as (3.40), a real second order sliding mode with respect to z_1 is established after a finite time.

3.7.2 Determination of the convergence domain

The TWC has been rewritten in the switching gain form. Thanks to this original formalism, the convergence domain is derived and given by the following theorem.

5. There exist singularities when $z_1 = 0$ or $z_2 = 0$; notice that for a sampled application, it is not practically possible that both variables are exactly equal to zero. Then, these singularities are not considered here.

Theorem 3.4. *[45] Consider system (3.1) where $\sigma-$dynamics read as (3.2) under Assumptions 3.1-3.5 and controlled by (3.38)-(3.39) with $\mathcal{T}_{\mathcal{H}}$ defined as (3.41). Then, if K_m and ϖ are tuned as in (3.40), the trajectories of system (3.4) converge in a finite time to*

$$|z_1| \leq \Big(\varrho + \frac{K_m^{max}}{2} + \frac{\varrho^2}{2K_M^{min}}\Big)T_e^2 \tag{3.44}$$

and

$$|z_2| \leq \varrho T_e \tag{3.45}$$

where ϱ is the positive solution of the second order equation

$$(\frac{1}{K_m^{max}} - \frac{1}{K_M^{min}})\varrho^2 - 4\varrho + 2K_m^{max} = (\frac{1}{K_m^{max}} - \frac{1}{K_M^{max}})(K_M^{max})^2 \tag{3.46}$$

with

$$\begin{aligned} K_m^{max} &= \max(K_m^*) = b_M K_m + a_M \\ K_m^{min} &= \min(K_m^*) = b_m K_m - a_M \\ K_M^{max} &= \max(K_M^*) = \varpi b_M K_m + a_M \\ K_M^{min} &= \min(K_M^*) = \varpi b_m K_m - a_M. \end{aligned} \tag{3.47}$$

Proof. Define $u^*(t)$ as

$$u^*(t) = \begin{cases} -K_m^*(t) \cdot \text{sign}(z_1(\varsigma T_e)) \text{ if} \varsigma T_e \notin \mathcal{T}_{\mathcal{H}} \\ -K_M^*(t) \cdot \text{sign}(z_1(\varsigma T_e)) \text{ if} \varsigma T_e \in \mathcal{T}_{\mathcal{H}} \end{cases} \tag{3.48}$$

with K_m^* and K_M^* defined by

$$\begin{aligned} K_m^*(t) &= b(x,t)K_m - a(x,t)\text{sign}(z_1(kT_e)) \\ K_M^*(t) &= b(x,t)\varpi K_m - a(x,t)\text{sign}(z_1(kT_e)) \end{aligned} \tag{3.49}$$

Then, system (3.4) can be rewritten as

$$\begin{aligned} \dot{z}_1 &= z_2 \\ \dot{z}_2 &= u^* \end{aligned} \tag{3.50}$$

Define $t = t_i$ the instant at which the system trajectory crosses z_2-axis for the i^{th} time (with $z_1(t_i) = 0$), T_s^i the time at which the i^{th} z_1-sign switching is *detected*[6] and τ_i^d the duration of the detection, *i.e.*

$$\text{sign}(z_1(T_s^i)) \neq \text{sign}(z_1(T_s^i - T_e)) \tag{3.51}$$

and

$$\tau_i^d = T_s^i - t_i. \tag{3.52}$$

Recall τ_i as the duration of the large control input, *i.e.*

$$[T_s^i,\ T_s^i + \tau_i] = \left\{\varsigma T_e | T_s^i \leq \varsigma T_e \leq T_s^{i+1} \text{ and } u(\varsigma T_e) = u_H\right\}. \tag{3.53}$$

6. A time value with capital letter T_*^* represents a sampling time whereas a time value with letter t_*^* is an instant on continuous time.

It yields that this duration is a multiple of the sampling period, *i.e.* for $i > 0$,

$$\tau_i \;=\; \varsigma_i T_e < T_s^{i+1} - T_s^i \tag{3.54}$$

ς_i being defined such that

$$\text{sign}(z_2(T_s^i + \varsigma_i T_e)) \neq \text{sign}(z_2(T_s^i + (\varsigma_i - 1)T_e)) \; . \tag{3.55}$$

Suppose that the controller has been tuned in order to guanrantee the convergence of the trajectory towards a vicinity of the origin. As shown in Figure 3.3, the gain switching point for the TWC occurs when the system trajectory crosses z_2-axis and is detected, that can be done only at a sampling time that potentially induces a delay.

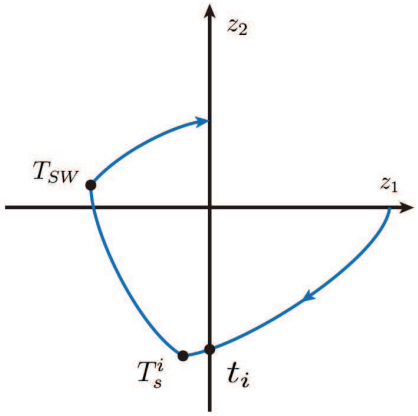

Figure 3.3 – TWC: trajectory in the (z_1, z_2)-phase plane.

Without loss of generality, suppose that at instant $t = t_i$, the system crosses z_2-axis for the i^{th} time, and at $t = T_s^i$ the i^{th} z_1-sign switching is detected. The delay of the detection between t_i and T_s^i is τ_i^d. As shown in (3.54)-(3.55), the large input u_H switches off just after the system trajectory crosses z_1-axis at instant $t = T_{SW}$.
If $z_2(t_i) < 0$, one has $z_2(T_{SW}) \geq 0$, otherwise $z_2(T_{SW}) \leq 0$ with $z_2(t_i) > 0$. It means that the length of the system trajectory projection on z_2-axis under large gain input is always larger than $|z_2(T_s^i)|$. It yields

$$\int_{T_s^i}^{T_s^i+\tau_i} K_M^*(t)\; \mathrm{d}t \geq |z_2(t_i)| + K_m^{max}\tau_i^d \; . \tag{3.56}$$

According to Theorem 1.1 (see Chapter 1 Section 1.3.2), it is clear that the first line of condition (1.46) is satisfied. On the other hand, one has

$$\int_{T_s^i}^{T_s^i+\tau_i} K_M^*(t)\; \mathrm{d}t \leq |z_2(T_s^i)| + |z_2(T_{SW})| \tag{3.57}$$

which leads to

$$\int_{T_s^i}^{T_s^i+\tau_i} K_M^*(t)\; \mathrm{d}t \leq |z_2(t_i)| + K_m^{max}\tau_i^d + |z_2(T_{SW})| \; . \tag{3.58}$$

Second line of condition (1.46) in Theorem 1.1 is fulfilled when $|z_2(T_{SW})| \leq \Delta'$.
Denote τ_{sw}^d the time delay to detect the i^{th} sign switching of z_2. So, one has $|z_2(T_{SW})| \leq K_M^{max}\tau_{sw}^d$.
According to Theorem 1.1, when $\Delta' \geq K_M^{max}\tau_{sw}^d$, the system trajectory will converge closer

to origin. If it is not the case, it means that the system trajectories have already reached the vicinity of zero. The system trajectories can no further converge to origin, when $\Delta' < K_M^{max}\tau_{sw}^d$. Therefore, the threshold value $K_M^{max}\tau_{sw}^d$ for Δ' enables to calculate the convergence domain. To this end, remark that the maximum value for the delay for a sign detection is T_e and suppose in the sequel $\tau_{sw}^d = T_e$ and $\tau_i^d = T_e$. Then, replacing Δ' by $K_M^{max}T_e$ into (1.48) and remarking that the maximum value of $|z_2|$ is obtained for $|z_2(T_s^i)| = |z_2(t_i)| + K_m^{max}T_e$, one gets, with (1.48) and (1.49), the final convergence domain (3.45) for z_2.
The maximum value of z_1 is obtained when the system crosses z_1-axis (just before instant T_{SW}) and the final convergence domain for z_1 is given by

$$|z_1| \leq |z_2(t_i)|T_e + K_m^{max}\frac{T_e^2}{2} + \frac{z_2^2(T_s^i)}{2K_M^{min}} \tag{3.59}$$

which leads to (3.44) thanks to (3.45). The establishment of real second order sliding mode is then proved *i.e.*

$$|z_1| \leq \mu_1 T_e^2, \qquad |z_2| \leq \mu_2 T_e \tag{3.60}$$

with $\mu_1 = \left(\varrho + \frac{K_m^{max}}{2} + \frac{\varrho^2}{2K_M^{min}}\right)$ and $\mu_2 = \varrho$ following (3.46). ■

Given that a formal definition of the TWC has been given, one tunes β, $\varepsilon_{\star,z_1}$ and $\varepsilon_{\star,z_2}$ of controllers (3.14)-(3.15) and (3.32)-(3.33) such that $\mathcal{S}_{real}^2 \subset \mathcal{B}_\star$ with $\star = \{s, a\}$. This is performed in order to get an efficient trade-off between accuracy and energy consumption.

3.8 Simulation results

3.8.1 Context

In this section, the effectiveness of the proposed controllers in this chapter is evaluated by simulations. Their performances are compared with respect to SOLSF and TWC. The simulations have been performed using Matlab/Simulink. The controller sampling period is $T_e = 1ms$ with Euler integration solver (sampling period step equal to $0.01ms$). The simulation duration is $5s$. The functions $\bar{a}(x,t)$ and $\bar{b}(x,t)$ (see Fig. 3.4) are generated using the MATLAB function 'rand' and are the same while testing all controllers. The bounds of these functions are

$$a_M = 4, \quad b_m = 0.96 \text{ and } b_M = 1.04$$

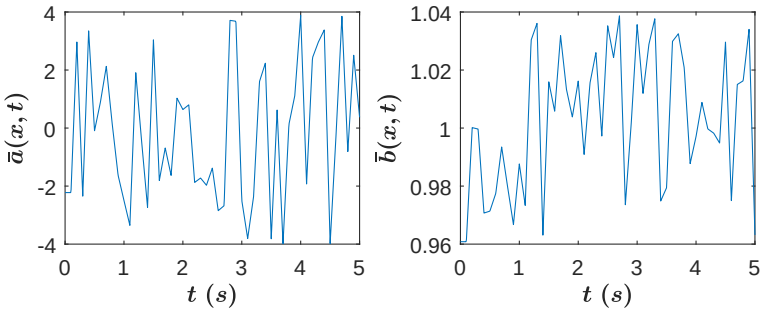

Figure 3.4 – **Left**: $\bar{a}(x,t)$ versus time (s); **Right**: $\bar{b}(x,t)$ versus time (s).

The gains are stated as $k_1 = 16$, $k_2 = 8$ for both controllers satisfying condition (3.9). Given the above information (bounds of $\bar{a}(x,t)$ and $\bar{b}(x,t)$, controllers gains and controller sampling period), the analytic bounds of z_1 and z_2 for the TWC are given following (3.44)-(3.46) as follows

$$\begin{aligned} |z_1| &< 1.71 \cdot 10^{-4}, \\ |z_2| &< 7.15 \cdot 10^{-2}. \end{aligned} \tag{3.61}$$

Hence, in order to obtain an effective adaptation for α, the first set (**Set 1**) of parameters ε_{s,z_1} and ε_{s,z_2} for the controller with switching$-\alpha$ approach (controller (3.14)-(3.15)) is chosen such that its theoretical convergence domain, following (3.18), is equal to the theoretical convergence domain TWC given in (3.61)

$$\varepsilon_{s,z_1} = 1.05 \cdot 10^{-4}, \qquad \varepsilon_{s,z_2} = 5.01 \cdot 10^{-2}.$$

Similarly, **Set 1** of parameters for the controller with algebraic$-\alpha$ approach (controller (3.32)-(3.33)) is given as follows

$$\beta = 2, \qquad \varepsilon_{a,z_1} = 1.71 \cdot 10^{-4}, \qquad \varepsilon_{a,z_2} = 7.15 \cdot 10^{-2}.$$

Since the convergence domain for the controller with dynamic$-\alpha$ approach is not determined, **Set 1** of its parameters is taken to obtain good performances as follows

$$k = 10, \qquad \varepsilon_{d,z_1} = 3 \cdot 10^{-5}, \qquad \varepsilon_{d,z_2} = 3 \cdot 10^{-2}.$$

In the second set (**Set 2**), only ε_{z_1} is changed and is multiplied by 2 for each controller. This is done to show how the trade-off between energy consumption and accuracy is achieved by changing the parameters of the controllers.

3.8.2 Results

For the controllers with variable α, the TWC (α=0) is initially applied (see Figure 3.7). When the system trajectories converge ($t \approx 1.5sec$), the adaptation starts (this phase will be called the steady state).
The theoretical and simulation bounds of the TWC controller are given in Table 3.1: Theorem 3.4 is confirmed. From Table 3.1, it can be seen that the bounds of the controllers with the switching and algebraic approaches obtained by simulation satisfy (3.18) and (3.35) respectively. Recall that the controllers with the switching and algebraic approaches parameters have been chosen as to obtain the same theoretical convergence domain as the TWC.
The energy consumed by the proposed controllers is much less than that of the TWC and comparable to that of the SOLSF (see $\mathcal{E}$ in Table 3.2). The accuracy versus $|z_1|$ ($mean(|z_1|)$ in Table 3.2 and Figure 3.5) with the proposed controllers is better than with the SOLSF and comparable to the TWC, whereas the accuracy versus $|z_2|$ ($mean(|z_2|)$ in Table 3.2 and Figure 3.5) with the proposed controllers is better than the other cases (concerning the TWC, this is mainly due to the attenuation of the chattering effect). An indicator used to quantify the chattering effect is the var function of the control input $var(u)$ (see Table 3.2): with the proposed controllers, this indicator is significantly less than with the TWC and larger than with the SOLSF. This can also be seen on the control input signals of both controllers (see Figure 3.6).
Concerning the comparison between **Set 1** and **Set 2** with the proposed controllers, it is done in order to show how the trade-off between energy consumption and accuracy is

achieved by changing the parameters of the controllers. One notices a better accuracy with **Set 1** than with **Set 2** (see Table 3.2). This is due to the larger weight on accuracy caused by a smaller value of ε_{z_1} with **Set 1**. The price to pay is that, with **Set 1**, a greater energy is consumed. Therefore, one can either favor accuracy or less energy consumption by tuning the different parameters of the proposed controllers.

Concerning the comparison between the different variable α approaches, it can be seen that, as predicted, the algebraic$-\alpha$ approach provides the smoother control (see $var(u)$ in Table 3.2). This is also corroborated by investigating the evolution of α with respect to time with the different variable α approaches in Figure 3.7. One notices that the evolution of α with the controller with algebraic$-\alpha$ approach is the smoothest. Indeed, a direct relation exits between α and the control input u (see (3.5)); hence, a smoother α induces a smoother control input u. Between the different variable α approaches, the least energy is consumed (see $\mathcal{E}$) by the controller with the algebraic$-\alpha$ approach. It also has comparable accuracy on z_1 and a much better one on z_2 with respect to the other two approaches.

	$max(\lvert z_1 \rvert)$	$max(\lvert z_2 \rvert)$
Theoretical bounds	$1.71 \cdot 10^{-4}$	$7.15 \cdot 10^{-2}$
Simulation bounds TWC	$8.86 \cdot 10^{-5}$	$4.65 \cdot 10^{-2}$
Simulation bounds controller with algebraic-α approach	$9.38 \cdot 10^{-5}$	$9.37 \cdot 10^{-3}$
Simulation bounds controller with switching-α approach	$1.71 \cdot 10^{-4}$	$4.11 \cdot 10^{-2}$

Table 3.1 – Theoretical and simulation bounds for TWC, controller with algebraic-α approach (**Set1**), controller with switching-α approach (**Set1**).

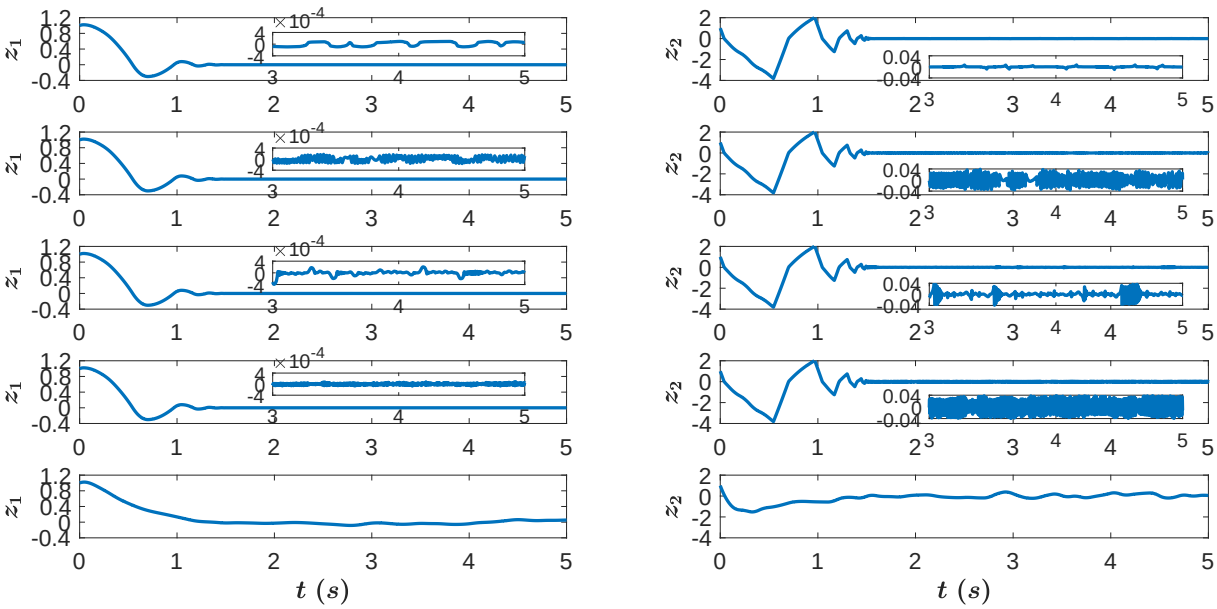

Figure 3.5 – Evolution of z_1 (**Left**) and z_2(**Right**) versus time (s). **Top to bottom**: controller with algebraic-α approach (**Set1**), controller with switching-α approach (**Set1**), controller with dynamic-α approach (**Set1**), TWC and SOLSF.

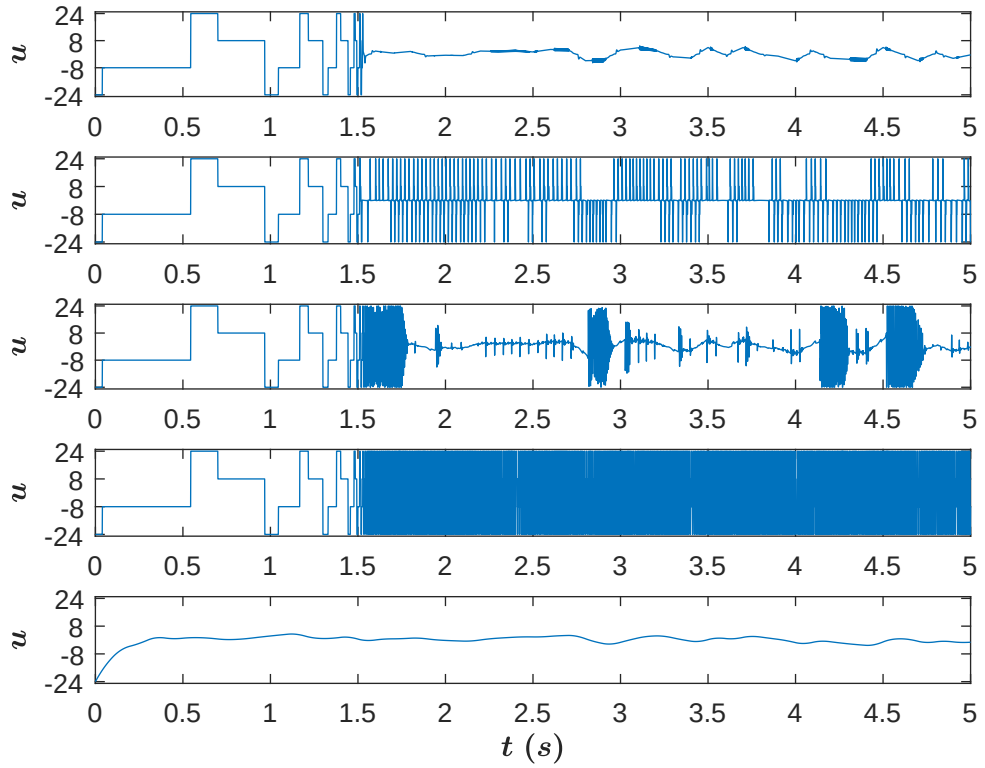

Figure 3.6 – Evolution of u versus time (s). **Top to bottom**: controller with algebraic-α approach (**Set1**), controller with switching-α approach (**Set1**), controller with dynamic-α approach (**Set1**), TWC and SOLSF.

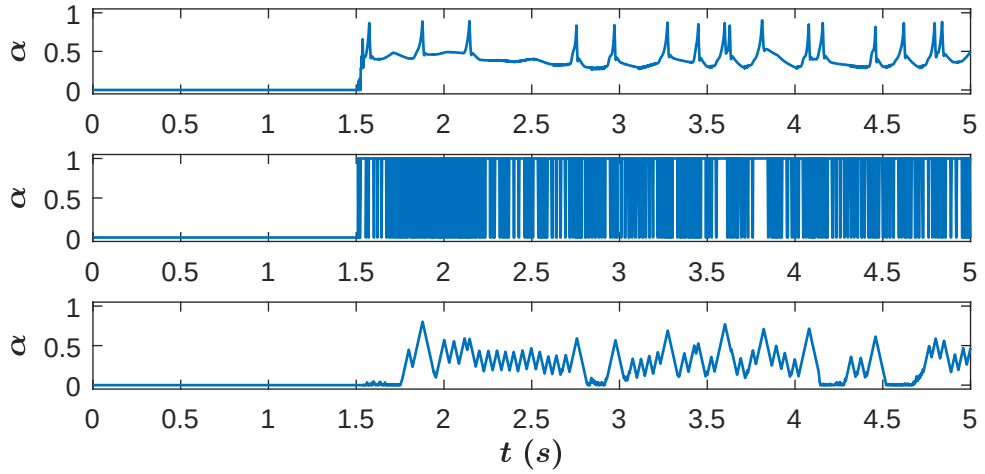

Figure 3.7 – Evolution of α versus time (s). **Top to bottom**: controller with algebraic-α approach (**Set1**), controller with switching-α approach (**Set1**), controller with dynamic-α approach (**Set1**).

3.9 Conclusion

The main contributions of this chapter can be summarized as follows

		Energy $\mathcal{E}$	$mean(\|z_1\|)$	$mean(\|z_2\|)$	$var(u)$	$mean(\alpha)$
	TWC	292.49	$2.19 \cdot 10^{-5}$	$1.63 \cdot 10^{-2}$	$2.57 \cdot 10^{4}$	
	SOLSF	2.05	$3.90 \cdot 10^{-2}$	$1.26 \cdot 10^{-1}$	$2.56 \cdot 10^{1}$	
Set1	Controller with algebraic-α approach	4.89	$7.07 \cdot 10^{-5}$	$9.42 \cdot 10^{-4}$	$4.72 \cdot 10^{2}$	0.40
	Controller with switching-α approach	57.04	$6.24 \cdot 10^{-5}$	$1.52 \cdot 10^{-2}$	$5.23 \cdot 10^{3}$	0.80
	Controller with dynamic-α approach	37.41	$4.13 \cdot 10^{-5}$	$4.64 \cdot 10^{-3}$	$3.80 \cdot 10^{3}$	0.29
Set2	Controller with algebraic-α approach	4.90	$1.29 \cdot 10^{-4}$	$1.73 \cdot 10^{-3}$	$1.66 \cdot 10^{2}$	0.42
	Controller with switching-α approach	41.43	$1.30 \cdot 10^{-4}$	$1.36 \cdot 10^{-2}$	$3.81 \cdot 10^{3}$	0.85
	Controller with dynamic-α approach	31.78	$1.07 \cdot 10^{-4}$	$7.54 \cdot 10^{-3}$	$2.71 \cdot 10^{3}$	0.32

Table 3.2 – Energy $\mathcal{E}$, mean accuracy on z_1, mean accuracy on z_2, $var(u)$ and average value of α in steady state with controller with algebraic-α approach, controller with switching-α approach, controller with dynamic-α approach, TWC and SOLSF.

- new controllers with variable α parameters for systems whose relative degree is equal to 2 is proposed.
- three variable α approaches have been explored: switching, dynamic and algebraic. They combine high accuracy and low energy consumption.
- the stability of the system controlled by these controllers is proved and the convergence domain is calculated for the switching and algebraic-α approaches.
- the convergence domain of the TWC in the case of a sampled controller is determined. This is done in order to ensure an effective variation of α.
- the effectiveness of the proposed controllers is shown via simulations and their performances are compared to those obtained with the TWC and SOLSF. They allow high accuracy tracking with reduced chattering and energy consumption.

4

Generalized algorithm for energy efficient controller based on HOSMC

Contents

4.1 Introduction

In Chapter 2, a controller with high accuracy and low energy consumption is designed for systems with relative degree 1. In Chapter 3, this result has been extended to systems with relative degree 2. The objective of this chapter is the design of a controller with similar properties (high accuracy and low energy consumption) such that the restriction on the relative degree is relieved, *i.e.* relative degree $r \geq 1$.
To achieve this objective, the proposed solution is inspired by sliding mode control (SMC) techniques. Indeed, higher order SMC (HOSMC) eliminate the restriction on the sliding variable relative degree. Among numerous HOSM solutions, one can cite [23] in which a HOSMC is designed using homogeneity tools. However, their design and analysis lack the link to classical sliding mode where a Lyapunov framework is used. In [53], [54] Lyapunov methods have been successfully applied to second order SMC, and attempts have been made to construct Lyapunov functions for HOSMC in [55], [56]. However, the result that seems to be the most complete is given in [29]. This latter proposes the design of a family of HOSMCs with finite time convergence using a Lyapunov framework. This is why a particular set of the family of HOSMCs controllers proposed in [29] is used in this thesis as a basis for the controller developed in the sequel.

Like many SMCs, the main drawback of the controller design in [29] is the chattering effect. The gains are overestimated leading to a high energy consuming controller which further amplifies the chattering effect. The objective of this chapter is to reduce this drawback by designing a new control strategy where a parameter α is introduced to the exponent term of the controller [29]. This parameter α is made variable and its evolution with respect to time is described with respect to the accuracy of the closed loop system. In a similar way to the previous controllers (Chapters 2 and 3), the value of α is increased in order to reduce the energy consumption whereas, when the accuracy is low, α is decreased to improve the robustness against matching perturbations/uncertainties.

4.2 Problem statement

Consider the following system

$$\begin{aligned} \dot{x} &= f(x,t) + g(x,t)u \\ \sigma &= \sigma(x,t) \end{aligned} \tag{4.1}$$

with $x \in \mathcal{X} \subset \mathbb{R}^n$ the state vector ($\mathcal{X}$ being an open bounded subset of $\mathbb{R}^n$ and n being the state dimension), f and g sufficiently differentiable uncertain functions, $u \in \mathcal{U} \subset \mathbb{R}$ the control input ($\mathcal{U}$ being a bounded open subset of $\mathbb{R}$) and σ the sliding variable. Assume that

Assumption 4.1. *The relative degree of (4.1), denoted r, is constant and known, i.e.*

$$\sigma^{(r)} = \bar{a}(x,t) + \bar{b}(x,t)u \tag{4.2}$$

Furthermore, one supposes that $r \geq 2$. [1] ■

Assumption 4.2. *$\bar{a}(x,t)$ and $\bar{b}(x,t)$ are unknown but bounded functions such that there exist positive constants a_M, b_m and b_M such that $\forall x \in \mathcal{X}, t \geq 0$ one has*

$$|\bar{a}(x,t)| \leq a_M, \quad 0 < b_m \leq \bar{b}(x,t) \leq b_M. \tag{4.3}$$

■

Assumption 4.3. *The internal dynamics of the system are bounded.* ■

Under these assumptions, σ-dynamics can re-written as

$$\begin{aligned} \dot{z}_1 &= z_2 \\ &\vdots \\ \dot{z}_r &= \bar{a}(x,t) + \bar{b}(x,t)u \end{aligned} \tag{4.4}$$

with $z = [z_1 \cdots z_r]^T = [\sigma \cdots \sigma^{(r-1)}] \in \mathcal{Z} \subset \mathbb{R}^r$. The control objective is achieved when z is evolving in a finite time around a vicinity of the origin in spite of perturbations/uncertainties. In [29], a family of HOSMCs is designed to control (4.4) and is based on control

1. When $r = 1$, the results developed in this chapter are the same as in Chapter 2. Then, in this chapter, one shall consider $r \geq 2$.

Lyapunov functions (CLFs). The focus here is made on a particular set of these HOSMCs, the control law u reading as

$$\begin{aligned} u =& -k_r \lceil \xi_r \rfloor^0, \\ \xi_i =& \lceil z_i \rfloor^{\frac{\epsilon_1}{\epsilon_i}} + k_{i-1}^{\frac{\epsilon_1}{\epsilon_i}} \xi_{i-1} \end{aligned} \tag{4.5}$$

with $2 \leq i \leq r$, $\epsilon = (\epsilon_1, \cdots, \epsilon_r) = (r, r-1, \cdots, 1)$ and $\xi_1 = z_1$. Furthermore, $(k_1, \cdots, k_r)$ are the controller gains where $(k_2, \cdots, k_r)$ can be written as a function of k_1 such that

$$\begin{aligned} & k_i = ß_{i-1} k_1^{\frac{r}{r-(i-1)}} \qquad \forall i = 2, \cdots, r-1 \\ & b_m k_r - a_M \geq ß_{r-1} k_1^r \end{aligned} \tag{4.6}$$

with the parameters $ß_{i-1}$ $(2 \leq i \leq r-1)$ calculated by evaluating homogeneous functions [30] and numerically finding their maxima on a homogeneous sphere (see Table 1.1 in Section 1.3.3 for proposed values of $ß_{i-1}$ $(2 \leq i \leq r-1)$ for $r = \{2, 3, 4\}$).
The controller (4.5) allows the establishment of a r^{th}-order sliding mode, *i.e.* z reaches zero in a finite time. However, it engenders the chattering phenomena caused by the unmodelled dynamics in the system. The controller is also high energy consuming from a control effort point of view since the gains have to be tuned in order to guarantee the finite time convergence in the "worst case" of perturbations and uncertainties. This last constraint induces the restrictions imposed by (4.6) on the gains of the controller. The chattering phenomena is further amplified by the gain overestimation.
In the sequel, a new controller is proposed based on (4.5) where a new parameter α is introduced as an exponent of ξ_r. The evolution of α is based on the accuracy of the closed-loop system and gives rise to an efficient trade-off between precision and energy consumption. It also allows to reduce the chattering phenomenon. In the next section, a formalization of this process is given and the closed loop stability is proven.

4.3 Controller design

The proposed controller, applied to system (4.4), reads as

$$\begin{aligned} u =& -k_r \lceil \xi_r \rfloor^{\alpha}, \\ \xi_i =& \lceil z_i \rfloor^{\frac{\epsilon_1}{\epsilon_i}} + k_{i-1}^{\frac{\epsilon_1}{\epsilon_i}} \xi_{i-1}, \quad 2 \leq i \leq r \end{aligned} \tag{4.7}$$

with $(k_1, \cdots, k_r)$ tuned as in (4.6) and α varying between 0 and 1 via the following variation law

$$\alpha = max\Big(-\beta \sum_{i=1}^{r} \frac{|z_i|}{|z_i| + \varepsilon_{z_i}} + 1, 0 \Big) \tag{4.8}$$

Parameters $\varepsilon_{z_i}, (1 \leq i \leq r)$ and β are positive constants set by the user with $\beta > 1$.

Energy consumption with controller (4.7)-(4.8). The control effort (in absolute value) of controller (4.7)-(4.8) is equal to $k_r |\xi_r|^{\alpha}$ whereas the control effort (in absolute value) of controller (4.5) is equal to k_r. Now, suppose that $|\xi_r| < 1$ [2]: therefore, by comparing the

2. It is not restrictive to consider $|\xi_r| < 1$ once the system trajectory converge to a vicinity of the origin.

control effort of both controllers $\forall \alpha \in [0,1]$ one has

$$k_r \geq k_r |\xi_r|^{\alpha} \tag{4.9}$$

where the left hand side of (4.9) and its right hand side are equal only when $\alpha = 0$. Then, it is clear that the control effort is smaller with controller (4.7)-(4.8) with respect to controller (4.5). Recall that the energy consumption is defined as (see Section 2.2.1)

$$\mathcal{E} = \int_{t_0}^{t_f} u^2(t) dt$$

with t_0 and t_f the initial and final instants respectively of the time interval over which the energy is evaluated. Then, the control effort is an image of the energy consumption. Hence, the energy consumed by controller (4.7)-(4.8) is less than that consumed by controller (4.5).

Notice also that $\forall \alpha_1, \alpha_2 \in [0,1]$ such that $\alpha_1 > \alpha_2$, one has

$$k_r |\xi_r|^{\alpha_1} < k_r |\xi_r|^{\alpha_2} \tag{4.10}$$

Then, the energy consumption decreases when α increases. Given the nonlinearity of the system, one cannot be sure that the system will follow the same trajectory with different values of α; therefore, one cannot be sure that (4.10) holds. However, the trend is visible in simulation that, as α increases, the energy consumption of the system decreases and vice-versa.

Remarks and parameters tuning.

- In order to guarantee the convergence of system (4.4) with controller (4.7)-(4.8) towards a vicinity of the origin, the gains $(k_1, \cdots, k_r)$ must be tuned following (4.6).
- A key point of this new control strategy is that its energy consumption is less than that of controller (4.5). Therefore, one should tune $\varepsilon_{z_i} (1 \leq i \leq r)$ and β in a way to make sure that inequality (4.9) is satisfied. This means that when $|\xi_r| \geq 1$, α should be equal to 0 which is ensured by introducing the following condition on the parameters of $\varepsilon_{z_i} (1 \leq i \leq r)$ and β in (4.8):[3]

$$\xi_r\left(\frac{\varepsilon_{z_1}}{\beta - 1}, \cdots, \frac{\varepsilon_{z_r}}{\beta - 1}\right) < 1. \tag{4.11}$$

- If the trajectories of the system are inside $\mathcal{D}$ defined as

$$\mathcal{D} = \{(z_1, \cdots, z_r) \in \mathcal{Z} \mid \alpha = -\beta \sum_{i=1}^{r} \frac{|z_i|}{|z_i| + \varepsilon_{z_i}} + 1 > 0\}, \tag{4.12}$$

  then the desired accuracy of the system is reached; therefore, the variation of α becomes possible and the value of α will vary between 0 and 1 following (4.8).
- If the trajectories of the system are outside $\mathcal{D}$, it means that the desired accuracy is not reached; it can be viewed as a loss of robustness versus perturbations and uncertainties. Hence, following (4.8), $\alpha = 0$: robust controller (4.5) is applied forcing the trajectories back to $\mathcal{D}$.

3. With abuse of notation, $\xi_r(\frac{\varepsilon_{z_1}}{\beta-1}, \cdots, \frac{\varepsilon_{z_r}}{\beta-1})$ is the value of ξ_r for $z = (\frac{\varepsilon_{z_1}}{\beta-1}, \cdots, \frac{\varepsilon_{z_r}}{\beta-1})$.

- Following (4.12), $\varepsilon_{z_i}, (1 \leq i \leq r)$ and β have a direct influence on $\mathcal{D}$ and therefore an influence on the accuracy of the controller. This fact is further discussed in the sequel.

Theorem 4.1. *[46] Consider system (4.1) under assumptions 4.1-4.3 where $\sigma-$dynamics read as (4.2) and controlled by (4.7)-(4.8). If $(k_1, \cdots, k_r)$ are tuned as (4.6), then there exist positive parameters $\varepsilon_{z_i}, (1 \leq i \leq r)$ and $\beta > 1$ satisfying (4.11) such that the trajectories of system (4.1) converge, in a finite time, to a vicinity of the origin.*

Proof: Suppose that the trajectory of the system is outside $\mathcal{D}$; then $\alpha = 0$ and controller (4.5) is applied. Given its finite time convergence property and supposing $(z_1(Q), z_2(Q))$ as the initial coordinates, the trajectory will converge to $\mathcal{D}$ in finite time (see trajectory $Q - R$ in Figure 4.1). Once the trajectory is inside $\mathcal{D}$, the variation of α takes effect following (4.8) decreasing the energy consumption (from a control effort point of view) and the chattering effect. Due to the loss of robustness versus perturbation/uncertainties $(\alpha \neq 0)$, the trajectory might leave $\mathcal{D}$ (see trajectory $R - S$ in Figure 4.1). Hence following (4.8), $\alpha = 0$ forcing the trajectory back to $\mathcal{D}$ (see trajectory $S - T$ in Figure 4.1) and so on. In fact, once the system trajectory converges to $\mathcal{D}$ for the first time, it evolves in a domain $\mathcal{D}'$ (see $\mathcal{D}'$ in Figure 4.1) that is slightly larger than $\mathcal{D}$. ε_{z_i} $(1 \leq i \leq r)$ and β influence the size of $\mathcal{D}$ and subsequently $\mathcal{D}'$; hence, they influence the ultimate accuracy of the controller.

■

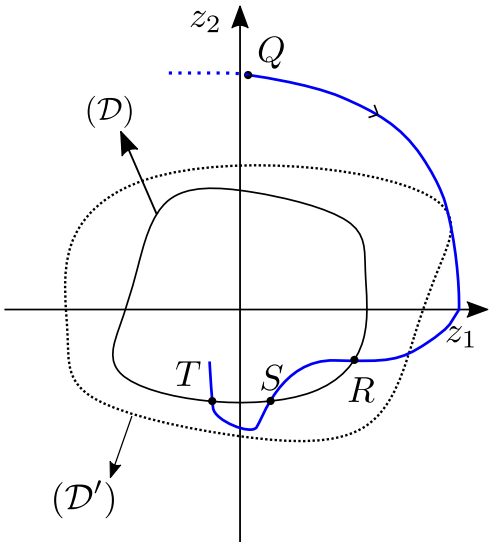

Figure 4.1 – Description of the system trajectory

Notice that, without loss of generality, note that Figure 4.1 is given for $r = 2$ in order to give a behavior illustration in the phase plan. In the sequel, the explicit expression of $\mathcal{D}'$ for $r = 2$ is determined.

Theorem 4.2. *[41] Consider system (4.1) under assumptions 4.1-4.3 where $\sigma-$dynamics read as (4.2) with $r = 2$ and controlled by (4.7)-(4.8). If k_1 and k_2 are tuned as in (4.6), then there exist positive parameters $\varepsilon_{z_1}, \varepsilon_{z_2}$ and β satisfying (4.11) with $\beta > 1$ such that the trajectories of system (4.1) converge, in a finite time, to*

$$\begin{aligned} \mathcal{D}' = \{x \in \mathcal{X} \mid |z_1| < max\left(\frac{\varepsilon_{z_1}}{\beta-1}, \frac{\varepsilon_{z_2}^2}{2(\beta-1)^2 K^*}\right) \\ |z_2| < max\left(\sqrt{\frac{2K^* k_1^2 \varepsilon_{z_1}}{(k_1^2+2K^*)(\beta-1)}}, \frac{\varepsilon_{z_2}}{\beta-1}\right) \end{aligned} \tag{4.13}$$

with $K^* = b_m k_2 - a_M$.

The proof of Theorem 4.2 is given in Appendix B. However, the outline of the proof is given as follows.
Recall $\mathcal{D}$ from (4.12) as the region around the origin in which the variation of α is possible (see Figure 4.2). Once the trajectory of the system is inside $\mathcal{D}$, it could potentially leave it due to loss of robustness versus perturbations and uncertainties ($\alpha \neq 0$, see trajectory $F - M$ in Figure 4.2). The trajectory of the system could leave $\mathcal{D}$ from

Case 1. $\widehat{AB}$ (resp. $\widehat{CD}$)

Case 2. a section of $\widehat{BC}$ (resp. $\widehat{DA}$)

Nevertheless, once the trajectory is evolving outside $\mathcal{D}$, the robustness property is increased ($\alpha = 0$) which will force the trajectory back to $\mathcal{D}$ (see $\widehat{ME}$ in Figure 4.2) and so on. In Appendix B, a formalization of the above discussion is given as well as the convergence domain $\mathcal{D}'$ of the proposed controller *i.e.* the convergence domain for when the trajectory of the system leaves $\mathcal{D}$ due to case 1 and case 2.

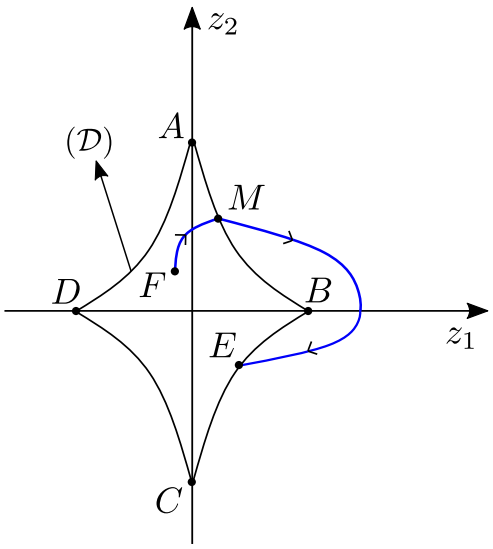

Figure 4.2 – Example of system trajectory in the phase plan with $r = 2$.

4.4 Simulation results

In this section, simulation results are given showing the effectiveness of the proposed controller (4.7)-(4.8). The software used is MATLAB/Simulink; the sampling period equals

0.1 ms with Euler integration solver. For simulation purposes, the relative degree of the system is taken equal to 3. This choice is made given that, in Chapters 2 and 3 systems with relative degree equal to 1 and 2 respectively have been considered. By this way, the applicability of the proposed method to high order systems ($r > 2$) and its effectiveness versus HOSMCs is shown.
Nevertheless, an example for which relative degree equals 2 is also considered. This is done in order to show that the system trajectories converge to the convergence domain $\mathcal{D}'$ defined in Theorem 4.2.

4.4.1 System with relative degree $r = 3$

Consider system (4.1) with $\sigma-$dynamics reading as (4.2) with $r = 3$. Then, the system is written as

$$\begin{aligned} \dot{z}_1 &= z_2, \\ \dot{z}_2 &= z_3, \\ \dot{z}_3 &= \bar{a}(x,t) + \bar{b}(x,t)u \end{aligned} \tag{4.14}$$

The functions $\bar{a}(x,t)$ and $\bar{b}(x,t)$ (Figure 4.3) are generated using the MATLAB function 'rand'. The bounds of these functions are

$$a_M = 5, \quad b_m = 0.96 \text{ and } b_M = 1.04 \tag{4.15}$$

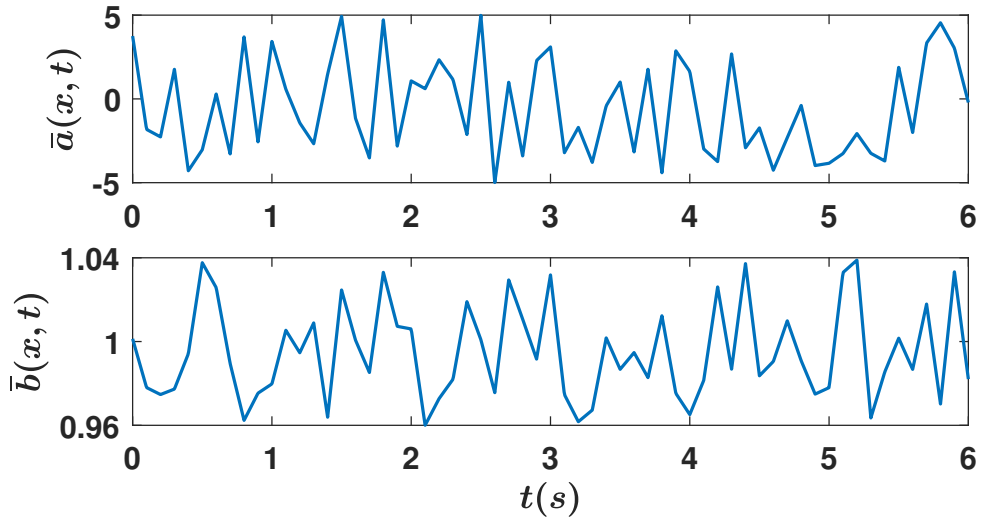

Figure 4.3 – Functions $\bar{a}(x,t)$ (top) and $\bar{b}(x,t)$ (bottom) versus time (s).

The gains are stated as $k_1 = 1$, $k_2 = 1.5$ and $k_3 = 35$ for both controllers satisfying condition (4.6). The parameters of α for controller (4.7)-(4.8) are taken

$$\beta = 4, \ \varepsilon_{z_1} = 10^{-7}, \ \varepsilon_{z_2} = 10^{-5} \text{ and } \varepsilon_{z_3} = 10^{-1}$$

satisfying condition (4.11).

Concerning controller (4.7)-(4.8), ($\alpha = 0$) is initially applied that ensures the convergence of the system towards a vicinity of the origin. When the system converges ($t \simeq 2.2\,s-$ see Figure 4.4), the $\alpha-$variation starts (see Figure 4.6). The phase where α is varying will be called the steady state.

The energy consumed by controller (4.7)-(4.8) is much less than that consumed by controller (4.5) (see $\mathcal{E}$ in Table 4.1 and control u in Figures 4.5 and 4.8). The average accuracy of $|z_1|, |z_2|$ and $|z_3|$ (see Figures 4.4 and 4.7, and $mean(|z_1|), mean(|z_2|)$ and $mean(|z_3|)$ in Table 4.1 for $3 \leq t \leq 5$ s) is high with both controllers. This means that variation of α has a low impact on the system accuracy but allows to reduced the energy consumption.

An indicator used to quantify the chattering effect is the var (see (2.25)) of the control input (see Table 4.1): it is significantly less with controller (4.7)-(4.8) than with controller (4.5). This can also be viewed on the control input signal u of both controllers (Figures 4.5 and 4.8).

	Controller (4.7)-(4.8)	Controller (4.5)
Energy $\mathcal{E}$	522.02	2450
$Mean(\|z_1\|)$	$7.13 \cdot 10^{-9}$	$1.57 \cdot 10^{-10}$
$Mean(\|z_2\|)$	$1.42 \cdot 10^{-6}$	$2.55 \cdot 10^{-7}$
$Mean(\|z_3\|)$	$1.54 \cdot 10^{-3}$	$1.83 \cdot 10^{-3}$
$var(u)$	$2.53 \cdot 10^{5}$	$1.17 \cdot 10^{6}$

Table 4.1 – Energy $\mathcal{E}$, average value of $|z_1|, |z_2|$ and $|z_3|$, $var(u)$ for controller (4.7)-(4.8) and controller (4.5) for $3 \leq t \leq 5$ s.

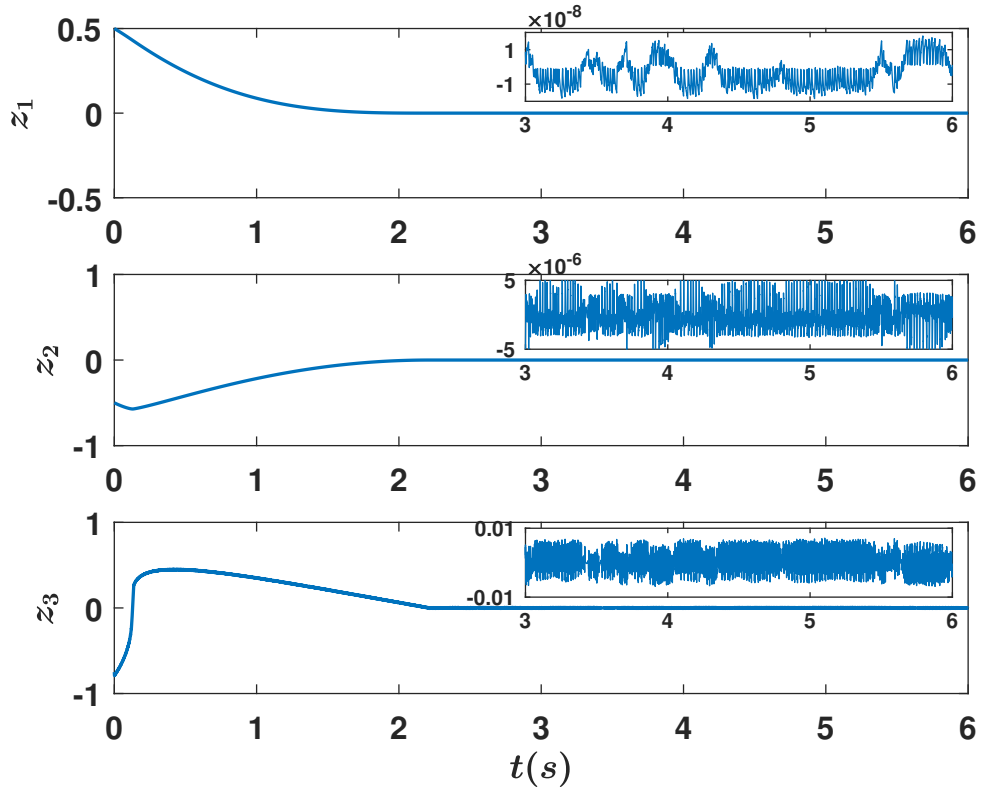

Figure 4.4 – **Controller (4.7)-(4.8). Top:** z_1 (with zoom) versus time (s). **Center:** z_2 (with zoom) versus time (s). **Bottom:** z_3 (with zoom) versus time (s).

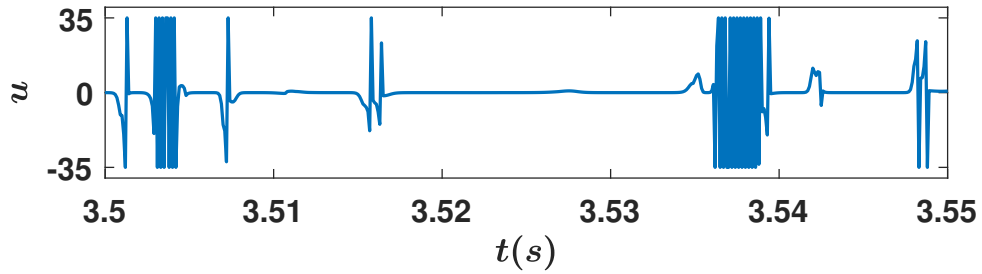

Figure 4.5 – Controller (4.7)-(4.8). Input u versus time (s).

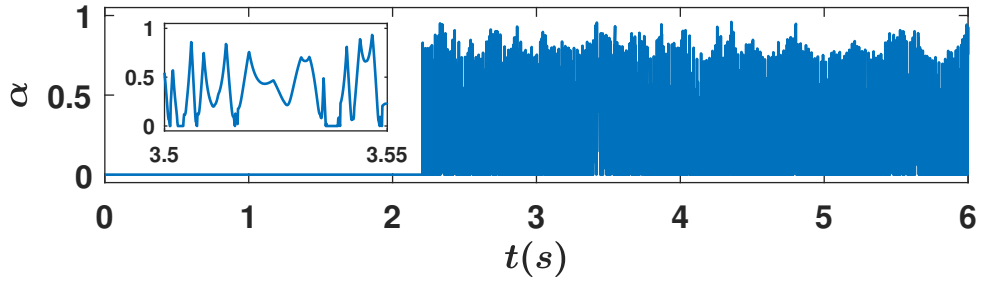

Figure 4.6 – Controller (4.7)-(4.8). α versus time (s).

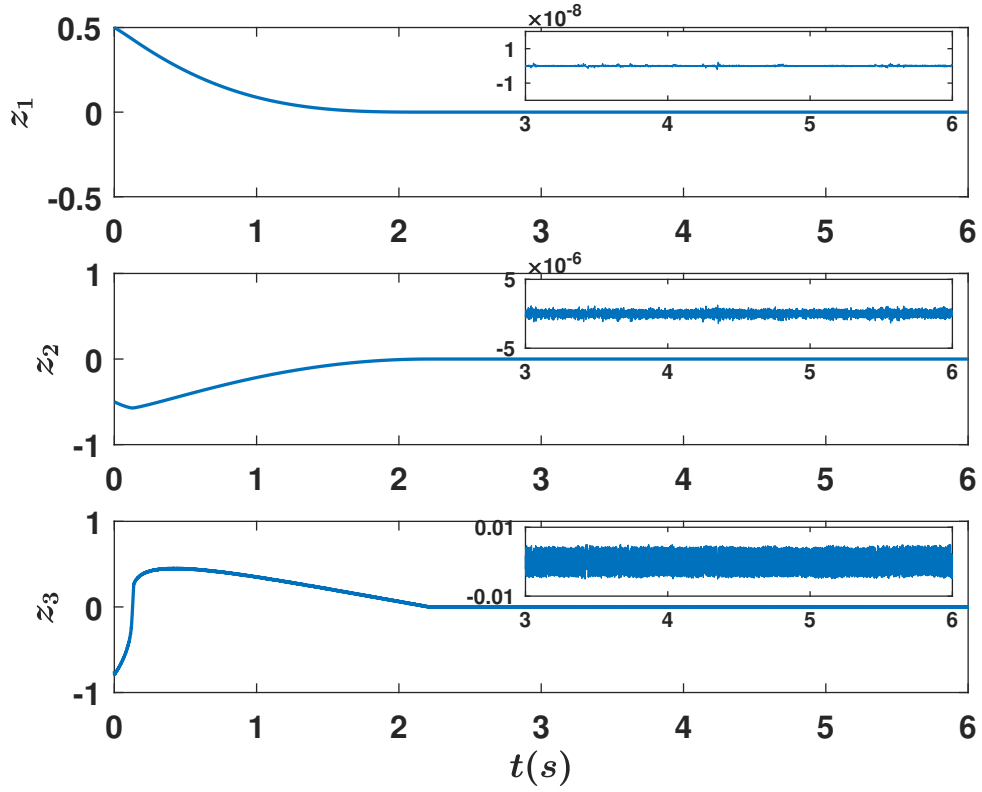

Figure 4.7 – **Controller** (4.5). **Top:** z_1 (with zoom) versus time (s). **Center:** z_2 (with zoom) versus time (s). **Bottom:** z_3 (with zoom) versus time (s).

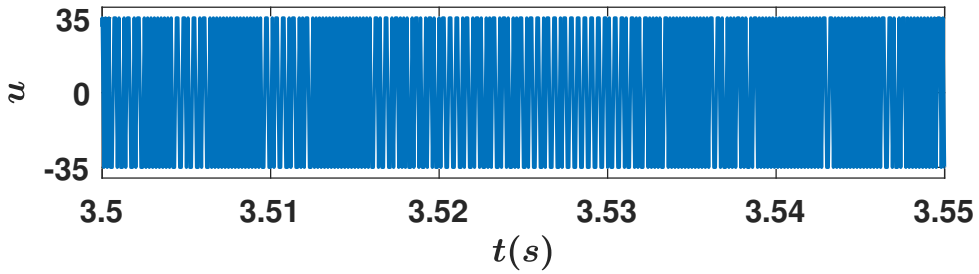

Figure 4.8 – **Controller (4.5).** Input u versus time (s).

4.4.2 Relative degree $r = 2$

Consider system (4.1) with $\sigma-$dynamics reading as (4.2) with $r = 2$. The objective of this section is to show that, when controller (4.7)-(4.8) is applied to (4.1), the system trajectories converge to the convergence domain $\mathcal{D}'$ defined in (4.13) in Theorem 4.2. The system is written as

$$\begin{aligned} \dot{z}_1 &= z_2, \\ \dot{z}_2 &= \bar{a}(x,t) + \bar{b}(x,t)u \end{aligned} \tag{4.16}$$

$\bar{a}(x,t)$ and $\bar{b}(x,t)$ are taken the same as in the previous section. The gains of controller (4.7)-(4.8) are stated as $k_1 = 1$ and $k_2 = 8$ satisfying condition (4.6). The parameters of α are taken

$$\beta = 9,\ \varepsilon_{z_1} = 5 \cdot 10^{-6} \text{ and } \varepsilon_{z_2} = 10^{-2}$$

satisfying condition (4.11). Then, according to (4.13), the theoretical convergence domain $\mathcal{D}'$ can be deduced as

$$\begin{aligned} |z_1| &< 7.28 \cdot 10^{-6}, \\ |z_2| &< 6.25 \cdot 10^{-3}. \end{aligned} \tag{4.17}$$

In the simulation test, the state variables converge into a vicinity of zero in a finite time (see Figure 4.9). After the transient behavior, the maximum values of $|z_1|$ and $|z_2|$ are

$$\begin{aligned} |z_1| &< 7.83 \cdot 10^{-7}, \\ |z_2| &< 1.50 \cdot 10^{-3}. \end{aligned} \tag{4.18}$$

Bounds (4.18) and Figure 4.9 clearly show that after a finite time, the system trajectories evolve in the convergence domain given by (4.17).

4.5 Prospective on α-variation

As viewed in Chapter 3, the choice for the variation law of α is not unique. Indeed, different laws could improve some features of the closed-loop system as accuracy or energy consumption. This fact is illustrated in this section without any convergence proof.

Define the following variation law

$$\alpha = max\Big(-\beta \frac{|\xi_r|}{|\xi_r| + \varepsilon} + 1, 0 \Big) \tag{4.19}$$

Parameters ε and β are positive constants set by the user with $\beta > 1$. One of the advantages of this variation law is that no matter the relative degree r of the system, the

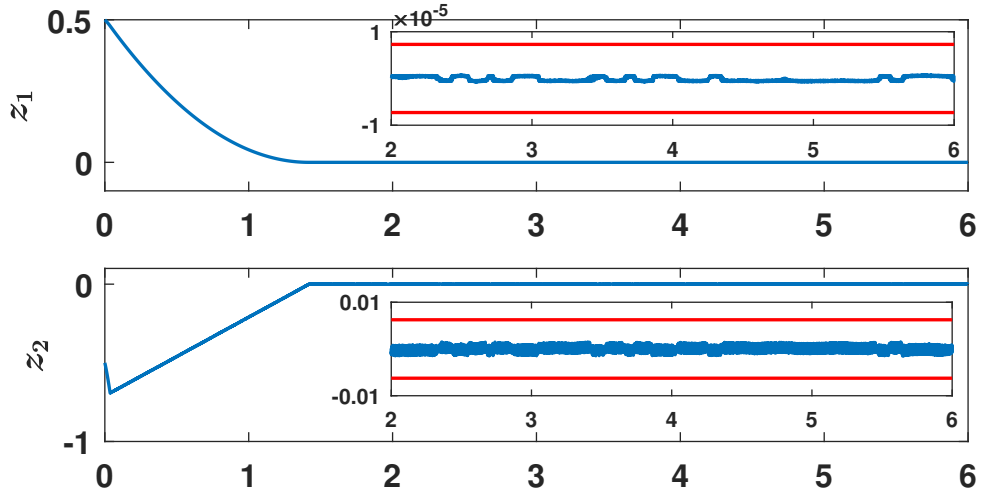

Figure 4.9 – **Controller** (4.7)-(4.8). **Top:** z_1 (with zoom) versus time (s). **Bottom:** z_2 (with zoom) versus time (s). The theoretical bounds of the convergence domain are plotted in red.

number of parameters of α does not change which reduces the parameter tuning effort. The logic of the controller is as follows. Recall

$$\begin{aligned}\xi_r &= \lceil z_r \rfloor^{\frac{\epsilon_1}{\epsilon_r}} + k_{r-1}^{\frac{\epsilon_1}{\epsilon_r}} \xi_{r-1} \\ \xi_i &= \lceil z_i \rfloor^{\frac{\epsilon_1}{\epsilon_i}} + k_{i-1}^{\frac{\epsilon_1}{\epsilon_i}} \xi_{i-1}, \quad 2 \leq i \leq r.\end{aligned}$$

This means that ξ_r is a function of the system states and could be used as an image of the system accuracy. Then, when $|\xi_r|$ is smaller than $\frac{\varepsilon}{\beta-1}$, α is increased and varies between 0 and 1 in order to decrease the energy consumption. On the other hand, when $|\xi_r| \geq \frac{\varepsilon}{\beta-1}$, α becomes 0 increasing the robustness of the system and so on.

Following the variation law (4.19), define $\mathcal{D}$ as the region where α is variable; it is given by

$$\mathcal{D} = \{x \in \mathcal{X} \mid |\xi_r| < \frac{\varepsilon}{\beta - 1}\}. \tag{4.20}$$

Notice that α begins varying as soon as $|\xi_r| < \frac{\varepsilon}{\beta-1}$ *i.e.* before z converges (see Figure 4.10); this is why, it has been difficult to perform the convergence proof.
For the simulations, consider system (4.1) with $\sigma-$dynamics reading as (4.2) with $r = 3$ as Section 4.4.1. Controller (4.7) & (4.19) is used to stabilize system (4.1) with the conditions and gains similar to Section 4.4.1. The parameters β and ε are taken equal to 9 and $4 \cdot 10^{-8}$ respectively. One notices that, for lower energy consumption, a better accuracy with (4.7) & (4.19) with respect to controller (4.7)-(4.8) on z_1, z_2 and z_3 is obtained. Furthermore, the accuracy is similar (z_1 and z_2) or better (z_3) than that obtained with controller (4.5), with a much reduced energy consumption (divided by 42 - see Table 4.2).

4.6 Conclusion

The main contributions of this chapter can be summarized as follows

- a generalized algorithm based on HOSMC for systems of arbitrary relative degree is proposed: it offers high accuracy tracking with reduced energy consumption with

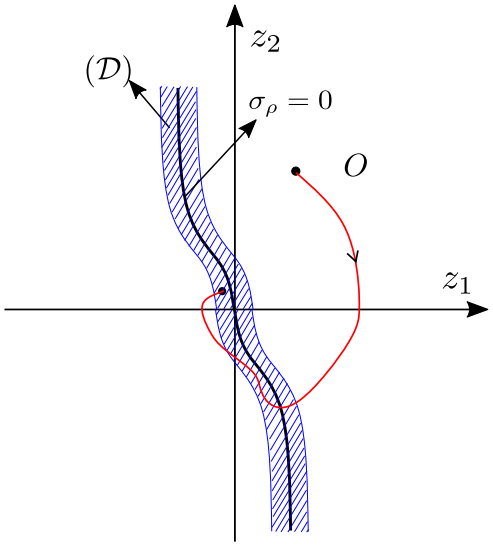

Figure 4.10 – Example of a system trajectory when controller (4.7) & (4.19) is applied to system (4.4) with $r = 2$

	Controller (4.7)-(4.8)	Controller (4.5)	Controller (4.7) & (4.19)
Energy $\mathcal{E}$	522.02	2450	57.93
$Mean(\|z_1\|)$	$7.13 \cdot 10^{-9}$	$1.57 \cdot 10^{-10}$	$1.05 \cdot 10^{-9}$
$Mean(\|z_2\|)$	$1.42 \cdot 10^{-6}$	$2.55 \cdot 10^{-7}$	$2.81 \cdot 10^{-7}$
$Mean(\|z_3\|)$	$1.54 \cdot 10^{-3}$	$1.83 \cdot 10^{-3}$	$4.42 \cdot 10^{-4}$
$var(u)$	$2.53 \cdot 10^{5}$	$1.17 \cdot 10^{6}$	$4.42 \cdot 10^{4}$

Table 4.2 – Energy $\mathcal{E}$, average value of $|z_1|, |z_2|$ and $|z_3|$, standard deviation of u for controller (4.7)-(4.8), controller (4.5) and controller (4.7) & (4.19) for $3 \leq t \leq 5$ s.

respect to HOSMC. This is performed by introducing a parameter α and varying it between 0 and 1;

- the stability of the system controlled by the later controller is given. The convergence domain is calculated for system with relative degree 2 with respect to the sliding variable;
- the effectiveness of the proposed controller is shown via simulations and its performances are compared to results obtained by controller [29]: the proposed controller allows high accuracy tracking with reduced energy consumption;
- for system with relative degree equal 2, simulations illustrating that the system trajectory converges to the theoretical convergence domain are given;
- a prospective on the variation of α decreasing the number of tuning parameters is also given. It has good closed-loop performances; however, no convergence proof is given.

Experimental applications

5

Application to an electropneumatic actuator

Contents

5.1 Introduction

Pneumatic actuators are very common in industrial applications due to their low cost and weight, easy installation and maintenance, and high power/weight ratio [57, 58, 59]. However, they are uncertain and complex systems which makes the control of their position quite difficult. Indeed, the nature of these actuators and their interaction with external elements make their modeling difficult and therefore their control. This makes sliding mode control an ideal tool to control this type of actuators thanks to its robustness property versus uncertainties and perturbations.
FOSMC has been used to control an electropneumatic actuator in [57]; however, the high frequency oscillations of the control input engender high frequency motion of the servodistributors mobile parts. This high frequency motion can deteriorate the components of the actuator and therefore must be reduced as much as possible. An alternative solution has been the use of higher order sliding mode approaches (see for example [60, 59, 61]): the interest of such control laws is a better accuracy and a reduction of the chattering. However, their tuning is not a simple task given that the bounds of the uncertainties and

perturbations, whose knowledge is important for the computation of the control parameters, are not easily determined and are very often overestimated. Then, another way consists in using adaptive versions (time-varying gain) of standard sliding mode controllers [62], or second order sliding mode controllers [63, 64]: these approaches allow to simplify the tuning of the controller gains but transiently reduce the performances of the closed-loop system (accuracy).
The main objective of this chapter is the control of the electropneumatic actuator position using the control laws developed in this thesis:

- the first order controller (2.15)-(2.16) from Chapter 2;
- the second order controller with the algebraic adaptive approach (3.32)-(3.33) from Chapter 3.

Another objective is to show the applicability of these methods to real physical systems. Thanks to these approaches, the advantages of the linear state feedback (low energy consumption) and sliding mode control (high accuracy tracking) is obtained. In order to apply the first order controller (respectively second order controller) the sliding variable is designed such that its relative degree is equal to 1 (respectively equal to 2).
All the experimental applications have been made on the electropneumatic system of LS2N (see Figure 5.1) which is described in the sequel.

Figure 5.1 – Photo of the electropneumatic setup.

5.2 System description

The electropneumatic actuator experimental set-up (see Figure 5.2) is composed of (for details, see [3, 64])

- a main actuator composed of two chambers denoted P (as positive) and N (as negative). The air mass flow rate entering in its chambers is controlled by 2 proportional 3-way servodistributors;
- a second actuator, mechanically identical to the main one and called “perturbation actuator”. The air mass flow rate is controlled by a 5-way servodistributor. The

purpose of this actuator is to apply a dynamical load force on the main one. Note that the force control of this actuator is performed by an analog PID controller developed by the bench manufacturer;

- the two actuators are mechanically linked, through a load carriage of mass M.

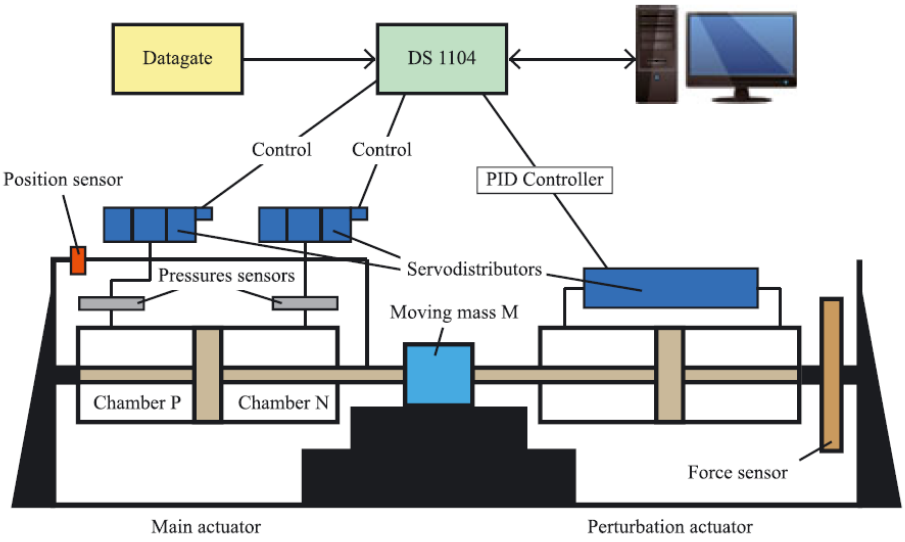

Figure 5.2 – Scheme of the control architecture of the electropneumatic setup [3].

The mathematical model of the electropneumatic system (details in [3]) reads as

$$\begin{aligned}
\dot{p}_P &= \frac{\varkappa RT}{V_P(y)}\left[\varphi_P + \psi_P.u - \frac{S}{RT}p_P v\right] \\
\dot{p}_N &= \frac{\varkappa RT}{V_P(y)}\left[\varphi_N - \psi_N.u + \frac{S}{RT}p_N v\right] \\
\dot{v} &= \frac{1}{M}\left[S(p_P - p_N) - b_v v - F_{\text{ext}}\right] \\
\dot{y} &= v
\end{aligned} \tag{5.1}$$

with y the piston position (*i.e.* system output), v its velocity, F_{ext} the external perturbation produced by the perturbation actuator, p_P and p_N the pressures in chambers P and N respectively, R the perfect gas constant, b_v the viscous friction coefficient, T the supply temperature, $\varkappa$ the polytropic constant, and S the piston surface. u is the control input of the system; physically, this input is a voltage acting on both servodistributors: given that there are two servodistributors, a voltage is applied to the first one whereas the opposite value is applied to the other one. The volume in each chamber depends on the position of the piston and reads as

$$\begin{aligned}
V_P(y) &= V_0 + S \cdot y \\
V_N(y) &= V_0 - S \cdot y
\end{aligned}$$

with V_0 the half-cylinder volume. The functions φ_P, φ_N, ψ_P and ψ_N describe the mass flow rate and are defined as 5^{th} order polynomials of the pressures as depicted in [65]. Note

that the dynamics of the servodistributors are not taken into account in the model. Then, the model (5.1) can be written as a nonlinear system affine in the control input u, *i.e.*

$$\dot{x} = f(x) + g(x)u \tag{5.2}$$

with x the state vector defined as $x = \begin{bmatrix} p_N & p_P & \upsilon & y \end{bmatrix}^T \in \mathcal{X}$, and u the control input. Furthermore, vectors $f(x)$ and $g(x)$ read as

$$f(x) = \begin{bmatrix} \dfrac{\varkappa RT}{V_P(y)}\left[\varphi_P - \dfrac{S}{RT}p_P\upsilon\right] \\ \dfrac{\varkappa RT}{V_P(y)}\left[\varphi_N + \dfrac{S}{RT}p_N\upsilon\right] \\ \dfrac{1}{M}\left[S(p_P - p_N) - b_\upsilon\upsilon - F_{\text{ext}}\right] \\ \upsilon \end{bmatrix}$$

$$g(x) = \begin{bmatrix} \dfrac{\varkappa RT}{V_P(y)}\psi_P \\ -\dfrac{\varkappa RT}{V_N(y)}\psi_N \\ 0 \\ 0 \end{bmatrix}$$

The operating domain $\mathcal{X}$ is as follows

$$\begin{aligned} \mathcal{X} = &\{x \in \mathbb{R}^4 \mid 1\ bar \leq p_N \leq 7\ bar, \\ &1\ bar \leq p_P \leq 7\ bar, |y| \leq 72\ mm, |\upsilon| \leq 1\ m.s^{-1}\} \end{aligned} \tag{5.3}$$

Note that the maximum force F_{ext} generated by the perturbation actuator is $2000N$. Mechanical and physical parameters of the main actuator are defined as

$$\begin{aligned} &M = 3.4\ kg,\ V_0 = 3.40 \cdot 10^{-4}\ m^3,\ S = 0.0045\ m^2, \\ &b_\upsilon = 50,\ k = 1.2,\ R = 287\ J.kg^{-1}.K^{-1},\ T = 293\ ^\circ K. \end{aligned}$$

5.3 Control design

In Part I of this thesis, first and second order controllers have been proposed. They have the advantages of both sliding mode control (robustness and accuracy) and linear state feedback (low energy consumption). In the sequel,

- a sliding variable is designed such that the system relative degree is equal to 1. Then, an electropneumatic actuator position controller based on the first order controller proposed in Chapter 2 is designed;
- another sliding variable is designed such that the system relative degree is equal to 2. Then, a position controller based on the second order controller proposed in Chapter 3 is designed. Among the different second order controllers designed in Chapter 3, the control strategy with the algebraic$-\alpha$ approach is chosen, given that it provides the best performances (most efficient trade-off between accuracy and energy consumption) as seen in Section 3.8.

First order and second order approaches are considered in order to show the applicability of the approaches developed in this thesis to real physical systems as well as their effectiveness with respect to sliding mode control and linear state feedback. One could also have designed a controller based on the approach presented in Chapter 4. However, it has been elected to keep the focus on the aforementioned controllers, the results of Chapter 4 being used for the control of a twin wind turbine in the next chapter.

5.3.1 Control problem statement with relative degree r equals 1

The objective is to control the position of the main electropneumatic actuator by tracking a sufficiently differentiable reference signal y_{ref}. Then, a suitable sliding variable is

$$\sigma = e_a + c_1 e_\upsilon + c_0 e_y \tag{5.4}$$

where e_a, e_υ and e_y are the tracking errors of the position, velocity and acceleration respectively, *i.e.*

$$e_y = y - y_{\text{ref}},\ e_\upsilon = \upsilon - \dot{y}_{\text{ref}},\ e_a = \dot{\upsilon} - \ddot{y}_{\text{ref}}.$$

c_1 and c_0 are chosen such as the Hurwitz condition (see (1.5) in Chapter 1). The relative degree of (5.2) with respect to σ defined by (5.4) equals 1 fulfilling Assumption 2.1. From (5.2)-(5.4), one has

$$\dot{\sigma} = \Psi_1(.) + \Phi_1(.)u \tag{5.5}$$

with

$$\begin{aligned}
\Psi_1(.) =& \frac{S\varkappa RT}{M}\left[\frac{\varphi_P}{V_P(y)} - \frac{\varphi_N}{V_N(y)}\right] - \frac{\dot{F}_{\text{ext}}}{M} + c_0\upsilon - y^{(3)}_{\text{ref}} \\
&- c_1\ddot{y}_{\text{ref}} - c_0\dot{y}_{\text{ref}} - \frac{S^2\varkappa\upsilon}{M}\left[\frac{p_P}{V_P(y)} + \frac{p_N}{V_N(y)}\right] \\
&+ \frac{c_1 M - b_\upsilon}{M^2}\left[S(p_P - p_N) - b_\upsilon\upsilon - F_{\text{ext}}\right] \\
\Phi_1(.) =& \frac{S\varkappa RT}{M}\left[\frac{\psi_P}{V_P(y)} + \frac{\psi_N}{V_N(y)}\right]
\end{aligned}$$

Functions $\Psi_1(.)$ and $\Phi_1(.)$ are uncertain ones due to parametric uncertainties (for example, the temperature T in the chamber is physically time-varying whereas it is supposed to be constant in the control design) and given that there is the external unknown perturbation F_{ext}. Then, the functions $\Psi_1(.)$ and $\Phi_1(.)$ can be written as

$$\begin{aligned}
\Psi_1(.) =& \Psi_{\text{Nom},1}(.) + \Delta\Psi_1(.) \\
\Phi_1(.) =& \Phi_{\text{Nom},1}(.) + \Delta\Phi_1(.)
\end{aligned} \tag{5.6}$$

with $\Psi_{\text{Nom},1}(.)$ and $\Phi_{\text{Nom},1}(.)$ the nominal terms and $\Delta\Psi_1(.)$ and $\Delta\Phi_1(.)$ the uncertain terms. In [59], it has been numerically observed that, under current operating conditions, $\Psi_{\text{Nom},1}$ and $\Phi_{\text{Nom},1}$ are bounded and only depend on measured or estimated variables. Furthermore, $\Phi_{\text{Nom},1} > 0\ \forall x \in \mathcal{X}$. Hence, the control input u is defined as

$$u = \frac{1}{\Phi_{\text{Nom},1}}(-\Psi_{\text{Nom},1} + \omega) \tag{5.7}$$

with ω defined in the sequel. After substituting (5.6)-(5.7) in (5.5), the closed loop behavior of $\sigma-$dynamics is described by

$$\dot{\sigma} = \underbrace{\Delta\Psi_1 - \Delta\Phi_1\Phi_{\text{Nom},1}^{-1}\Psi_{\text{Nom},1}}_{\bar{a}(x,t)} + \underbrace{(1 + \Delta\Phi_1\Phi_{\text{Nom},1}^{-1})}_{\bar{b}(x,t)} \cdot \omega \tag{5.8}$$

As previously mentioned, under the considered operating conditions, the functions Ψ_1 and Φ_1 are bounded with $\Phi_{\text{Nom},1} > 0$ [59]. Therefore, there exist positive constants a_M, b_m and b_M such that, $\forall x \in \mathcal{X}$ and $t \geq 0$,

$$\begin{aligned} &|\bar{a}(x,t)| \leq a_M \\ &0 < b_m \leq \bar{b}(x,t) \leq b_M. \end{aligned} \tag{5.9}$$

Assumption 2.2 is fulfilled. The term ω will be defined in Section 5.4, to ensure the convergence of σ to a vicinity of the origin.

5.3.2 Sliding variable relative degree $r = 2$

Consider now the following sliding variable

$$\sigma = e_\upsilon + c_0 e_y \tag{5.10}$$

with $c_0 > 0$. In this case, the relative degree of (5.1) with respect to σ equals 2 and is constant, that makes Assumption 3.1 fulfilled. From (5.2)-(5.10), one gets

$$\ddot{\sigma} = \Psi_2(.) + \Phi_2(.)u \tag{5.11}$$

with

$$\begin{aligned} \Psi_2(.) =& \frac{S\varkappa RT}{M}\left[\frac{\varphi_P}{V_P(y)} - \frac{\varphi_N}{V_N(y)}\right] - \frac{1}{M}(\dot{F}_{\text{ext}} + My_{\text{ref}}^{(3)}) \\ &- \frac{S^2\varkappa\upsilon}{M}\left[\frac{p_P}{V_P(y)} + \frac{p_N}{V_N(y)}\right] - \lambda\ddot{y}_{\text{ref}} \\ &+ \frac{Mc_0 - b_\upsilon}{M^2}\left[S(p_P - p_N) - b_\upsilon\upsilon - F_{\text{ext}}\right] \\ \Phi_2(.) =& \frac{SkRT}{M}\left[\frac{\psi_P}{V_P(y)} + \frac{\psi_N}{V_N(y)}\right] \end{aligned}$$

Functions $\Psi_2(.)$ and $\Phi_2(.)$ are uncertain functions due to parametric uncertainties and can be written as

$$\begin{aligned} \Psi_2(.) =& \Psi_{\text{Nom},2}(.) + \Delta\Psi_2(.) \\ \Phi_2(.) =& \Phi_{\text{Nom},2}(.) + \Delta\Phi_2(.) \end{aligned} \tag{5.12}$$

with $\Psi_{\text{Nom},2}(.)$ and $\Phi_{\text{Nom},2}(.)$ being the nominal terms and $\Delta\Psi_2(.)$ and $\Delta\Phi_2(.)$ the uncertain terms. As previously, under current operating conditions, $\Psi_{\text{Nom},2}$ and $\Phi_{\text{Nom},2}$ are bounded and only depend on measured or estimated variables. Furthermore, $\Phi_{\text{Nom},2} > 0\ \forall x \in \mathcal{X}$. Hence, the control input u is defined as

$$u = \frac{1}{\Phi_{\text{Nom},2}}(-\Psi_{\text{Nom},2} + \omega) \tag{5.13}$$

with ω defined in the sequel. After substituting (5.12)-(5.13) in (5.11), the closed loop behavior of $\sigma-$dynamics is described by

$$\ddot{\sigma} = \underbrace{\Delta\Psi_2 - \Delta\Phi_2\Phi_{\text{Nom},2}^{-1}\Psi_{\text{Nom},2}}_{\bar{a}(x,t)} + \underbrace{(1 + \Delta\Phi_2\Phi_{\text{Nom},2}^{-1})}_{\bar{b}(x,t)} \cdot\omega \tag{5.14}$$

There exist positive constants a_M, b_m and b_M satisfying (5.9) $\forall x \in \mathcal{X}$ and $t \geq 0$. Assumption 3.2 is fulfilled. By a similar way to the previous section, the term ω will be defined in Section 5.4, to ensure the convergence of σ and $\dot{\sigma}$ to a vicinity of the origin.

5.4 Experimental context

The controllers are implemented on the experimental setup using MATLAB/Simulink coupled with dSpace DS1104 datacard. The sampling period is $T_e = 0.2\ ms$. The position y of the mass load as well as the pressures p_P and p_N are measured via sensors. The velocity and the acceleration are obtained using supertwisting differentiators [66]. The mass load connected to the main actuator has to track a reference trajectory defined as (see Figure 5.3)

$$\begin{aligned} y_{\text{ref}} &= 0.04sin(0.15\pi t + \pi) && \text{for} \quad 0 \leq t < 20\ s \\ y_{\text{ref}} &= 0 && \text{for} \quad 20 \leq t < 40\ s \\ y_{\text{ref}} &= 0.04sin(0.3\pi t) && \text{for} \quad 40 \leq t \leq 60\ s \end{aligned}$$

This reference trajectory has been defined in order to evaluate the performances of both controllers versus different dynamics (sinusoidal references) or in case of constant position. All the tests are made by considering perturbations. Thus, the selected reference trajectory for the perturbation actuator is $F_{\text{ext}} = 1000sin(0.34\pi t)\ (N)$ (Figure 5.3). This trajectory is tracked using a PID controller parametrized by the setup manufacturer. Note that the perturbation is considered unknown by the controller, only its bound is known.

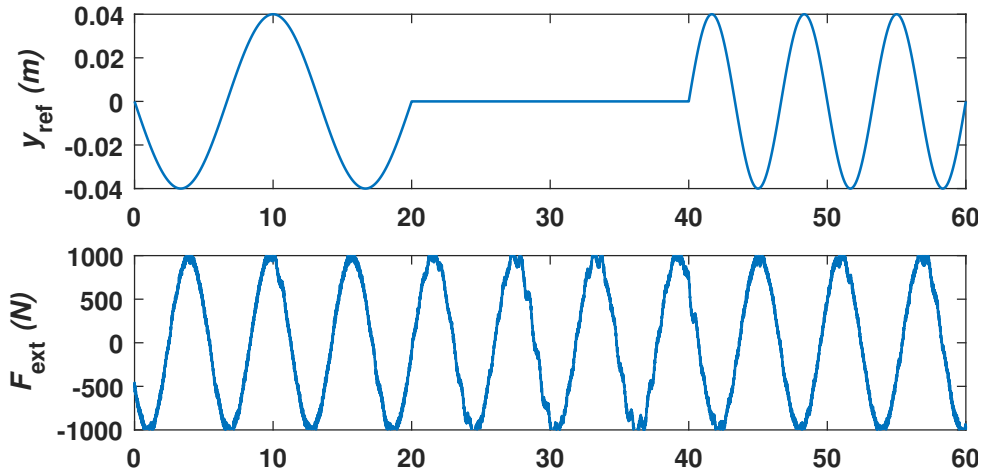

Figure 5.3 – **Top.** Reference trajectory $y_{ref}\ (m)$ for the actuator position versus time (s). **Bottom.** External perturbation $F_{ext}(N)$ versus time (s).

Sliding variable with relative degree equals 1. First-of-all, the performances of controller (5.7) with ω defined by 3 different ways are analyzed. Indeed, the term ω is defined as

- (2.15)-(2.16)

$$\omega = -k\lceil\sigma\rfloor^{\alpha}, \text{ with } \alpha = max(-\beta\frac{|\sigma|}{|\sigma|+\varepsilon} + 1\,,\, 0)$$

- FOLSF ($\alpha = 1$)

$$\omega = -k\sigma$$

- FOSMC ($\alpha = 0$)

$$\omega = -ksign(\sigma)$$

This analysis/comparison is made by evaluating

- the tracking error e_y;
- the energy consumption $\mathcal{E}$ from (2.13) defined as

$$\mathcal{E} = \int_{t_0}^{t_f} u^2(t)dt$$

  with t_0 and t_f the initial and final instants respectively of the time interval over which the energy is evaluated;
- $var(u)$ which is an indicator of the presence (or not) of chattering.

The gain k of the three controllers is set to 4000 satisfying (2.7). This choice has been made in order to get the best performances during the experimentation, for all controllers. The parameters β and ε of (2.15)-(2.16) are chosen as 11 and 2 respectively.

Sliding variable with relative degree equals 2. Then, the performances of controller (5.13) with ω defined as

- controller (3.32)-(3.33)

$$\omega = -k_1\lceil\sigma\rfloor^{\frac{\alpha}{2-\alpha}} - k_2\lceil\dot{\sigma}\rfloor^{\alpha} \text{ with } \alpha = \max(-\beta(\frac{|\sigma|}{|\sigma|+\varepsilon_{a,\sigma}} + \frac{|\dot{\sigma}|}{|\dot{\sigma}|+\varepsilon_{a,\dot{\sigma}}}) + 1\,,\, 0),$$

- SOLSF ($\alpha = 1$)

$$u = -k_1\sigma - k_2\dot{\sigma} \tag{5.15}$$

- TWC ($\alpha = 0$)

$$u = -k_1\text{sign}(\sigma) - k_2\text{sign}(\dot{\sigma}) \tag{5.16}$$

are analyzed by a similar way than previously. The gains k_1 and k_2 are taken as 3000 and 1500 respectively. The parameters of (3.32)-(3.33) are chosen as $\beta = 7$, $\varepsilon_{a,\sigma} = 0.01$ and $\varepsilon_{a,\dot{\sigma}} = 0.9$.

Remark 5.1. *The controllers for systems with relative degree 1 on one side, and 2 on an other side will be separately analyzed since there is no concrete way to formally compare their energy consumptions, their gains being different.* ■

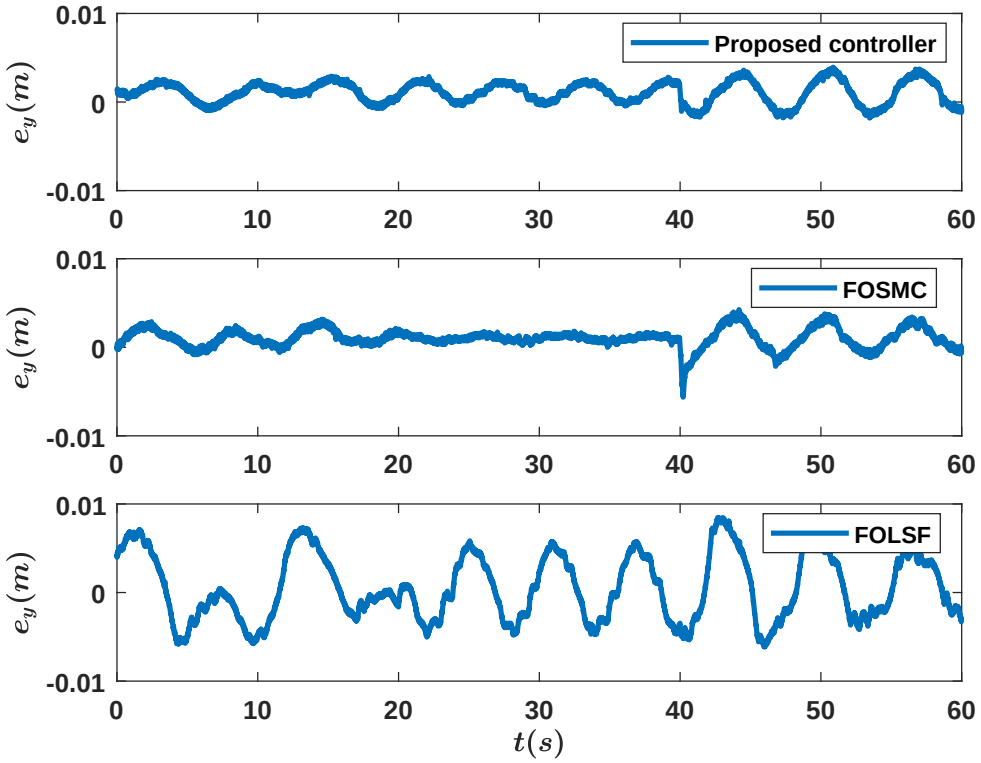

Figure 5.4 – Tracking error e_y (m) versus time (s) for controller (2.15)-(2.16) (**Top**), FOSMC (**Middle**) and FOLSF (**Bottom**).

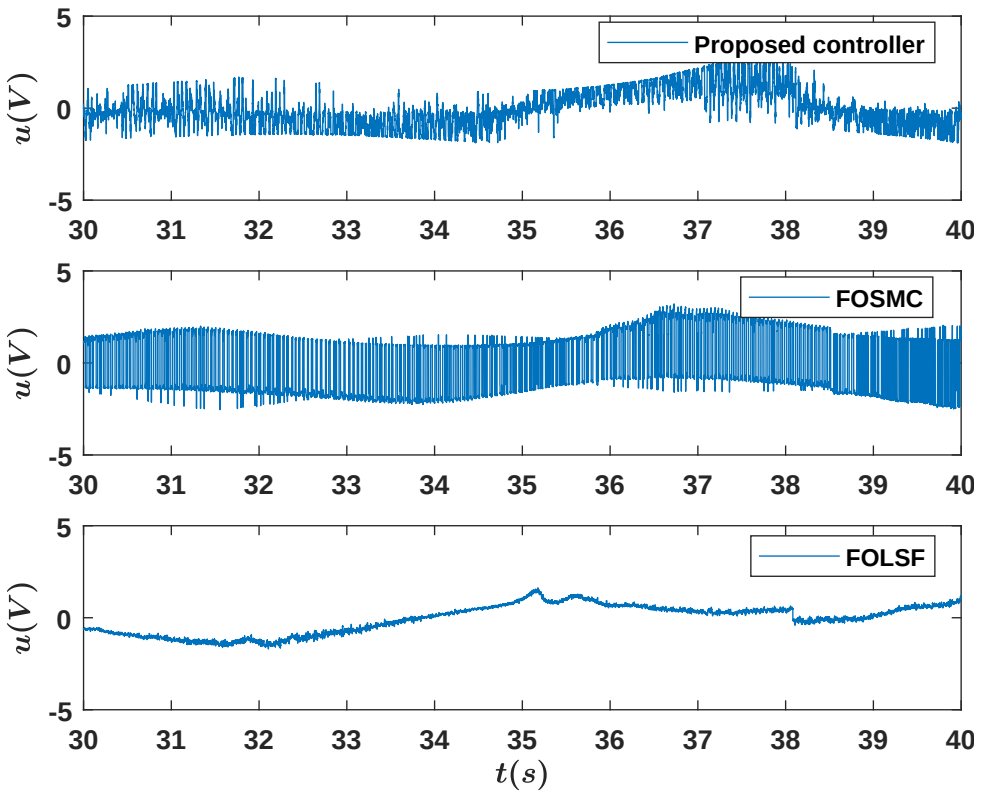

Figure 5.5 – Control input u (V) versus time (s) for controller (2.15)-(2.16) (**Top**), FOSMC (**Middle**) and FOLSF (**Bottom**) for $30 \leq t \leq 40s$.

	Controller (2.15)-(2.16)	FOSMC ($\alpha = 0$)	FOLSF ($\alpha = 1$)
Energy $\mathcal{E}$	63.61	173.94	56.61
Mean($\lvert e_y \rvert$)	$1.36 \cdot 10^{-3}$	$1.25 \cdot 10^{-3}$	$5.98 \cdot 10^{-3}$
$var(u)$	$1.23 \cdot 10^{4}$	$2.22 \cdot 10^{4}$	$2.46 \cdot 10^{3}$
Mean(α)	0.43		

Table 5.1 – Energy $\mathcal{E}$, average value of the tracking error $|e_y|$, standard deviation of u and average value of α with controller (2.15)-(2.16), FOSMC and FOLSF for $0 \leq t \leq 60$ s.

5.5 Experimental results

5.5.1 Controller with sliding variable relative degree equals 1

As it can be seen from Figure 5.4 and Table 5.1 (thanks to the average value of $|e_y|$), controller (2.15)-(2.16) and the FOSMC lead to a better tracking of the reference trajectory than the FOLSF.
As expected, from Figure 5.5 and Table 5.1, it appears that the consumed energy $\mathcal{E}$ evaluated for $0 \leq t \leq 60$ s by controller (2.15)-(2.16) is less than the consumed energy with the FOSMC and slightly greater than with the FOLSF. The average value (Figure 5.6) of α is 0.43; this means that even if $\alpha \neq 0$, the accuracy is kept at a very high level (see $mean(|e_y|)$ in Table 5.1). The indicator used to quantify the reduction of the chattering is the var function of the control input u: from Table 5.1, it can be seen that, thanks to the controller (2.15)-(2.16), $var(u)$ is much less than that of the FOSMC.
Note that in the 3 cases, as seen in Figure 5.7, the pressures p_N and p_N are well within their operating domain $1\ bar \leq p_N \leq 7\ bar, 1\ bar \leq p_P \leq 7\ bar$ (see (5.3)).

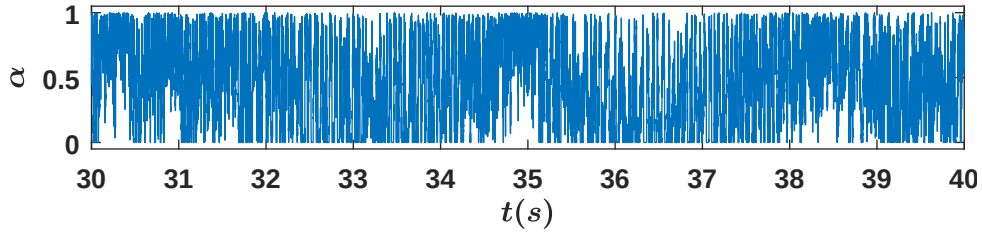

Figure 5.6 – Parameter α versus time (s) for $30 \leq t \leq 40s$ with controller (2.15)-(2.16).

5.5.2 Controller with sliding variable relative degree equals 2

Similar conclusions can be deduced when controllers (3.32)-(3.33), TWC, SOLSF are applied. Controller (3.32)-(3.33) induces a better accuracy than the SOLSF and a similar one with respect to TWC (see Figure 5.8 and Table 5.2). Moreover, the energy consumption and $var(u)$ due to the controller (3.32)-(3.33) are less than those obtained with the TWC. This means that controller (3.32)-(3.33) is less energy consuming and with less chattering, that is confirmed by Figure 5.9 and Table 5.2. The evolution of α with controller (3.32)-(3.33) is depicted Figure 5.10 for $30 \leq t \leq 40s$ and induces an average value of 0.33 (see Table 5.2): high accuracy can be achieved with $\alpha \neq 0$.
Notice that the pressures p_N and p_N are well within their operating domain (see (5.3)

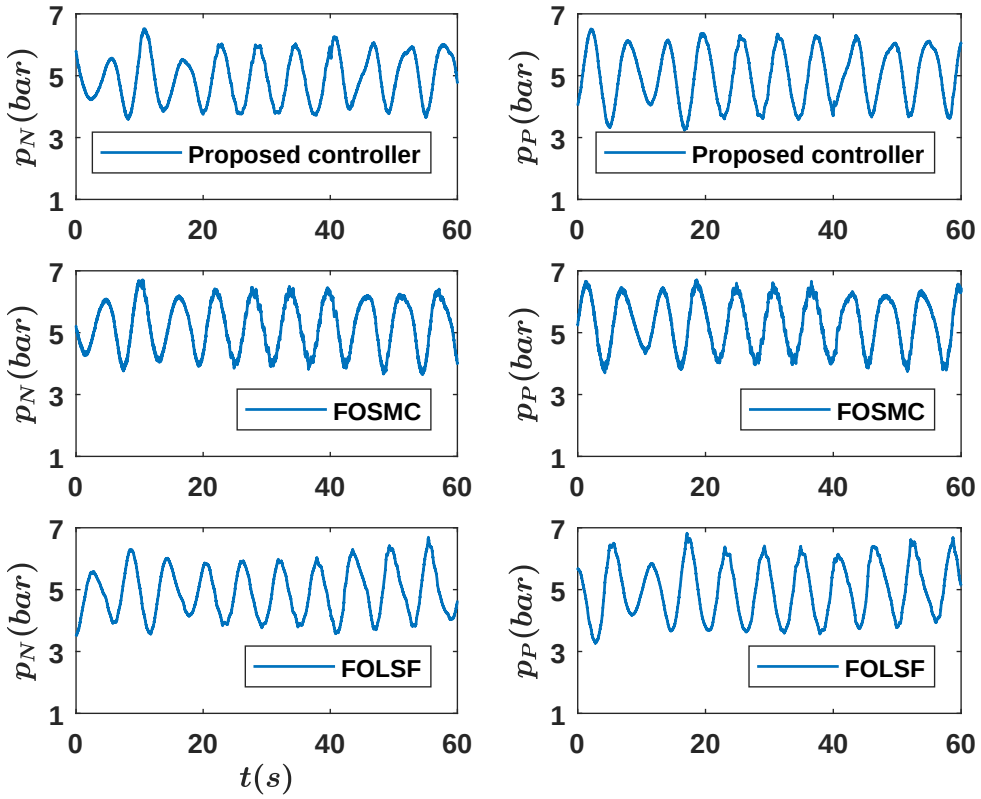

Figure 5.7 – **Left** pressure $p_N(bar)$ versus time (s) **Right** pressure $p_P(bar)$ versus time (s) for controller (2.15)-(2.16) (**Top**), FOSMC (**Middle**) and FOLSF (**Bottom**).

and Figure 5.11). Notice also that in case sliding mode control and variable α approach are applied to the system, the accuracy of the closed loop system is improved when σ is designed such that $r = 2$ with respect to when σ is designed such that $r = 1$ (see Figures 5.4 and 5.8 and $mean(|e_y|)$ in Tables 5.1 and 5.2).

	Controller (3.32)-(3.33)	TWC ($\alpha = 0$)	SOLSF ($\alpha = 1$)
Energy $\mathcal{E}$	237.45	431.17	35.45
$Mean(\|e_y\|)$	$5.25 \cdot 10^{-4}$	$2.59 \cdot 10^{-4}$	$1.12 \cdot 10^{-2}$
$var(u)$	$1.66 \cdot 10^{5}$	$2.13 \cdot 10^{5}$	$3.99 \cdot 10^{4}$
$Mean(\alpha)$	0.33		

Table 5.2 – Energy $\mathcal{E}$, average value of the tracking error $|e_y|$, standard deviation of u and average value of α for controller (3.32)-(3.33), TWC and SOLSF for $0 \leq t \leq 60$ s.

5.6 Conclusion

This chapter deals with the position control problem of an electropneumatic system which is an uncertain and perturbed nonlinear system. It also shows the applicability of the control methods developed in this thesis to real physical systems. The main contributions are:

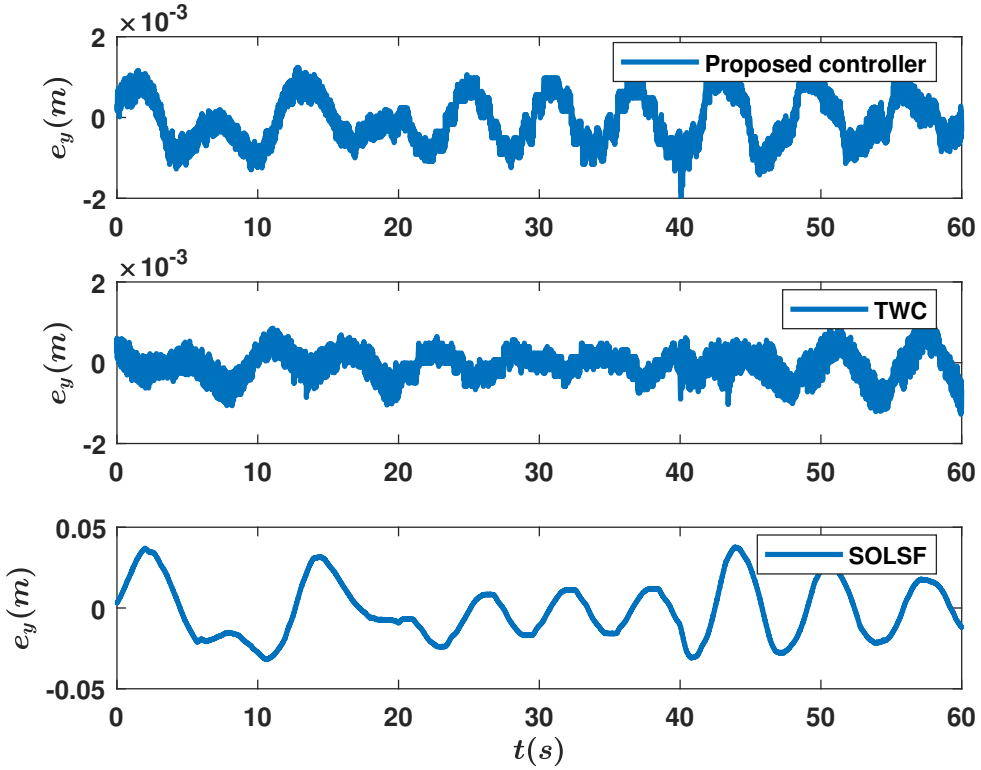

Figure 5.8 – Tracking error e_y (m) versus time (s) for controller (3.32)-(3.33) (**Top**), TWC (**Middle**) and SOLSF (**Bottom**).

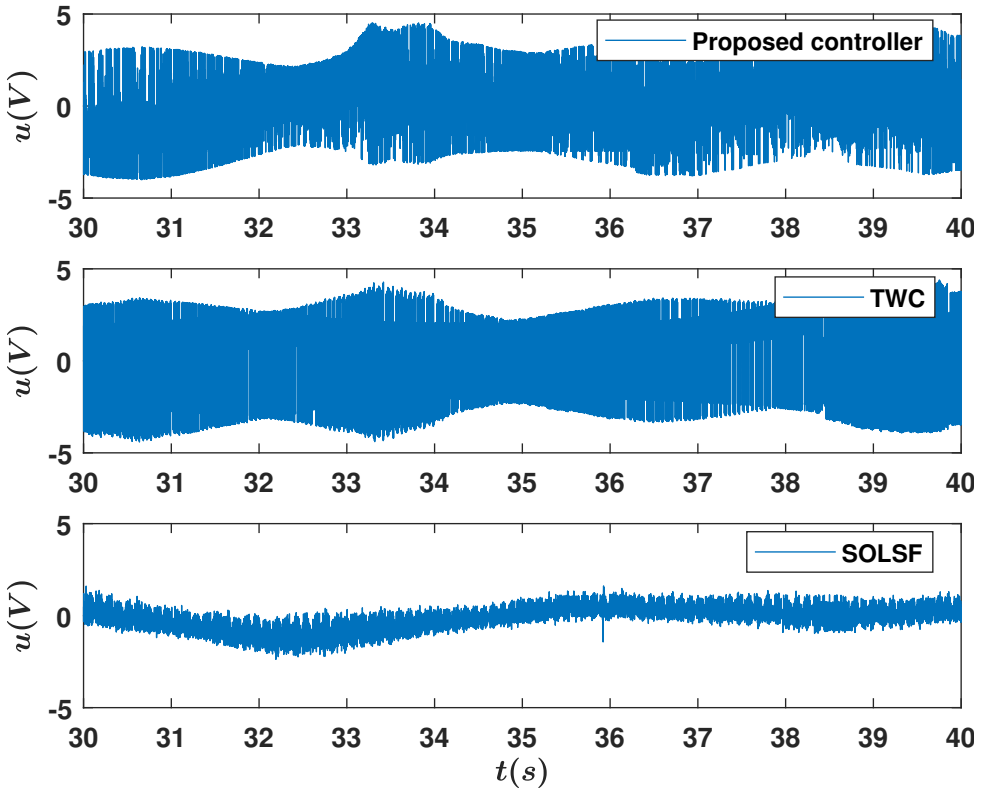

Figure 5.9 – Control input u (V) versus time (s) for controller (3.32)-(3.33) (**Top**), TWC (**Middle**) and SOLSF (**Bottom**) for $30 \leq t \leq 40s$.

- the design of two controllers based on the first order controller (2.15)-(2.16) and

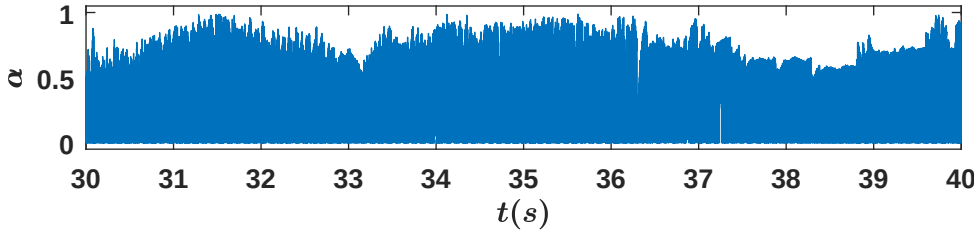

Figure 5.10 – Parameter α versus time (s) for $30 \leq t \leq 40s$ with controller (3.32)-(3.33).

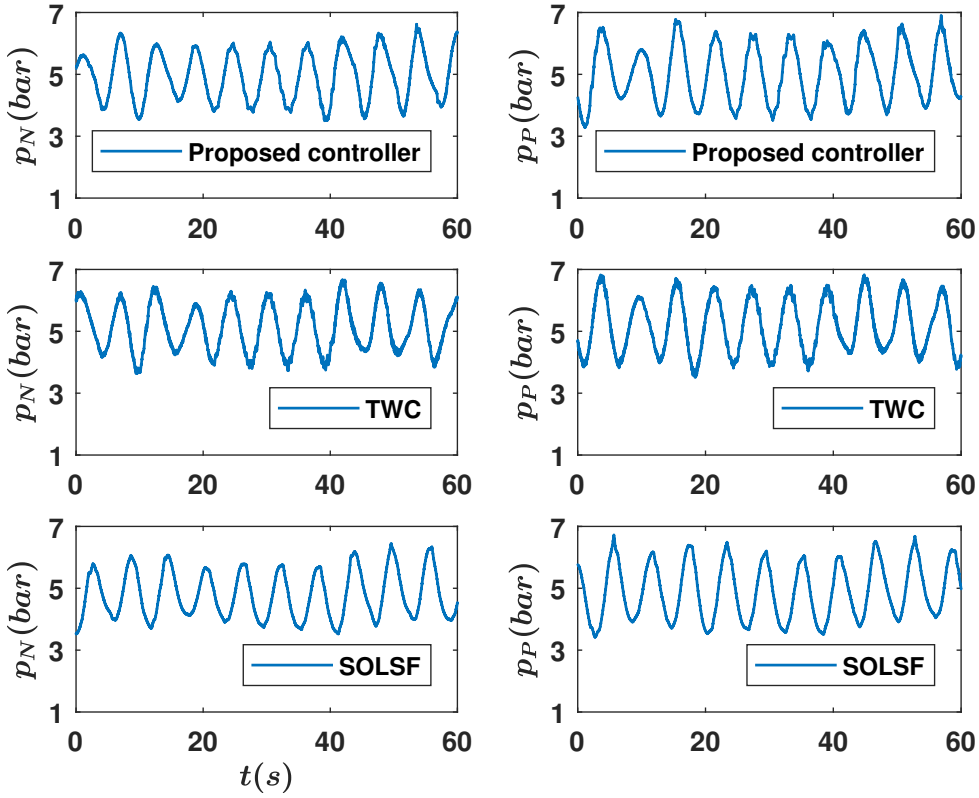

Figure 5.11 – **Left** pressure $P_N(bar)$ versus time (s) **Right** pressure $p_P(bar)$ versus time (s) for controller (3.32)-(3.33) (**Top**), TWC (**Middle**) and SOLSF (**Bottom**).

the second order controller (3.32)-(3.33) for the aforementioned electropneumatic actuator.

- the experimental implementation of the two previously mentioned controllers. The proposed first order (resp. second order) controllers performances are compared to FOSMC (resp. TWC) and FOLSF (resp. SOLSF).
- the proposed controllers allow to obtain high accuracy position tracking with reduced chattering and energy consumption.

6

Application to a twin wind turbine

Contents

6.1 Introduction

Fossil fuels produce three quarters of the world's energy. However, the burning of fossil fuels releases carbon dioxide, one of the main greenhouse gases, considered to be partly responsible for global warming. Given this problem, associated with the scarcity of fossil fuels, it is imperative to switch to other means to produce energy. Thus, renewable energy sources such as wind turbines offer great potential for a massive reduction of carbon dioxide emissions and decrease the dependency of the energy market on fossil fuels.
An original structure of twin wind turbines (TWT),named SEREO [4], is considered in this chapter. It includes two identical wind turbines ridden on the same tower that can pivot freely in front of the wind with no additional actuator. Therefore, the motion of the arms carrying the TWT is free. The rotation motion is performed by creating a difference between the drag forces of both wind turbines, this difference inducing the yaw motion.
The advantages of such structure versus traditional wind turbines are

- given that there is no yaw actuation, failures risks are reduced, as well as maintenance;
- furthermore, on a same tower, two turbines are available. For a given nominal power for the whole system, especially for the large power turbines (>10 MW), it is more interesting by a weight point-of-view to have two turbines, than only a single one.

The objective of this chapter is the design of a control strategy to align the turbines face the wind while having maximal power production. This is performed by controlling the rotor speed of the TWT and the yaw rotation without the use of a yaw actuator. The

control strategy is based on controller (4.7)-(4.8) presented in Chapter 4. Two aspects of the control are considered

- **mechanical:** controlling the yaw motion of the structure in order to force it face the wind by acting on the blade pitch angle of both twin turbines;
- **electrical:** forcing the direct current of both generators to 0 for the limitation of the ripple effect on the electromagnetic torque and controlling the angular velocities of both generators in order to optimize the electrical power output. This is achieved by acting on the direct and quadrature stator voltages.

As it will be explained in the sequel, once the system is decoupled, the relative degree vector of the system is composed of elements equal to 1, 2 and 3. This fact makes the control strategy proposed in Chapter 4, ideal given that the proposed controller has no restriction on the relative degree.

6.2 System description

The SEREO Twin Wind Turbine (see Figures 6.1 and 6.2) includes two identical wind turbines mounted on the same tower. It can rotate face the wind without a yaw driving motor. Given that the motion of the arms carrying the TWT is free, the yaw motion is induced by creating a difference between the drag forces of both wind turbines. This difference is created by acting on the blade pitch angles. The idea is to create a difference between the blade pitch angles of both wind turbines around their optimal value in order to generate a difference of drag forces, and therefore a yaw motion.

Figure 6.1 – SEREO structure [4] composed of twin wind turbines.

The SEREO system can be written as a nonlinear system affine with respect to the control input vector [67]

$$\dot{x} = f(x) + g(x) \cdot u \tag{6.1}$$

with x the state vector and u the input vector respectively defined as

$$\begin{aligned} x &= \begin{bmatrix} \beta_1 & \beta_2 & \psi & \dot{\psi} & i_{d1} & i_{q1} & \Omega_1 & i_{d2} & i_{q2} & \Omega_2 \end{bmatrix}^T, \\ u &= \begin{bmatrix} \Delta\beta_1 & \Delta\beta_2 & V_{d1} & V_{q1} & V_{d2} & V_{q2} \end{bmatrix}^T, \end{aligned} \tag{6.2}$$

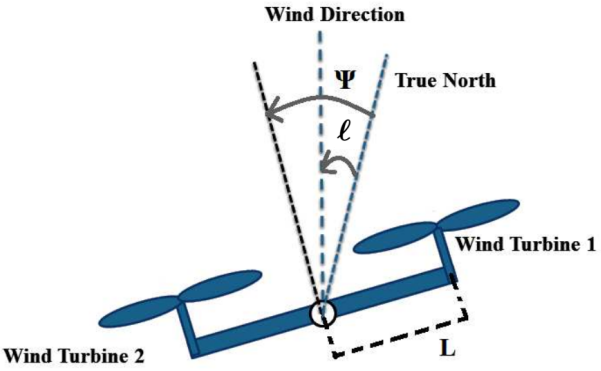

Figure 6.2 – Simplified model of the twin wind turbines (view from the top).

the vector $f(x)$ and the matrix $g(x)$ reading as

$$f(x) = \begin{bmatrix} \frac{1}{T_{\beta 1}}(\beta_1^{opt} - \beta_1) \\ \frac{1}{T_{\beta 2}}(\beta_2^{opt} - \beta_2) \\ \dot{\psi} \\ \frac{1}{K_r}\left(-D_r\ \dot{\psi} + (F_{d,1} - F_{d,2})\ L\right) \\ \frac{-R_s}{L_d}\, i_{\mathrm{d}1} + \frac{pL_q}{L_d}\, i_{\mathrm{q}1}\, \Omega_1 \\ \frac{-R_s}{L_q}\, i_{\mathrm{q}1} - \frac{pL_d}{L_q}\, i_{\mathrm{d}1}\, \Omega_1 - \frac{p\phi_f}{L_q}\, \Omega_1 \\ \frac{1}{J}\Gamma_{a1}(\beta_1, \Omega_1, \psi) - \frac{p\phi_f}{J}\, i_{\mathrm{q}1} - \frac{p(L_d - L_q)}{J}\, i_{\mathrm{d}1}\, i_{\mathrm{q}1} - \frac{f_v}{J}\, \Omega_1 \\ \frac{-R_s}{L_d}\, i_{\mathrm{d}2} + \frac{pL_q}{L_d}\, i_{\mathrm{q}2}\, \Omega_2 \\ \frac{-R_s}{L_q}\, i_{\mathrm{q}2} - \frac{pL_d}{L_q}\, i_{\mathrm{d}2}\, \Omega_2 - \frac{p\phi_f}{L_q}\, \Omega_2 \\ \frac{1}{J}\Gamma_{a2}(\beta_2, \Omega_2, \psi) - \frac{p\phi_f}{J}\, i_{\mathrm{q}2} - \frac{p(L_d - L_q)}{J}\, i_{\mathrm{d}2}\, i_{\mathrm{q}2} - \frac{f_v}{J}\, \Omega_2 \end{bmatrix} \tag{6.3}$$

$$g(x) = \begin{bmatrix} \frac{1}{T_{\beta 1}} & 0 & 0 & 0 & 0 & 0 \\ 0 & \frac{1}{T_{\beta 2}} & 0 & 0 & 0 & 0 \\ 0 & 0 & 0 & 0 & 0 & 0 \\ 0 & 0 & 0 & 0 & 0 & 0 \\ 0 & 0 & \frac{1}{L_d} & 0 & 0 & 0 \\ 0 & 0 & 0 & \frac{1}{L_q} & 0 & 0 \\ 0 & 0 & 0 & 0 & 0 & 0 \\ 0 & 0 & 0 & 0 & \frac{1}{L_d} & 0 \\ 0 & 0 & 0 & 0 & 0 & \frac{1}{L_q} \\ 0 & 0 & 0 & 0 & 0 & 0 \end{bmatrix}, \tag{6.4}$$

where

- the first two equations are the pitch angle dynamics with β_i ($i \in \{1, 2\}$ being the number of the wind turbine) the pitch angles, β_i^{opt} the optimal pitch angle giving maximum power output and considered constant (see Table 6.1) and $T_{\beta i}$ the time constant of the blades actuation systems. $\Delta\beta_i$ is the control input controlling the rotation of the structure. This latter can be viewed as the difference between β_i^{opt} and β_i.
- the third and fourth equations are yaw-dynamics with K_r and D_r the inertia moment and the friction coefficient, respectively, associated to the yaw motion and L the distance between each hub and the tower axis (see Figure 6.2). The drag forces $F_{d,i}$ are given as

$$F_{d,i} = \frac{1}{2}\rho\pi(RV\cos(\psi - \ell))^2 C_{d,i} \tag{6.5}$$

  with R the radius of the wind turbines blades, ρ the air density, V the wind velocity. ℓ (resp. ψ) is the angle between the True North and the wind direction (resp. the orientation of the wind turbines defined by an axis that is perpendicular to the arm connecting the two turbines) (see Figure 6.2) and $C_{d,i}$ the drag force coefficient which is a nonlinear function of the tip-speed ratio (TSR), λ_i, and the pitch angle [68]. λ_i is defined as

$$\lambda_i = \frac{\Omega_i}{Vcos(\psi - \ell)}R, \tag{6.6}$$

  with Ω_i being the rotational speed of the turbine.
- the last six equations represent the electrical model with Ω_i the rotational speed, Γ_{ai} the aerodynamic torque, $i_{di}, i_{qi}, V_{di}, V_{qi}$ respectively the direct/quadrature currents and voltages, L_d, L_q the dq-axis inductances, R_s the stator resistance, p the number of pole pairs, ϕ_f the permanent-magnet flux, J the total inertia and f_v the friction coefficient. Note that the considered generator for each twin turbine is a permanent magnet synchronous generator (PMSG).

As detailed in the sequel, rotational velocities Ω_1 and Ω_2 are forced to follow the same reference value Ω^* for a given optimal TSR λ_{opt} *i.e.* the tip speed ratio giving the optimal

power production (considered constant, see Table 6.1). Therefore, one considers that Ω_1 and Ω_2 are almost the same. Hence, one has

$$\lambda_1 \approx \lambda_2 \approx \lambda \text{ and } \beta_1^{opt} \approx \beta_2^{opt} \approx \beta^{opt}. \tag{6.7}$$

Given that the rotation is made thanks to $F_{d,1}$ and $F_{d,2}$, one states a symmetric behavior by considering $\Delta\beta_1 = -\Delta\beta_2 = \Delta\beta$. Therefore, define the new control input $\bar{u}$ as

$$\bar{u} = \begin{bmatrix} \Delta\beta & V_{d1} & V_{q1} & V_{d2} & V_{q2} \end{bmatrix}^T \tag{6.8}$$

The input u (6.2) is a 6×1 vector whereas $\bar{u}$ (6.8) is a 5×1-vector, these two vectors being linearly linked by

$$u = \begin{bmatrix} 1 & 0 & 0 & 0 & 0 \\ -1 & 0 & 0 & 0 & 0 \\ 0 & 1 & 0 & 0 & 0 \\ 0 & 0 & 1 & 0 & 0 \\ 0 & 0 & 0 & 1 & 0 \\ 0 & 0 & 0 & 0 & 1 \end{bmatrix} \cdot \bar{u}. \tag{6.9}$$

Mechanical parameters		**Parameters of PMSG**	
Blade radius R	39 m	Rated power	2 MW
Air density ρ	1.205 kg/m^3	Stator resistance R_s	50 $\mu\Omega$
Rated wind speed	12 m/s	d axis inductance L_d	0.0055 H
Maximum power coefficient	0.4	q axis inductance L_q	0.00375 H
Total inertia J	10,000 $kg\,m^2$	pole pairs number p	11
Yaw inertia K_r	$5 \cdot 10^5$ $kg\,m^2$	field flux ϕ_f	136.25 Wb
Yaw friction coefficient D_r	200 $N\,m\,/(rad/s)$		
Length L	40 m		
Optimal blade pitch angle β_{opt}	2 °		
Optimal TSR λ_{opt}	7.3		

Table 6.1 – Parameters of the wind turbines.

6.3 Control objective

In this case study, one considers that the TWT is operating in Region II *i.e.* the wind speed $V \in [V_{min},\ V_n]$ with V_{min} being the minimal wind velocity for which the rotors of the TWT start to spin and V_n being a nominal value [69]. Then, the primary control objective is to ensure that the SEREO Twin Wind Turbines has optimal power production. This objective is achieved by orienting the structure face the wind, while each turbine must operate at its maximum conversion efficiency. Therefore, a yaw angle control is required to maintain the nacelle at optimal orientation [70], together with a MPPT control setup acting on the turbines rotational speeds. Then, three control problems have to be managed and can be summarized as follows

- to force the structure to be face the wind, *i.e.* control $\psi - \ell$ to 0; when it is not the case, the pitch angles of the two wind turbines blades must be changed to produce a difference between the drag forces F_{d1} and F_{d2}. Thanks to this difference, a yawing torque is induced forcing the rotating motion;

- to control the angular velocities of the wind turbines, in order to optimize the electrical power. This is achieved by keeping their tip-speed ratios at their optimal values λ_{opt}, for given pitch angles of the wind turbines blades. Therefore, the rotational speeds of both wind turbines are controlled at a reference

$$\Omega^* = \frac{V\cos(\psi - \ell)}{R}\,\lambda_{opt}, \tag{6.10}$$

- to force the direct currents of both generators $i_{d,1}$ and $i_{d,2}$ to 0 in order to avoid the ripple effects on the electromagnetic torque, which may increase the fatigue loads in the mechanical shaft of the wind turbine and affect the produced power.

6.4 Control design

The control objective described above is now applied to the TWT structure described in Section 6.2. The control strategy is designed from the nonlinear system (6.1). Firstly, given the control objectives displayed in the previous section, the output vector is defined as

$$y = \begin{bmatrix} y_\psi \\ y_{\Omega_1} \\ y_{i_{d1}} \\ y_{\Omega_2} \\ y_{i_{d2}} \end{bmatrix} = \begin{bmatrix} \psi - \ell \\ \Omega_1 - \Omega^* \\ i_{d1} \\ \Omega_2 - \Omega^* \\ i_{d2} \end{bmatrix}. \tag{6.11}$$

Consider that each element of y corresponds to a sliding variable. Then, the control objective is to force each sliding variable, then each component of y, to a vicinity of 0 in a finite time.

The relative degree of y_ψ of system (6.1) is equal to 3 such that

$$y_\psi^{(3)} = \Theta_1(x,t) + \Lambda_1(x,t)\cdot\Delta\beta \tag{6.12}$$

The relative degree of y_{Ω_1} and y_{Ω_2} of (6.1) is 2 such that

$$\begin{aligned} \ddot{y}_{\Omega_1} &= \Theta_2(x,t) + \Lambda_{2,1}(x,t)\cdot V_{d1} + \Lambda_{2,2}(x,t)\cdot V_{q1} \\ \ddot{y}_{\Omega_2} &= \Theta_4(x,t) + \Lambda_{4,1}(x,t)\cdot V_{d2} + \Lambda_{4,2}(x,t)\cdot V_{q2} \end{aligned} \tag{6.13}$$

whereas the relative degree of i_{d1} and i_{d2} is 1 given that

$$\begin{aligned} \dot{y}_{i_{d1}} &= \Theta_3(x,t) + \Lambda_3(x,t)\cdot V_{d1} \\ \dot{y}_{i_{d2}} &= \Theta_5(x,t) + \Lambda_5(x,t)\cdot V_{d2} \end{aligned} \tag{6.14}$$

Then, one gets

$$\begin{bmatrix} y_\psi^{(3)} \\ \ddot{y}_{\Omega_1} \\ \dot{y}_{i_{d1}} \\ \ddot{y}_{\Omega_2} \\ \dot{y}_{i_{d2}} \end{bmatrix} = \Theta(x,t) + \Lambda(x,t)\cdot\bar{u} \tag{6.15}$$

where

$$\Theta(x,t) = \begin{bmatrix} \Theta_1(x,t) \\ \Theta_2(x,t) \\ \Theta_3(x,t) \\ \Theta_4(x,t) \\ \Theta_5(x,t) \end{bmatrix} \text{ and } \Lambda(x,t) = \begin{bmatrix} \Lambda_1(x,t) & 0 & 0 & 0 & 0 \\ 0 & \Lambda_{2,1}(x,t) & \Lambda_{2,2}(x,t) & 0 & 0 \\ 0 & \Lambda_3(x,t) & 0 & 0 & 0 \\ 0 & 0 & 0 & \Lambda_{4,1}(x,t) & \Lambda_{4,2}(x,t) \\ 0 & 0 & 0 & 0 & \Lambda_5(x,t) \end{bmatrix}$$

the expressions of $\Theta(x,t)$ and $\Lambda(x,t)$ being given in Appendix C.

The parameters on which uncertainties have been considered are the inductance L_d, the stator resistance R_s and the drag force coefficients $C_{d,i}$. Therefore, each of these parameters can be divided into a nominal part and an uncertain one. Subsequently, $\Theta(x,t)$ and $\Lambda(x,t)$ can be written as follows

$$\Theta(x,t) = \bar{\Theta}(x,t) + \Delta\Theta(x,t), \quad \Lambda(x,t) = \bar{\Lambda}(x,t) + \Delta\Lambda(x,t) \tag{6.16}$$

where $\bar{\Theta}(x,t)$ and $\bar{\Lambda}(x,t)$ are the nominal (known) parts of $\Theta(x,t)$ and $\Lambda(x,t)$, respectively, and $\Delta\Theta(x,t)$ and $\Delta\Lambda(x,t)$ are the uncertain (unknown) parts, respectively. Define the control input $\bar{u}$ as

$$\bar{u} = \Big[\bar{\Lambda}(x,t)\Big]^{-1}\Big[-\bar{\Theta}(x,t) + \vartheta\Big] \tag{6.17}$$

which gives

$$\begin{bmatrix} y_\psi^{(3)} \\ \ddot{y}_{\Omega_1} \\ \dot{y}_{i_{d1}} \\ \ddot{y}_{\Omega_2} \\ \dot{y}_{i_{d2}} \end{bmatrix} = \underbrace{\Big(\Delta\Theta(x,t) - \bar{\Lambda}(x,t)^{-1}\bar{\Theta}(x,t)\Delta\varphi_2\Big)}_{\varphi_1} + \underbrace{\Big(I_{5\times5} + \bar{\Lambda}(x,t)^{-1}\Delta\Lambda(x,t)_2\Big)}_{\varphi_2}\vartheta \tag{6.18}$$

The matrix $\Lambda(x,t)$ and its nominal value $\Lambda_N(x,t)$ are invertible if

$$\psi - \ell \neq (\pm 2k+1)\frac{\pi}{2} \tag{6.19}$$

with $k \in \mathbb{N}$. This condition corresponds to the case that the wind direction is not strictly parallel to the arm linking the two wind turbines: in that case, difference of drag force cannot be created. Hence, one considers that condition (6.19) is satisfied.
It is reasonable to consider that the parametric uncertainties have limited magnitudes with respect to the nominal values, which gives that φ_2 is a diagonally dominate matrix. It means that, thanks to the control law (6.17), dynamics of (6.15) is almost decoupled. It also gives that φ_1 and φ_2 are bounded satisfying Assumption 4.2. Finally, the new control input reads as (See Section 4.3 and (4.7)-(4.8))

$$\vartheta = \begin{bmatrix} -k_\psi \lceil S_\psi \rfloor^{\alpha_\psi} \\ -k_{\Omega 1}\lceil S_{\Omega_1} \rfloor^{\alpha_{\Omega_1}} \\ -k_{d1}\lceil S_{i_{d1}} \rfloor^{\alpha_{i_{d1}}} \\ -k_{\Omega 2} \lceil S_{\Omega_2} \rfloor^{\alpha_{\Omega_2}} \\ -k_{d2} \lceil S_{i_{d2}} \rfloor^{\alpha_{i_{d2}}} \end{bmatrix}. \tag{6.20}$$

Accordingly with the output relative degree

- S_ψ and α_ψ are calculated following (4.7)-(4.8) respectively where S_ψ corresponds to ξ_r for $r = 3$ and z_1 corresponds to y_ψ. *i.e.*

$$\begin{aligned} S_\psi &= \lceil \ddot{y}_\psi \rfloor^3 + k_2^3(\lceil \dot{y}_\psi \rfloor^{\frac{3}{2}} + k_1^{\frac{3}{2}} y_\psi), \\ \alpha_\psi &= max(-\beta(\frac{|\ddot{y}_\psi|}{|\ddot{y}_\psi| + \varepsilon_{\ddot{y}_\psi}} + \frac{|\dot{y}_\psi|}{|\dot{y}_\psi| + \varepsilon_{\dot{y}_\psi}} + \frac{|y_\psi|}{|y_\psi| + \varepsilon_{y_\psi}}) + 1, 0) \end{aligned} \tag{6.21}$$

- S_{Ω_1} and α_{Ω_1} (respectively S_{Ω_2} and α_{Ω_2}) are calculated for $r = 2$ where $z_1 = y_{\Omega_1}$ (respectively $z_1 = y_{\Omega_2}$) *i.e.*

$$\begin{aligned} S_{\Omega_1} &= \lceil \dot{y}_{\Omega_1} \rfloor^2 + k_1^2 y_{\Omega_1}, \quad \alpha_{\Omega_1} = max(-\beta(\frac{|\dot{y}_{\Omega_1}|}{|\dot{y}_{\Omega_1}| + \varepsilon_{\dot{y}_{\Omega_1}}} + \frac{|y_{\Omega_1}|}{|y_{\Omega_1}| + \varepsilon_{y_{\Omega_1}}}) + 1, 0) \\ S_{\Omega_2} &= \lceil \dot{y}_{\Omega_2} \rfloor^2 + k_1^2 y_{\Omega_2}, \quad \alpha_{\Omega_2} = max(-\beta(\frac{|\dot{y}_{\Omega_2}|}{|\dot{y}_{\Omega_2}| + \varepsilon_{\dot{y}_{\Omega_2}}} + \frac{|y_{\Omega_2}|}{|y_{\Omega_2}| + \varepsilon_{y_{\Omega_2}}}) + 1, 0) \end{aligned} \tag{6.22}$$

- $S_{i_{d1}}$ and $\alpha_{i_{d1}}$ (respectively $S_{i_{d2}}$ and $\alpha_{i_{d2}}$) are calculated for $r = 1$ where $z_1 = y_{i_{d1}}$ (respectively $z_1 = y_{i_{d2}}$) *i.e.*

$$\begin{aligned} S_{i_{d1}} &= y_{i_{d1}}, \quad \alpha_{i_{d1}} = max(-\beta\frac{|y_{i_{d1}}|}{|y_{i_{d1}}| + \varepsilon_{y_{\Omega_1}}}) + 1, 0) \\ S_{i_{d2}} &= y_{i_{d2}}, \quad \alpha_{i_{d2}} = max(-\beta\frac{|y_{i_{d2}}|}{|y_{i_{d2}}| + \varepsilon_{y_{\Omega_2}}}) + 1, 0) \end{aligned} \tag{6.23}$$

The output vector y converges to a vicinity of the origin in a finite time, by setting the gains sufficiently large following (4.6). The parameters tuning will be detailed in the next section.

6.5 Simulation results

The proposed controller is implemented on the twin wind turbine structure. The main parameters of the twin wind turbines [71] are listed in Table 6.1. Simulations have been performed using MATLAB/Simulink with sampling period $Te = 0.1ms$. The proposed controller is compared to the HOSMC presented in [29]:

$$\vartheta = \begin{bmatrix} -k_\psi \ \lceil S_\psi \rfloor^0 \\ -k_{\Omega 1} \lceil S_{\Omega_1} \rfloor^0 \\ -k_{d1} \lceil S_{i_{d1}} \rfloor^0 \\ -k_{\Omega 2} \ \lceil S_{\Omega_2} \rfloor^0 \\ -k_{d2} \ \lceil S_{i_{d2}} \rfloor^0 \end{bmatrix}. \tag{6.24}$$

with S_ψ, S_{Ω_1}, S_{Ω_2}, $S_{i_{d1}}$ and $S_{i_{d2}}$ defined as in (6.21), (6.22) and (6.23) respectively. The comparison is performed by evaluating different performances such as oscillations of the electromagnetic torques and the pitch angles, as well as the mean generated power. The indicator used to evaluate the oscillations is the function *var* defined as

$$var_{[\zeta_1,\zeta_2]}(h) = \sum_{i=0}^{N-1} |h(t_{i+1}) - h(t_i)| \tag{6.25}$$

where h is a real valued function and the set of instants $\{t_0, t_1, \cdots, t_N\}$ is a partition of $[\zeta_1, \zeta_2]$. Simulation results of wind turbine 1 are displayed only, since the ones obtained for

wind turbine 2 are similar. In order to check the behavior of the closed-loop system, the wind speed is modeled as

$$V = (V_m + V_d) \cdot \cos(\psi - \ell)$$

with V_m the mean wind speed set at 10 m/s, and V_d a time-varying term defined as a white noise. In order to test the robustness of the controllers to parametric uncertainties, a 20%-variation with respect to their nominal value is taken on R_s and L_d and a 50%-variation is taken on C_{di}. The parameters of the proposed controller are tuned as displayed in Table 6.2. Recall that controller (6.24) has the same structure as the proposed controller but with $\alpha = 0,\ \forall t > 0$. Hence, the latter's gains are taken equal to those of the proposed controller (see gain k_r in Table 6.2) for an effective performance comparison between the two. Also, this choice of the gains has been made as to ensure finite time convergence and good performances for both controllers.

Controlled variable	Gain k_r	β	ε_{z_1}	ε_{z_2}	ε_{z_3}
Yaw angle ($r = 3$)	2.2	1.1	$5 \cdot 10^{-5}$	10^{-3}	10^{-1}
Velocities Ω_1 and Ω_2 ($r = 2$)	100	11	$2 \cdot 10^{-1}$	5	-
Direct currents ($r = 1$)	10	11	$3 \cdot 10^{-3}$	-	-

Table 6.2 – Parameters of the proposed controller.

The wind direction ℓ changes between $10°$ and $-10°$ (Figure 6.3 - **Top**). When the wind direction is changing, the pitch angles β_1 and β_2 are actuated (Figure 6.3 - **Bottom**) in order to generate a drag force difference which engenders the rotation of the whole system (Figure 6.3 - **Top**). Notice that once the structure has been stabilized face the wind, $\beta_1 \simeq 2$.

Initially the value of α_ψ is equal to zero (see Figure 6.4 - **Left**): this is due to the fact that the yaw angle ψ does not track the wind direction ℓ; hence, $\alpha_\psi = 0$ forcing ψ to ℓ. When $\psi = \ell$, a steady state is attained ($10 < t < 35\ sec$), then α_ψ starts varying between 0 and 1 reducing the chattering phenomena. A similar logic can be applied to α_{Ω_1} (see Figure 6.4 - **Right**) and $\alpha_{i_{d1}}$ (in fact in this case $\alpha_{i_{d1}} = 1$ almost all the time meaning that the direct currents are not affected by the uncertainties considered in this simulation).

The reduction of the chattering in the steady state caused by the variation of α ($\alpha \neq 0$) is manifested by the reduction of the oscillations of the electromagnetic torque Γ_{em1} and the pitch angle β_1 (Figure 6.5 - **Bottom**, see Figure 6.3 - **Middle**, and $var(\Gamma_{em1})$ and $var(\beta_1)$ in Table 6.5) all while keeping good yaw tracking and optimal power production. This fact is important in decreasing the fatigue loads hence increasing the lifetime of the structure. Notice that controller (6.24) has a faster convergence to the required yaw angle than the proposed controller (see Figure 6.3 - **Top** $43 < t < 45\ sec$); however, it does not affect the mean power produced by the system (see power generated in Figure 6.5 and mean power in Table 6.3).

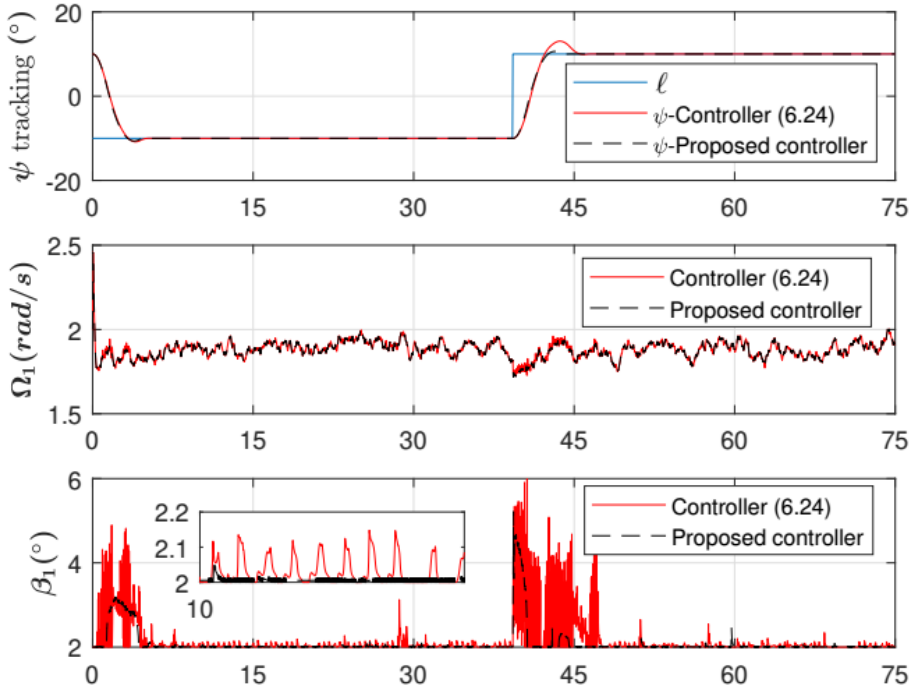

Figure 6.3 – Comparison controller (6.24) and the proposed controller - **Top** - Yaw angle tracking $\psi - \ell$ (°) versus time (sec). **Middle** -Rotational speed Ω_1 and rotational speed reference $\Omega^*(rad/s)$ versus time (sec). **Bottom** - Pitch angle for Wind Turbine 1 (°) versus time (sec).

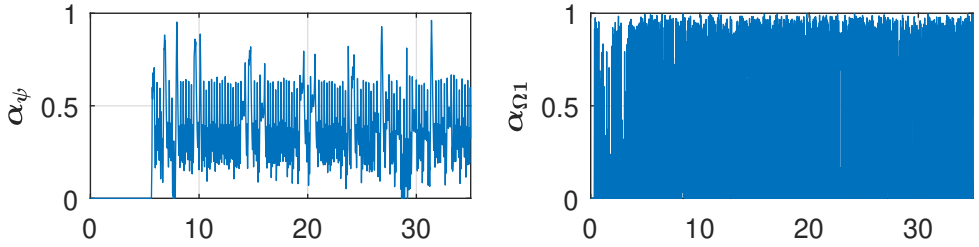

Figure 6.4 – **Left** - α_ψ versus time (sec). **Right** - α_{Ω_1} versus time (sec).

	Controller (6.24)	Proposed controller
$var(\Gamma_{em1})\,(N \cdot m)$	$9.487 \cdot 10^6$	$7.800 \cdot 10^6$
$var(\beta_1)\,(°)$	75.030	18.994
Mean power (W)	$1.153 \cdot 10^6$	$1.151 \cdot 10^6$

Table 6.3 – Comparison controller (6.24) and proposed controller - $var(\Gamma_{em1})\,(N \cdot m)$ and $var(\beta_1)\,(°)$ in the steady state $(10 < t < 35\ sec)$ and mean power.

6.6 Conclusion

This chapter deals with the control problem of a TWT which is a nonlinear perturbed system. The contributions in this Chapter can be summarized as follows:

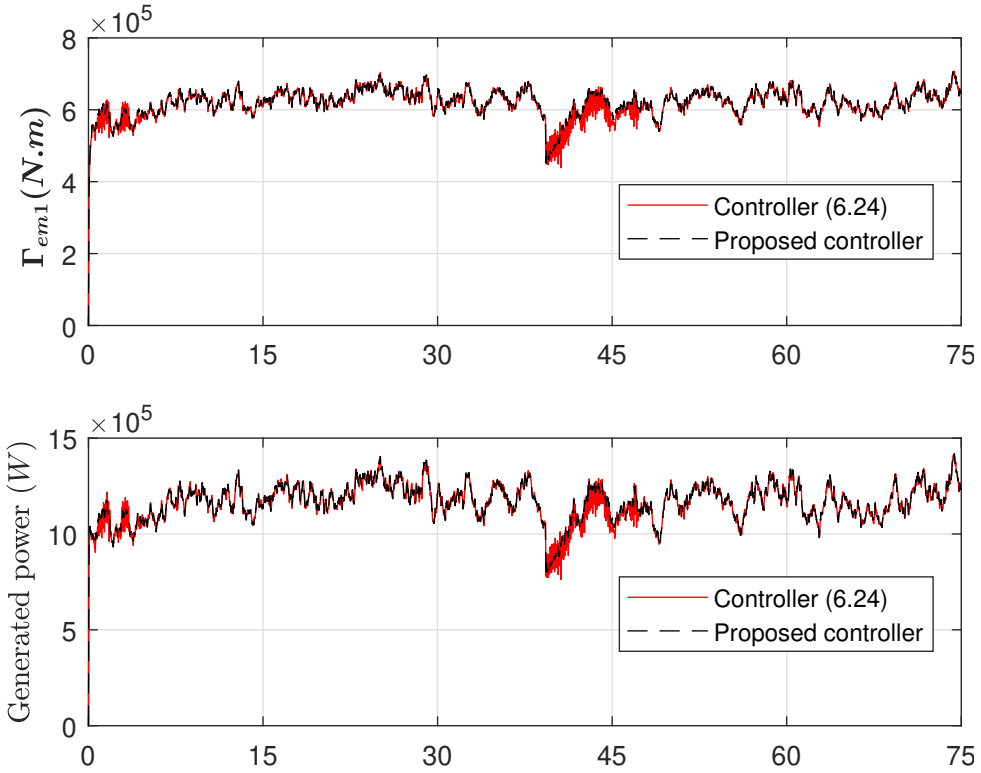

Figure 6.5 – Comparison controller (6.24) and the proposed controller - **Top** - Electromagnetic torque Γ_{em1} $(N.m)$ versus time (sec). **Bottom** - Generated power for Wind Turbine 1 (W) versus time (sec).

- the design and implementation of a controller based on controller (4.7)-(4.8) presented in Chapter 4 for the TWT is given;
- its performances are analyzed with respect to those of one based on controller [29].
- thanks to the proposed controller, high accuracy tracking of the TWT facing the wind is achieved with reduced oscillations of the electromagnetic torque and pitch angle. This is performed while keeping optimal energy production.

Concluding remarks and future works

In this thesis, new robust control schemes have been developed based on sliding mode control and linear approaches for nonlinear, perturbed and uncertain systems. The main idea, that is a novelty, is to use a time-varying parameter allowing to balance the control law between sliding mode control and the linear state feedback. The objectives are high accuracy, robustness and reduced chattering.

In Chapter 2, a controller for system whose relative degree is equal to 1 is proposed. It has the advantages of the standard first order sliding mode control (accuracy and robustness) and the first order linear state feedback (low energy consumption). This is done by varying a parameter α on the exponent term of the proposed controller. The stability of the closed-loop system is proved and the convergence domain size is calculated. The effectiveness of the proposed controller is shown via simulations and its performances for the control of an uncertain/perturbed system are compared to those of the first order sliding mode control, first order linear state feedback and saturation function. It allows high accuracy tracking with reduced chattering and energy consumption.

Moreover, **in Chapter 3**, a controller balancing between the twisting algorithm and second order linear state feedback is proposed. It combines high accuracy tracking with low energy consumption. It is shown that several variable approaches for α can be considered. Indeed, three approaches have been considered: switching, adaptive and algebraic. It is obvious that these different control laws implicate different closed loop performances such as accuracy and energy consumption. In the case of a sampled controller (finite switching frequency), it has been shown that the twisting algorithm converges to a domain that has been formally calculated for the first time. Simulations show the effectiveness of the proposed control methods versus twisting algorithm and second order linear state feedback. They allow high accuracy tracking with reduced energy consumption.

In Chapter 4, an algorithm for systems of arbitrary relative degree combining high accuracy and low energy consumption is presented. It is based on the higher order sliding mode control presented in [29]. It introduces the parameter α as an exponent of this controller, α being time-varying. Simulations showing the effectiveness of the proposed control are also given: the proposed controller allows high accuracy tracking with reduced energy consumption. A prospective on the variation of α inducing high closed-loop performances is also given.

Chapter 5 presents an application of several control laws to an experimental system. The position control problem of an electropneumatic system has been considered. This is a

typically nonlinear system with uncertainties and perturbations. The first order controller presented in Chapter 2 is applied to the system: it allows to obtain an efficient trade-off between the standard first order sliding mode control (high accuracy and robustness) and the first order linear state feedback (low energy consumption). Then, the second order controller with algebraic$-\alpha$ approach is implemented: high accuracy tracking is achieved with reduced chattering and energy consumption. Then, efficacy on a real system is established.

In Chapter 6, the control strategy developed in Chapter 4 is applied to a twin wind turbine. It ensures high accuracy tracking while decreasing the control effort and the chattering. The effectiveness of the new methodology for the control of a twin wind turbine is shown. The proposed control law ensures power output maximization, with reduced electromagnetic torque and limited pitch angle oscillations, resulting in the improvement of the structure lifetime.

Some works remain to be developed in the future. This includes in particular the following topics

- as discussed in Chapter 1, adaptive gain sliding mode control does not require the knowledge of the uncertainties and perturbations bounds. This is an interesting aspect of this control strategy given that the identification of these bounds is a hard task and often leads to overestimated gains which in its turn amplifies the chattering effect. Furthermore, experimental application of such control strategies has been proven effective for chattering attenuation. An interesting topic would be the coupling of two time-varying approaches for chattering attenuation: adaptive gain and variable exponent parameter. Indeed, it would allow to further attenuate the chattering effect without the knowledge of the uncertainties and perturbations bounds.
- in [72], research on variable exponent parameters applied to differentiators is performed. They have been applied to an mecatronic system in [73] Then, it would also be worth to further explore such differentiators (which is not treated in this thesis), couple them with time varying exponent controllers, to study the closed-loop stability and analyze the obtained performances.
- applications of the above strategies to an electropneumatic actuator and a twin wind turbine can also be envisioned. Future works can also be dedicated to apply the aforementioned control strategies to floating wind systems which have an increased implementation complexity. Notice that this kind of systems is nonlinear, uncertain and their models very difficult to establish. Then, floating wind turbines would be an interesting field of application of the proposed and further strategies.

Proof of Theorem 3.3

Recall system (3.1) with $\sigma-$dynamics reading as

$$\begin{aligned} \dot{z}_1 &= z_2 \\ \dot{z}_2 &= \bar{a}(x,t) + \bar{b}(x,t)u \end{aligned} \tag{A.1}$$

such that $\sigma = z_1$. Recalling the controller as

$$u = -k_1 \lceil z_1 \rfloor^{\frac{\alpha}{2-\alpha}} - k_2 \lceil z_2 \rfloor^{\alpha} \tag{A.2}$$

with α varying such that

$$\alpha = \max(-\beta(\frac{|z_1|}{|z_1| + \varepsilon_{a,z_1}} + \frac{|z_2|}{|z_2| + \varepsilon_{a,z_2}}) + 1\,,\, 0). \tag{A.3}$$

The objective is to prove the stability of the system when controlled by (A.2)-(A.3) and calculate the convergence domain. ■

From (A.3) one has that $\alpha = 0$ when

$$|z_2| \geq \frac{-(\beta-1)\varepsilon_{a,z_2}|z_1| + \varepsilon_{a,z_1}\varepsilon_{a,z_2}}{(2\beta-1)|z_1| + \varepsilon_{a,z_1}(\beta-1)}. \tag{A.4}$$

In other words, the TWC is applied when the trajectory of the system is outside $\mathcal{D}_a$ defined as (see $(\mathcal{D}_a)$ in Figure A.1)

$$\mathcal{D}_a = \left\{ (z_1, z_2) \mid |z_2| < \frac{-(\beta-1)\varepsilon_{a,z_2}|z_1| + \varepsilon_{a,z_1}\varepsilon_{a,z_2}}{(2\beta-1)|z_1| + \varepsilon_{a,z_1}(\beta-1)} \right\}. \tag{A.5}$$

Consider the general case such that the trajectory of the system is initially outside $\mathcal{D}_a$. Then, the TWC ($\alpha = 0$) is applied and the trajectory of the system will converge to $\mathcal{D}_a$ in finite time (see (3.8) and trajectory $O - O'$ in Figure A.1): the variation of α starts and α takes values in $(0, 1]$ following the first part of equation (A.3). Since $\alpha \neq 0$, the controller is less robust; furthermore, due to perturbations and uncertainties, the trajectory might potentially leave $\mathcal{D}_a$. However as soon as that happens, $\alpha = 0$ and the TWC is applied bringing back the trajectory to $\mathcal{D}_a$ and so on.

Therefore, the proof of Theorem 2 is outlined as follows

Step 1. Evaluation of the convergence boundary of the (z_1, z_2)-trajectory when this latter leaves $\mathcal{D}_a$ through the segments $\widehat{\text{GH}}$ or $\widehat{\text{IJ}}$.

Step 2. Evaluation of the convergence boundary of the (z_1, z_2)-trajectory when this latter leaves $\mathcal{D}_a$ through the segments $\widehat{\text{HI}}$ or $\widehat{\text{JG}}$.

Step 3. Calculation of the ultimate convergence boundary.

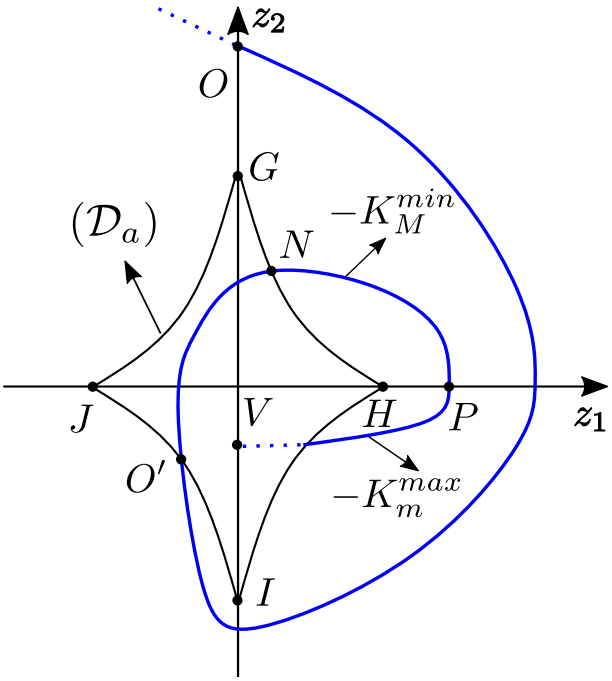

Figure A.1 – **Step 1** - Example of system trajectory in the phase plan (z_1, z_2).

Step 1. Suppose that the trajectory of the system leaves $\mathcal{D}_a$ passing through a point N on $\widehat{\text{GH}}$ (see trajectory $O' - N$ in Figure A.1). Then, from (A.5), the following relation exists between $z_1(N)$ and $z_2(N)$ [1]

$$z_1(N) = \frac{\varepsilon_{a,z_1}\varepsilon_{a,z_2} - (\beta-1)\varepsilon_{a,z_1} z_2(N)}{(2\beta-1)z_2(N) + \varepsilon_{a,z_2}(\beta-1)} \tag{A.6}$$

Consider $\dot{z}_2 = -K_M^{min}$. In fact, this case can be viewed as the "worst" case: indeed, it gives the most external trajectory from N, knowing that K_M^{min} is the smallest variation in absolute value of z_2 when the large gain of the controller is applied (see (3.19)). Note that while calculating the trajectory from N, one might find that the trajectory enters $\mathcal{D}_a$ again even before crossing the z_1-axis. In that case, the boundaries of z_1 and z_2 are

$$|z_1| \leq \frac{\varepsilon_{a,z_1}}{\beta-1}, \quad |z_2| \leq \frac{\varepsilon_{a,z_2}}{\beta-1}, \tag{A.7}$$

that correspond to the maximum values of z_1 and z_2 on $\widehat{\text{GH}}$ ($z_1(H)$ and $z_2(G)$ can be easily derived from (A.5)).
Now, the concern is to find the boundaries when the trajectory enters $\mathcal{D}_a$ after crossing the

1. With abuse of notation, $z_1(N)$ and $z_2(N)$ are respectively the values of z_1 and z_2 at the point N of the phase plan. These notations will be used throughout the paper.

z_1-axis at a point P such that $z_2(P) = 0$ (see trajectory $N - P$ in Figure A.1). Recalling that $\dot{z}_2 = -K_M^{min}$, the expression of $z_1(P)$ is

$$z_1(P) = \frac{z_2^2(N)}{2K_M^{min}} + z_1(N) \tag{A.8}$$

Combined with (A.6), the previous equation gives a relation between $z_1(P)$ and $z_2(N)$

$$z_1(P) = \frac{z_2^2(N)}{2K_M^{min}} + \frac{\varepsilon_{a,z_1}\varepsilon_{a,z_2} - (\beta-1)\varepsilon_{a,z_1} z_2(N)}{(2\beta-1)z_2(N) + \varepsilon_{a,z_2}(\beta-1)} \tag{A.9}$$

The objective is now to find for which value of $z_2(N)$ the value of $z_1(P)$ is maximal. Firstly, compute

$$\frac{\partial z_1(P)}{\partial z_2(N)} = \frac{\Gamma_1(z_2(N))}{\Lambda_1(z_2(N))} \tag{A.10}$$

with

$$\begin{aligned} \Gamma_1 =& (2\beta-1)^2 z_2^3(N) + 2\varepsilon_{a,z_2}(\beta-1)(2\beta-1)z_2^2(N) \\ &+ \varepsilon_{a,z_2}^2(\beta-1)^2 z_2(N) - \varepsilon_{a,z_1}\varepsilon_{a,z_2}\beta^2 K_M^{min} \\ \Lambda_1 =& K_M^{min}\Big[(2\beta-1)z_2(N) + \varepsilon_{a,z_2}(\beta-1)\Big]^2. \end{aligned} \tag{A.11}$$

Γ_1 has the same sign as (A.10) given that $\Lambda_1 > 0\ \forall z_2(N)$. Γ_1 is a third order polynomial versus $\dot{z}_1(N)$, its discriminant Δ_1 being

$$\begin{aligned} \Delta_1 =& -4\varepsilon_{a,z_1}\varepsilon_{a,z_2}^4(\beta-1)^3(2\beta-1)^3\beta^2 K_M^{min} \\ &- 27\varepsilon_{a,z_1}^2\varepsilon_{a,z_2}^2(2\beta-1)^4\beta^4 K_M^{min^2} \end{aligned} \tag{A.12}$$

that is negative. Then, Γ_1 has a single real root ∇_1. Given that

$$\begin{aligned} \Gamma_1(0) &= -\varepsilon_{a,z_1}\varepsilon_{a,z_2}\beta^2 K_M^{min} \\ \lim_{z_2(N)\to+\infty} \Gamma_1(z_2(N)) &= +\infty, \end{aligned} \tag{A.13}$$

it is also obvious that $\nabla_1 \geq 0$. Furthermore, in the studied case, the analysis is pertinent on $[0, \frac{\varepsilon_{a,z_2}}{\beta-1}]$ *i.e.* the range of $z_2(N)$ on $[GH]$. In this case, analysis can be made from the variations table in Figure A.2 for $\nabla_1 \in [0, \frac{\varepsilon_{a,z_2}}{\beta-1}]$.

$z_2(N)$	0		∇_1		$\frac{\varepsilon_{a,z_2}}{\beta-1}$
$\frac{\partial z_1(P)}{\partial z_2(N)}$		$-$	0	$+$	
$z_1(P)$	$\frac{\varepsilon_{a,z_1}}{\beta-1}$	↘		↗	$\frac{\varepsilon_{a,z_2}^2}{2(\beta-1)^2 K_M^{min}}$

Figure A.2 – Variations table of $\frac{\partial z_1(P)}{\partial z_2(N)}$ for $\nabla_1 \in [0, \frac{\varepsilon_{a,z_2}}{\beta-1}]$.

One notices that one of the boundaries of $z_2(N)$ evaluated on $[0, \frac{\varepsilon_{a,z_2}}{\beta-1}]$ gives the maximum value of $z_1(P)$ following (A.9); these bounds depend on system and controller parameters. Note that if $\nabla_1 \in [\frac{\varepsilon_{a,z_2}}{\beta-1}, +\infty]$, the maximum value of $z_1(P)$ is given uniquely by $z_2(N) = 0$ $\left(\frac{\partial z_1(P)}{\partial z_2(N)} < 0 \ \forall z_2(N) \in [0, \frac{\varepsilon_{a,z_2}}{\beta-1}]\right)$.
If $z_2(N) = \frac{\varepsilon_{a,z_2}}{\beta-1}$ leads to the maximum of $z_1(P)$, then point N coincides with point G (see Figure A.1): the trajectory is entering $\mathcal{D}_a$ crossing $\widehat{\text{HI}}$.
This latter can be proved by showing that $\widehat{\text{PV}}$ intersects $\widehat{\text{HI}}$, with $\widehat{\text{PV}}$ being the trajectory from P if the twisting algorithm is applied all the time and $z_1(V) = 0$ (see trajectory (P-V) in Figure A.1). The worst case is when $\ddot{z}_1 = -K_m^{max}$ that gives the most external trajectory from P, K_m^{max} engendering the largest variation of z_2 in absolute value when the small gain of the controller is applied. By integrating $\ddot{z}_1 = -K_m^{max}$, one gets

$$z_2(V) = -\frac{\varepsilon_{a,z_2}}{\beta-1}\sqrt{\frac{K_m^{max}}{K_M^{min}}} = z_2(I)\sqrt{\frac{K_m^{max}}{K_M^{min}}} \tag{A.14}$$

From (3.9), one has $K_m^{max} > K_M^{min}$; therefore, $z_2(V) > z_2(I)$. Then, the trajectory enters $\mathcal{D}_a$ through $\widehat{\text{HI}}$.
If $z_2(N) = 0$ leads to the maximum of $z_1(P)$, then point N coincides with point H. It also means that if the trajectory leaves $\mathcal{D}_a$ from any other point on $\widehat{\text{GH}}$, it will enter in $\mathcal{D}_a$ again before crossing the z_1-axis. That corresponds to the results found in (A.7). Notice that the trajectory leaving $\mathcal{D}_a$ through point H on $\widehat{\text{GH}}$ can be seen as leaving $\mathcal{D}_a$ through H on $\widehat{\text{HI}}$ and therefore will be studied in **Step 2**. Finally one concludes that if the trajectory leaves $\mathcal{D}_a$ through $\widehat{\text{GH}}$ (excluding point H) one has

$$\begin{aligned} |z_1| \leq & max(\frac{\varepsilon_{a,z_1}}{\beta-1}, \frac{\varepsilon_{a,z_2}^2}{2(\beta-1)^2 K_M^{min}}) \\ |z_2| \leq & \frac{\varepsilon_{a,z_2}}{\beta-1} \end{aligned} \tag{A.15}$$

Remark that, due to symmetry, similar results are obtained when the trajectory leaves $\mathcal{D}_a$ through $\widehat{\text{IJ}}$ (excluding point J).

■

Step 2. Suppose that the trajectory of the system leaves $\mathcal{D}_a$ passing through a point Q on $\widehat{\text{HI}}$ (see trajectory $O' - Q$ in Figure A.3). Then, from (A.5), the following relation exists between $z_1(Q)$ and $z_2(Q)$

$$z_1(Q) = \frac{\varepsilon_{a,z_1}\varepsilon_{a,z_2} + (\beta-1)\varepsilon_{a,z_1} z_2(Q)}{-(2\beta-1)z_2(Q) + \varepsilon_{a,z_2}(\beta-1)} \tag{A.16}$$

Considering the worst case, take $\ddot{z}_1 = -K_m^{max}$ that gives the most external trajectory from Q. When the trajectory enters $\mathcal{D}_a$ after crossing the z_2-axis at a point R such that $z_1(R) = 0$ (see trajectory $Q - R$ in Figure A.3). The expression of $z_2(R)$ is

$$z_2(R) = -\sqrt{z_2^2(Q) + 2K_m^{max} z_1(Q)} \tag{A.17}$$

which combined with (A.16) gives the following relation between $z_2(R)$ and $z_2(Q)$

$$z_2(R) = -\sqrt{z_2^2(Q) + 2K_m^{max}\frac{\varepsilon_{a,z_1}\varepsilon_{a,z_2} + (\beta-1)\varepsilon_{a,z_1} z_2(Q)}{-(2\beta-1)z_2(Q) + \varepsilon_{a,z_2}(\beta-1)}} \tag{A.18}$$

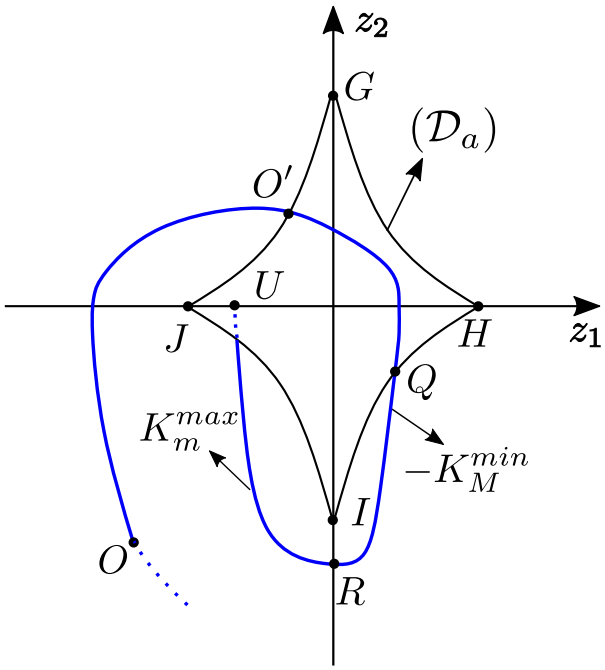

Figure A.3 – Example of system trajectory in the phase plan (z_1, z_2) - **Case 2.**

The objective is now to find which value of $z_2(Q)$ gives the maximum value for $z_2(R)$. Hence, the first step is to calculate $\frac{\partial z_2(R)}{\partial z_2(Q)}$ which reads as

$$\frac{\partial z_2(R)}{\partial z_2(Q)} = \frac{\Gamma_2(z_2(Q))}{\Lambda_2(z_2(Q))} \tag{A.19}$$

with

$$\begin{aligned}\Gamma_2 =& -2(2\beta-1)^2 z_2^3(Q) + 4\varepsilon_{a,z_2}(\beta-1)(2\beta-1)z_2^2(Q) \\ & - 2\varepsilon_{a,z_2}^2(\beta-1)^2 z_2(Q) - \varepsilon_{a,z_1}\varepsilon_{a,z_2}\beta^2 K_m^{max} \\ \Lambda_2 =& -\Big[(2\beta-1)z_2(Q) + \varepsilon_{a,z_2}(\beta-1)\Big]^2 z_2(R).\end{aligned} \tag{A.20}$$

By a similar way to Step 1, one finds that Γ_2 has only one real root ∇_2 which is negative. This results in the variations table with $\nabla_2 \in [-\frac{\varepsilon_{a,z_2}}{\beta-1}, 0]$ in Figure A.4. One notices that one of the boundaries of $z_2(Q)$ evaluated on $[-\frac{\varepsilon_{a,z_2}}{\beta-1}, 0]$ gives the maximum value of $z_2(R)$. Note that if $\nabla_2 \in]-\infty, -\frac{\varepsilon_{a,z_2}}{\beta-1}]$, the maximum is given uniquely by $z_2(Q) = -\frac{\varepsilon_{a,z_2}}{\beta-1}$.
If $z_2(Q) = 0$ leads to the maximum of $z_2(R)$, then point Q coincides with point H and the trajectory will enter $\mathcal{D}_a$ crossing $\widehat{\mathrm{IJ}}$. It can be proven as in **Step 1** by showing that $\widehat{\mathrm{RU}}$ intersects $\widehat{\mathrm{IJ}}$ where $\widehat{\mathrm{RU}}$ is the trajectory from R if the TWC is applied all the time with $z_2(U) = 0$ (see trajectory $R - U$ in Figure A.3).
If $z_2(Q) = -\frac{\varepsilon_{a,z_2}}{\beta-1}$ leads to the maximum of $z_2(R)$, then point Q coincides with point I. It also means that if the trajectory leaves $\mathcal{D}_a$ from any other point on $\widehat{\mathrm{HI}}$, it will enter $\mathcal{D}_a$ again before crossing the z_2-axis. This corresponds to the results found in (A.7). The trajectory leaving $\mathcal{D}_a$ through point I on $\widehat{\mathrm{HI}}$ can be seen as leaving $\mathcal{D}_a$ through I on $\widehat{\mathrm{IJ}}$ and which leads back to **Step 1**.

Finally one concludes that if the trajectory leaves $\mathcal{D}_a$ through $\widehat{\mathrm{HI}}$ (excluding point I) one

$z_2(Q)$	$-\frac{\varepsilon_{a,z_2}}{\beta-1}$	∇_2	0
$\frac{\partial z_2(R)}{\partial z_2(Q)}$	$+$	0	$-$
$z_2(R)$	$-\frac{\varepsilon_{a,z_2}}{\beta-1}$		$-\sqrt{\frac{2K_m^{max}\varepsilon_{a,z_1}}{\beta-1}}$

Figure A.4 – Table of variations of $\frac{\partial z_1(P)}{\partial z_2(N)}$ if $\nabla_2 \in [-\frac{\varepsilon_{a,z_2}}{\beta-1}, 0]$.

has

$$\begin{aligned} |z_1| \leq & \frac{\varepsilon_{a,z_1}}{\beta-1} \\ |z_2| \leq & max(\frac{\varepsilon_{a,z_2}}{\beta-1}, \sqrt{\frac{2K_m^{max}\varepsilon_{a,z_1}}{\beta-1}}). \end{aligned} \tag{A.21}$$

Remark that due to symmetry, the same results are obtained in case the trajectory leaves $\mathcal{D}_a$ through $\widehat{\text{JG}}$. ■

Step 3. Finally, by combining the results obtained in (A.15) and (A.21) the ultimate convergence boundaries of z_1 and z_2 are

$$\begin{aligned} |z_1| \leq & max(\frac{\varepsilon_{a,z_1}}{\beta-1}, \frac{\varepsilon_{a,z_2}^2}{2(\beta-1)^2 K_M^{min}}) \\ |z_2| \leq & max(\frac{\varepsilon_{a,z_2}}{\beta-1}, \sqrt{\frac{2K_m^{max}\varepsilon_{a,z_1}}{\beta-1}}) \end{aligned} \tag{A.22}$$

which concludes the proof. ■

B

Proof of Theorem 4.2

Recall system (4.1) with $\sigma-$dynamics with $r = 2$ reading as

$$\begin{aligned} \dot{z}_1 &= z_2 \\ \dot{z}_2 &= \bar{a}(x,t) + \bar{b}(x,t)u \end{aligned} \tag{B.1}$$

such that $\sigma = z_1$. Recalling the controller as

$$u = -k_2 \left\lceil \lceil z_2 \rfloor^2 + k_1^2 z_1 \right\rfloor^{\alpha} \tag{B.2}$$

with α varying such that

$$\alpha = \max(-\beta(\frac{|z_1|}{|z_1| + \varepsilon_{z_1}} + \frac{|z_2|}{|z_2| + \varepsilon_{z_2}}) + 1\,,\, 0). \tag{B.3}$$

The objective is to prove the stability of the system when controlled by (B.2)-(B.3) and calculate the convergence domain. ■

When the relative degree of the system with respect to the sliding variable is equal to 2, *i.e.* $r = 2$, the suitable controller from [29] is discontinuous on the same curve in the phase plan as the controller from [23] ($u = -k_2 \left\lceil z_2 + k_1 \lceil z_1 \rfloor^{\frac{1}{2}} \right\rfloor^0$) described as $z_2 = -k_1 \lceil z_1 \rfloor^{\frac{1}{2}}$ (see $\mathcal{L}$ in Figure B.1). Hence, following [25], if the gains are tuned as (4.6), the system trajectory inevitably hits the manifold $\mathcal{L}$ and then will slide on it until the origin is reached. This fact is essential in the determination of the domain of convergence of the trajectory when controller (4.7)-(4.8) is applied to system (4.1) with $\sigma-$dynamics reading as (4.4) and $\rho = 2$ which will be detailed in the following.

By a general point-of-view, the trajectory of the system is outside $\mathcal{D}$: therefore, $\mu = 0$ and the controller from [29] is applied. As previously mentioned, the system trajectory will hit $\mathcal{L}$ and slide on it; therefore, it will reach $\mathcal{D}$ in a finite time. However, due to the presence of perturbations and uncertainties, the trajectory will potentially leave $\mathcal{D}$ from

Case 1. $\widehat{AB}$ (resp. $\widehat{CD}$)

Case 2. $\widehat{BE}$ (resp. $\widehat{DF}$)

The trajectory cannot leave $\mathcal{D}$ through $\overset{\frown}{EC}$ since at $\overset{\frown}{EC}$, $\mu = 0$ meaning that $\dot{z}_2 > 0$ and $z_2 < 0$; therefore, z_2 cannot decrease and z_1 cannot increase. Similarly, the trajectory cannot leave $\mathcal{D}$ through $\overset{\frown}{FA}$.
The domain of convergence for each case will be presented in the sequel.

Case 1: Suppose that the trajectory leaves $\mathcal{D}$ through $\overset{\frown}{AB}$ at a point M (see M in Figure B.1a). Considering the worst case, $\dot{z}_2 = -K^* = -b_m k_2 + a_M$ gives the most external trajectory from the origin. Therefore, the expression of $\overset{\frown}{MN}$ is [1]

$$z_1 = \frac{-z_2^2 + z_2^2(M)}{2K^*} + z_1(M) \tag{B.4}$$

From (4.8) the expression of $z_1(M)$ is

$$z_1(M) = \frac{\varepsilon_{z_1}\varepsilon_{z_1} - (\beta-1)\varepsilon_{z_2} z_2(M)}{(2\beta-1)z_2(M) + \varepsilon_{z_2}(\beta-1)} \tag{B.5}$$

Hence, combining (B.4) and (B.5) the expression of $z_1(N)$ is deduced:

$$z_1(N) = \frac{z_2^2(M)}{2K^*} + \frac{\varepsilon_{z_1}\varepsilon_{z_1} - (\beta-1)\varepsilon_{z_2} z_2(M)}{(2\beta-1)z_2(M) + \varepsilon_{z_2}(\beta-1)}. \tag{B.6}$$

The maximum of this expression on the interval $z_2(M) \in \left[0, \frac{\varepsilon_{z_2}}{\beta-1}\right]$ is

$$max(z_1(N)) = max\left(\frac{\varepsilon_{z_1}}{\beta-1}, \frac{\varepsilon_{z_2}^2}{2(\beta-1)^2 K^*}\right) \tag{B.7}$$

After the trajectory crosses the $z_1 - axis$ it will enter again $\mathcal{D}$ through $\overset{\frown}{BC}$ (see $\overset{\frown}{NO}$ in Figure B.1a). This is due to the fact that $\overset{\frown}{MN}$ and $\overset{\frown}{NO}$ are symmetric with respect to $z_1 - axis$. Note that in case the trajectory hits $\mathcal{L}$ before hitting $\overset{\frown}{BC}$ (see $\overset{\frown}{NO}$' in Figure B.1a) then it will slide on $\mathcal{L}$ and then enter $\mathcal{D}$ through $\overset{\frown}{BC}$ (see $\overset{\frown}{O'E}$ in Figure B.1a). This fact, combined with the result from (B.7) gives that if the trajectory leaves $\mathcal{D}$ from $\overset{\frown}{AB}$ and $\overset{\frown}{CD}$ (due to symmetry) then

$$\begin{aligned} |z_1| \leq & max\left(\frac{\varepsilon_{z_1}}{\beta-1}, \frac{\varepsilon_{z_2}^2}{2(\beta-1)^2 K^*}\right) \\ |z_2| \leq & \frac{\varepsilon_{z_2}}{\beta-1} \end{aligned} \tag{B.8}$$

Case 2. When the trajectory leaves $\mathcal{D}$ at a point H on $\overset{\frown}{BC}$ (see H in Figure B.1b), $\mu = 0$; then, the controller from [29] is applied. As previously mentioned, the manifold defined by $\mathcal{L}$ in the phase plan is attractive; therefore, the trajectory will hit $\mathcal{L}$ at point I and start converging towards the origin (see $\overset{\frown}{IE}$ in Figure B.1b). Still considering the worst case, $\dot{z}_2 = -K^*$, the expression of $\overset{\frown}{HI}$ is also given by

$$z_1 = \frac{-z_2^2 + z_2^2(H)}{2K^*} + z_1(H). \tag{B.9}$$

At point I one has:

$$z_1(I) = \frac{1}{k_1^2} z_2^2(I) \tag{B.10}$$

1. Denote $z_1(M)$ (resp. $z_2(M)$) as the z_1 (resp. z_2) coordinate of point M.

Hence, by combining (B.10) and (B.9) the following expression of $z_2(I)$ is obtained:

$$z_2^2(I) = \frac{k_1^2}{k_1^2 + 2K^*}\left(z_2^2(H) + 2K^* \frac{\varepsilon_{z_1}\varepsilon_{z_2} + (\beta-1)z_2(H)\varepsilon_{z_1}}{-(2\beta-1)z_2(H) + (\beta-1)\varepsilon_{z_2}}\right) \tag{B.11}$$

The maximum of the latter is obtained when $z_2(H) = 0$

$$z_2(I) = -\sqrt{\frac{2K^* k_1^2 \varepsilon_{z_1}}{(k_1^2 + 2K^*)(\beta-1)}} \tag{B.12}$$

or when H coincides with point E which is the intersection between $\mathcal{L}$ and $\mathcal{D}$ (see E in Figure B.1b). Considering the worst case, that is, when $z_2(E)$ maximal in absolute value and therefore coinciding with point C (*i.e.* $k_1 \to \infty$ and therefore $z_2(H) = -\frac{\varepsilon_{z_2}}{\beta-1}$)

$$z_2(I) = -\frac{\varepsilon_{z_2}}{\beta-1}\sqrt{\frac{k_1^2}{k_1^2 + 2K^*}}. \tag{B.13}$$

Note that the latter expression gives a boundary for z_2 smaller than that in (B.8) and therefore will be discarded when calculating the ultimate convergence domain. In addition to that, with $k_1 \to \infty$ one has the same convergence domain as in (B.8). However, one states that if the system trajectory leaves from $\widehat{\text{BE}}$ and $\widehat{\text{AF}}$ (due to symmetry) , the convergence boundary is

$$\begin{aligned} |z_1| &< \frac{\varepsilon_{z_1}}{\beta-1} \\ |z_2| &< max\left(\sqrt{\frac{2K^* k_1^2 \varepsilon_{z_1}}{(k_1^2 + 2K^*)(\beta-1)}}, \frac{\varepsilon_{z_2}}{\beta-1}\sqrt{\frac{k_1^2}{k_1^2 + 2K^*}}\right) \end{aligned} \tag{B.14}$$

■

As a conclusion, by combining the 2 previous cases, the ultimate convergence boundary of the system is

$$\begin{aligned} |z_1| &< max\left(\frac{\varepsilon_{z_1}}{\beta-1}, \frac{\varepsilon_{z_2}^2}{2(\beta-1)^2 K^*}\right) \\ |z_2| &< max\left(\sqrt{\frac{2K^* k_1^2 \varepsilon_{z_1}}{(k_1^2 + 2K^*)(\beta-1)}}, \frac{\varepsilon_{z_2}}{\beta-1}\right) \end{aligned} \tag{B.15}$$

■

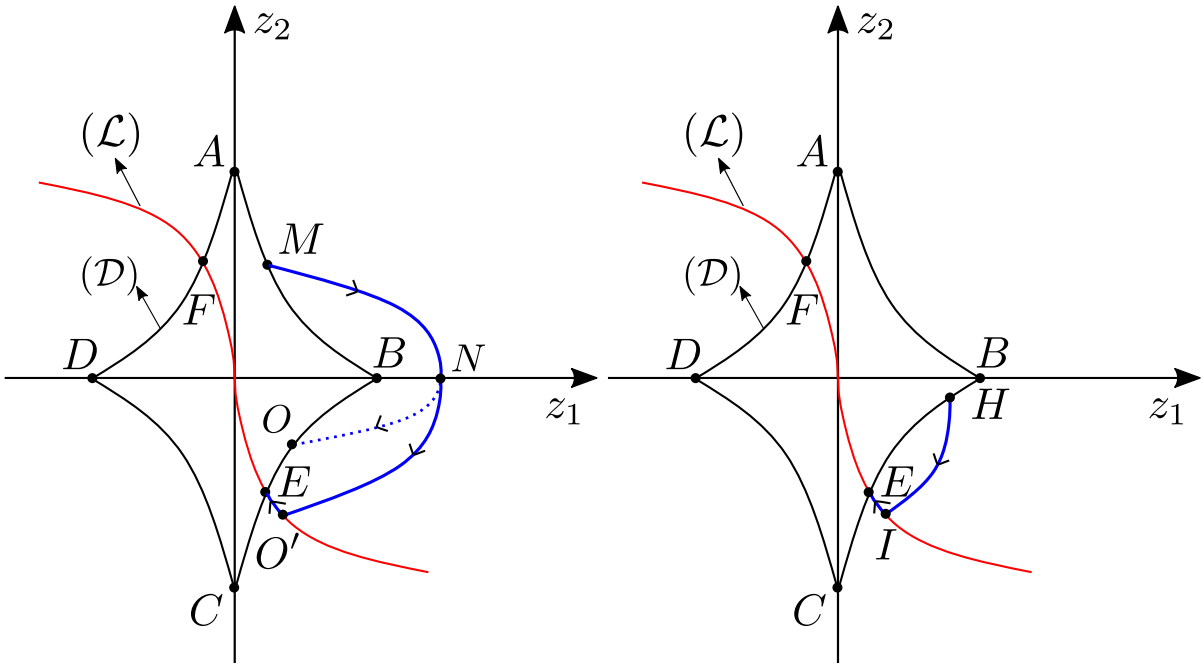

(a) Case 1 (b) Case 2

Figure B.1 – Description of the system trajectory in the phase plan (z_1, z_2).

C

Expressions of $\Theta(x,t)$ and $\Lambda(x,t)$

The expressions of $\Theta(x,t)$ and $\Lambda(x,t)$ of (6.15) are given. Let f_i, $i \in \{1,2,..,7\}$

$$f_1 = \frac{p\phi_f}{J}, f_2 = \frac{p(L_d - L_q)}{J}, f_3 = \frac{R_s}{L_q}, f_4 = \frac{pL_d}{L_q}, f_5 = \frac{p\phi_f}{L_q}, f_6 = \frac{R_s}{L_d}, f_7 = \frac{pL_q}{L_d}. \tag{C.1}$$

Note that the expression of $F_{d,1} - F_{d,2}$ is given as [1]

$$F_{d,1} - F_{d,2} = \mathcal{C}\mathcal{B}(\beta_1 - \beta_2) \tag{C.2}$$

where $\mathcal{C} = \frac{1}{2}\rho\pi(V cos(\psi - \ell))^2$ and $\mathcal{B} = b_0 + b_1\ \lambda_i + b_2\ \lambda_i^2 + b_3\ \lambda_i^3$ with $b_0 = -0.008608$, $b_1 = 0.0063$, $b_2 = -0.0015$ and $b_3 = 0.000118$.
The time derivative of the terms $\mathcal{B}$ and $\mathcal{C}$ appearing in the matrix $\Theta(x,t)$ depend on λ, Ω, ψ, V. These derivatives are given as following

$$\begin{aligned}
\dot{\mathcal{B}} &= \frac{\partial \mathcal{B}}{\partial t} = \frac{\partial \mathcal{B}}{\partial \lambda} \cdot \frac{\partial \lambda}{\partial t} = (b_1 + 2\,b_2\,\lambda + 3\,b_3\,\lambda^2) \cdot \frac{\partial}{\partial t}\left(\frac{\Omega\,R}{V\,cos(\psi - \ell)}\right) \\
&= (b_1 + 2\,b_2\,\lambda + 3\,b_3\,\lambda^2) \cdot \left(\frac{R}{V\,cos(\psi - \ell)}\,\dot{\Omega} + \lambda\,\mathrm{tg}(\psi - \ell)\,\dot{\psi} - \frac{\lambda}{V}\,\dot{V}\right) \\
\dot{\mathcal{C}} &= \frac{\partial \mathcal{C}}{\partial t} = \frac{\partial \mathcal{C}}{\partial V} \cdot \frac{\partial V}{\partial t} + \frac{\partial \mathcal{C}}{\partial \psi} \cdot \frac{\partial \psi}{\partial t} \\
&= \frac{2\,\mathcal{C}}{V}\,\dot{V} - 2\,\mathrm{tg}(\psi - \ell)\,\dot{\psi}
\end{aligned}$$

Note that the derivative of V is estimated by $\frac{s}{\tau\,s + 1}$. Then the expressions of $\Theta(x,t)$ and $\Lambda(x,t)$ are

1. For more details on how this expression is obtained the reader is referred to [67].

$$\Theta(x,t) = \begin{bmatrix} -\dfrac{D_r}{K_r}\,\ddot{\psi} + \dfrac{\mathcal{C}L}{K_r\,T_\beta}\,\mathcal{B}\,(\beta_1-\beta_2) + \dfrac{\mathcal{C}L}{K_r}\,(\beta_1-\beta_2)\,\dot{\mathcal{B}} + \dfrac{\mathcal{B}L}{K_r}\,(\beta_1-\beta_2)\,\dot{\mathcal{C}} \\ \dfrac{1}{J}\,\dot{\Gamma}_{a1} - (f_1+f_2\,i_{d1})[-f_3 i_{q1} - f_4\,\Omega_1\,i_{d1} - f_5\,\Omega_1] - f_2\,i_{q1}\,[-f_6\,i_{d1} + f_7\,\Omega_1\,i_{q1}] \\ -\dfrac{f_v}{J}\,\dot{\Omega}_1 - \ddot{\Omega}_1^* \\ \dfrac{-R_s}{L_d}\,i_{d1} + \dfrac{P\,L_q}{L_d}\,\Omega_1\,i_{q1} \\ \dfrac{1}{J}\,\dot{\Gamma}_{a2} - (f_1+f_2\,i_{d2})[-f_3 i_{q2} - f_4\,\Omega_2\,i_{d2} - f_5\,\Omega_2] - f_2\,i_{q2}\,[-f_6\,i_{d2} + f_7\,\Omega_2\,i_{q2}] \\ -\dfrac{f_v}{J}\,\dot{\Omega}_2 - \ddot{\Omega}_2^* \\ \dfrac{-R_s}{L_d}\,i_{d2} + \dfrac{P\,L_q}{L_d}\,\Omega_2\,i_{q2} \end{bmatrix}$$

$$\Lambda(x,t) = \begin{bmatrix} \dfrac{-2}{K_r\,T_\beta}\,L\,\mathcal{C}\,\mathcal{B} & 0 & 0 & 0 & 0 \\ 0 & \dfrac{-f_2}{L_d}\,i_{q1} & \dfrac{-1}{L_q}(f_1+f_2\,i_{d1}) & 0 & 0 \\ 0 & \dfrac{1}{L_d} & 0 & 0 & 0 \\ 0 & 0 & 0 & \dfrac{-f_2}{L_d}\,i_{q2} & \dfrac{-1}{L_q}(f_1+f_2\,i_{d2}) \\ 0 & 0 & 0 & \dfrac{1}{L_d} & 0 \end{bmatrix}.$$

Bibliography

[1] A. Levant, "Sliding order and sliding accuracy in sliding mode control," *International Journal of Control*, vol. 58, no. 6, pp. 1247–1263, 1993. 3, 13, 21, 43, 44, 45

[2] X. Yan, M. Primot, and F. Plestan, "An unified formalism based on gain switching for second order sliding mode control," in *14th International Workshop on Variable Structure Systems (VSS)*, Nanjing, China, 2016. 3, 13, 22, 23, 24, 44, 54

[3] A. Girin and F. Plestan, "A new experimental test bench for a high performance double electropneumatic actuator system," in *American Control Conference (ACC)*, St. Louis, Missouri, USA, 2009. 6, 78, 79

[4] A. Herskovits, O. Laffitte, P. Thome, and A. Tobie, "V-shaped, bi-rotor wind generator on a spar floating structure," *French Patent WO2014060420 A*, vol. 1, p. 2014, 2012. 6, 91, 92

[5] V. V. Vantsevich and M. V. Blundell, *Advanced Autonomous Vehicle Design for Severe Environments*, vol. 44. IOS Press, 2015. 13

[6] T. Madani and A. Benallegue, "Backstepping control for a quadrotor helicopter," in *2006 IEEE/RSJ International Conference on Intelligent Robots and Systems*, pp. 3255–3260, IEEE, 2006. 14

[7] D. Jabri, K. Guelton, N. Manamanni, A. Jaadari, and C.-D. Chinh, "Robust stabilization of nonlinear systems based on a switched fuzzy control law," vol. 14, no. 2, pp. 40–49, 2012. 14

[8] B. Mansouri, N. Manamanni, K. Guelton, and M. Djemai, "Robust pole placement controller design in lmi region for uncertain and disturbed switched systems," *Nonlinear Analysis: Hybrid Systems*, vol. 2, no. 4, pp. 1136–1143, 2008. 14

[9] Y. Shtessel, C. Edwards, L. Fridman, and A. Levant, *Sliding mode control and observation*. Springer, New York, USA, 2014. 14, 20

[10] V. I. Utkin, *Sliding modes in control and optimization*. Springer, Berlin, Germany, 1992. 14, 15, 16, 33, 34, 35

[11] A. Isidori, *Nonlinear control systems*. Springer, London, UK, 2013. 14

[12] V. Utkin, "Variable structure systems with sliding modes," *IEEE Transactions on Automatic control*, vol. 22, no. 2, pp. 212–222, 1977. 15

[13] H. K. Khalil, *Nonlinear Systems*. Pearson, 2001. 15

[14] V. Utkin and H. Lee, "Chattering problem in sliding mode control systems," in *9th International Workshop on Variable Structure Systems (VSS)*, Alghero, Italy, 2006. 18, 27, 33

[15] V. Utkin and J. Shi, "Integral sliding mode in systems operating under uncertainty conditions," in *IEEE Conference on Decision and Control (CDC)*, Kobe, Japan, 1996. 18

[16] J. Guldner and V. Utkin, "The chattering problem in sliding mode systems," in *14th Intenational Symposium of Mathematical Theory of Networks and systems (MTNS)*, Perpignan, France, 2000. 18

[17] J. Burton and A. S. Zinober, "Continuous approximation of variable structure control," *International Journal of Systems Science*, vol. 17, no. 6, pp. 875–885, 1986. 19, 38

[18] X. Yu and R. B. Potts, "Analysis of discrete variable structure systems with pseudo-sliding modes," *International Journal of Systems Science*, vol. 23, no. 4, pp. 503–516, 1992. 19

[19] A. Levant, "Higher-order sliding modes, differentiation and output-feedback control," *International Journal of Control*, vol. 76, no. 9-10, pp. 924–941, 2003. 20, 35

[20] G. Bartolini, A. Pisano, and E. Usai, "Digital second-order sliding mode control for uncertain nonlinear systems," *Automatica*, vol. 37, no. 9, pp. 1371–1377, 2001. 21

[21] İ. Eker, "Second-order sliding mode control with experimental application," *ISA Transactions*, vol. 49, no. 3, pp. 394–405, 2010. 21

[22] F. Plestan, E. Moulay, A. Glumineau, and T. Cheviron, "Robust output feedback sampling control based on second-order sliding mode," *Automatica*, vol. 46, no. 6, pp. 1096–1100, 2010. 21, 22

[23] A. Levant, "Homogeneity approach to high-order sliding mode design," *Automatica*, vol. 41, no. 5, pp. 823–830, 2005. 21, 25, 27, 63, 111

[24] E. Bernuau, D. Efimov, W. Perruquetti, and A. Polyakov, "On homogeneity and its application in sliding mode control," *Journal of the Franklin Institute*, vol. 351, no. 4, pp. 1866–1901, 2014. 21, 25, 27

[25] A. Levant, "Principles of 2-sliding mode design," *Automatica*, vol. 43, no. 4, pp. 576–586, 2007. 21, 111

[26] Y. V. Orlov, *Discontinuous systems: Lyapunov analysis and robust synthesis under uncertainty conditions*. Springer, 2008. 21, 25

[27] A. Polyakov and A. Poznyak, "Lyapunov function design for finite-time convergence analysis:"twisting" controller for second-order sliding mode realization," *Automatica*, vol. 45, no. 2, pp. 444–448, 2009. 21, 25

[28] A. Polyakov and A. Poznyak, "Unified Lyapunov function for a finite-time stability analysis of relay second-order sliding mode control systems," *IMA Journal of Mathematical Control and Information*, vol. 29, no. 4, pp. 529–550, 2012. 21, 25

[29] E. Cruz-Zavala and J. A. Moreno, *"Lyapunov approach to higher-order sliding mode design"*. in *Recent trends in sliding mode control* Eds. L. Fridman, J.-P. Barbot and F. Plestan. The Institution of Engineering and Technology, pp. 3-28, London, UK, 2016. 21, 25, 28, 63, 64, 74, 98, 101, 103, 111, 112

[30] A. Bacciotti and L. Rosier, *Liapunov functions and stability in control theory*. Springer, Berlin, Germany, 2006. 25, 65

[31] C. Edwards and Y. Shtessel, "Adaptive dual-layer super-twisting control and observation," *International Journal of Control*, vol. 89, no. 9, pp. 1759–1766, 2016. 26

[32] F. Plestan, Y. Shtessel, V. Bregeault, and A. Poznyak, "New methodologies for adaptive sliding mode control," *International Journal of Control*, vol. 83, no. 9, pp. 1907–1919, 2010. 26

[33] Y. Shtessel, M. Taleb, and F. Plestan, "A novel adaptive-gain supertwisting sliding mode controller: Methodology and application," *Automatica*, vol. 48, no. 5, pp. 759–769, 2012. 26

[34] V. I. Utkin and A. S. Poznyak, *"Adaptive sliding mode control"*. in *Advances in sliding mode control* Eds. B. Bandyopadhyay, S. Janardhanan, S. K. Spurgeon. Springer, pp. 21-53, Berlin, Germany, 2013. 26

[35] V. I. Utkin and A. S. Poznyak, "Adaptive sliding mode control with application to super-twist algorithm: Equivalent control method," *Automatica*, vol. 49, no. 1, pp. 39–47, 2013. 26

[36] Z. Guo, J. Chang, J. Guo, and J. Zhou, "Adaptive twisting sliding mode algorithm for hypersonic reentry vehicle attitude control based on finite-time observer," *ISA Transactions*, vol. 77, pp. 20–29, 2018. 26

[37] Y. B. Shtessel, J. A. Moreno, and L. M. Fridman, "Twisting sliding mode control with adaptation: Lyapunov design, methodology and application," *Automatica*, vol. 75, pp. 229–235, 2017. 26

[38] C. Edwards and Y. B. Shtessel, "Adaptive continuous higher order sliding mode control," *Automatica*, vol. 65, pp. 183–190, 2016. 26

[39] A. Levant, "Universal single-input-single-output (siso) sliding-mode controllers with finite-time convergence," *IEEE Transactions on Automatic Control*, vol. 46, no. 9, pp. 1447–1451, 2001. 27

[40] E. Tahoumi, M. Ghanes, F. Plestan, and J.-P. Barbot, "New robust schemes based on both linear and sliding mode approaches: design and application to an electro-pneumatic setup," *IEEE Transactions on Control System Technology*, accepted with modifications, 2019. 29, 37, 54

[41] E. Tahoumi, M. Ghanes, F. Plestan, and J.-P. Barbot, "Energy efficient control with time varying parameters derived from homogeneous algorithm - application to a wind system," *Control Engineering Practice*, under second round of revision, 2019. 29, 68

[42] E. Tahoumi, M. Ghanes, F. Plestan, and J.-P. Barbot, "A new controller switching between linear and twisting algorithms," in *American Control Conference (ACC)*, Milwaukee, Wisconsin, USA, 2018. 29, 48

[43] E. Tahoumi, F. Plestan, M. Ghanes, and J.-P. Barbot, "A controller switching between twisting and linear algorithms for an electropneumatic actuator," in *European Control Conference (ECC)*, Limasol, Cyrpus, 2018. 29

[44] E. Tahoumi, F. Plestan, M. Ghanes, and J.-P. Barbot, "Adaptive exponent parameter: a robust control solution balancing between linear and twisting controllers," in *15th International Workshop on Variable Structure Systems (VSS)*, Gratz, Austria, 2018. 29, 52

[45] M. Primot, E. Tahoumi, X. Yan, and F. Plestan, "Determination of the convergence domain of the twisting algorithm thanks to a switching gain approach," in *IEEE Conference on Decision and Control (CDC)*, Miami, Florida, USA, 2018. 29, 56

[46] E. Tahoumi, F. Plestan, M. Ghanes, and J.-P. Barbot, "Robust and energy efficient control schemes based on higher order sliding mode," in *European Control Conference (ECC)*, Naples, Italy, 2019. 29, 67

[47] C. Zhang, E. Tahoumi, S. Gutierrez, F. Plestan, and J. De Leon Morales, "Adaptive robust control of floating offshore wind turbine based on sliding mode," in *IEEE Conference on Decision and Control (CDC)*, Nice, France, 2019. 29

[48] E. Moulay and W. Perruquetti, "Finite time stability conditions for non-autonomous continuous systems," *International Journal of control*, vol. 81, no. 5, pp. 797–803, 2008. 34

[49] E. Bernuau, D. Efimov, W. Perruquetti, and A. Polyakov, "On homogeneity and its application in sliding mode control," *Journal of the Franklin Institute*, vol. 351, no. 4, pp. 1866–1901, 2014. 34

[50] A. Levant, "Chattering analysis," *IEEE Transactions on Automatic Control*, vol. 55, no. 6, pp. 1380–1389, 2010. 35

[51] S. P. Bhat and D. S. Bernstein, "Finite-time stability of homogeneous systems," in *American Control Conference (ACC)*, Albuquerque, New Mexico, USA, 1997. 44, 45, 47

[52] S. P. Bhat and D. S. Bernstein, "Continuous finite-time stabilization of the translational and rotational double integrators," *IEEE Transactions on Automatic Control*, vol. 43, no. 5, pp. 678–682, 1998. 44, 45, 47

[53] J. A. Moreno, "Lyapunov approach for analysis and design of second order sliding mode algorithms," in *Sliding Modes after the first decade of the 21st Century*, pp. 113–149, Springer, 2011. 63

[54] A. Polyakov and A. Poznyak, "Lyapunov function design for finite-time convergence analysis:"twisting" controller for second-order sliding mode realization," *Automatica*, vol. 45, no. 2, pp. 444–448, 2009. 63

[55] T. Sánchez and J. A. Moreno, "Construction of lyapunov functions for a class of higher order sliding modes algorithms," in *IEEE Conference on Decision and Control (CDC)*, Maui, Hawai, USA, 2012. 63

[56] M. Harmouche, S. Laghrouche, and Y. Chitour, "Robust and adaptive higher order sliding mode controllers," in *IEEE Conference on Decision and Control (CDC)*, Maui, Hawai, USA, 2012. 63

[57] M. Bouri and D. Thomasset, "Sliding control of an electropneumatic actuator using an integral switching surface," *IEEE Transactions on Control Systems Technology*, vol. 9, no. 2, pp. 368–375, 2001. 77

[58] X. Brun, S. Sesmat, D. Thomasset, and S. Scavarda, "A comparative study between two control laws of an electropneumatic actuator," in *European Control Conference (ECC)*, Karlsruhe, Germany, 1999. 77

[59] S. Laghrouche, M. Smaoui, F. Plestan, and X. Brun, "Higher order sliding mode control based on optimal approach of an electropneumatic actuator," *International Journal of Control*, vol. 79, no. 2, pp. 119–131, 2006. 77, 81, 82

[60] A. Estrada and F. Plestan, "Second order sliding mode output feedback control with switching gains—application to the control of a pneumatic actuator," *Journal of the Franklin Institute*, vol. 351, no. 4, pp. 2335–2355, 2014. 77

[61] X. Yan, F. Plestan, and M. Primot, "A new third-order sliding-mode controller—application to an electropneumatic actuator," *IEEE Transactions on Control Systems Technology*, vol. 25, no. 2, pp. 744–751, 2016. 77

[62] F. Plestan, Y. Shtessel, V. Bregeault, and A. Poznyak, "Sliding mode control with gain adaptation—application to an electropneumatic actuator," *Control Engineering Practice*, vol. 21, no. 5, pp. 679–688, 2013. 78

[63] Y. Shtessel, M. Taleb, and F. Plestan, "A novel adaptive-gain supertwisting sliding mode controller: Methodology and application," *Automatica*, vol. 48, no. 5, pp. 759–769, 2012. 78

[64] M. Taleb, A. Levant, and F. Plestan, "Pneumatic actuator control: Solution based on adaptive twisting and experimentation," *Control Engineering Practice*, vol. 21, no. 5, pp. 727–736, 2013. 78

[65] M. Belgharbi, S. Sesmat, S. Scavarda, and D. Thomasset, "Analytical model of the flow stage of a pneumatic servo-distributor for simulation an nonlinear control," in *Scandinavian International Conference on Fluid Power (SICFP)*, Tampere, Finland, 1999. 79

[66] A. Levant, "Robust exact differentiation via sliding mode technique," *Automatica*, vol. 34, no. 3, pp. 379–384, 1998. 83

[67] I. Guenoune, F. Plestan, A. Chermitti, and C. Evangelista, "Modeling and robust control of a twin wind turbines structure," *Control Engineering Practice*, vol. 69, pp. 23–35, 2017. 92, 115

[68] S. Georg, H. Schulte, and H. Aschemann, "Control-oriented modelling of wind turbines using a takagi-sugeno model structure," in *IEEE International Conference on Fuzzy Systems*, Brisbane, Queensland, Australia, 2012. 94

[69] I. Guenoune, "Commande non-linéaires robustes de système éoliens," *PhD Dissertation, Ecole Centrale de Nantes, Nantes, France*, 2018. 95

[70] H. Shariatpanah, R. Fadaeinedjad, and M. Rashidinejad, "A new model for PMSG-based wind turbine with yaw control," *IEEE Transactions on Energy Conversion*, vol. 28, no. 4, pp. 929–937, 2013. 95

[71] A. Uehara, A. Pratap, T. Goya, T. Senjyu, A. Yona, N. Urasaki, and T. Funabashi, "A coordinated control method to smooth wind power fluctuations of a PMSG-based wecs," *IEEE Transactions on energy conversion*, vol. 26, no. 2, pp. 550–558, 2011. 98

[72] M. Ghanes, J.-P. Barbot, L. Fridman, and A. Levant, "A novel differentiator: a compromise between super twisting and linear algorithms," in *IEEE Conference on Decision and Control (CDC)*, Melbourne, Victoria, Australia, 2017. 104

[73] S. Derbel, N. Feki, F. Nicolau, J. P. Barbot, M. Abbes, and M. Haddar, "Application of homogeneous observers with variable exponent to a mechatronic system," *Journal of Mechanical Engineering Science*, vol. 233, no. 18, 2019. 104

Titre : Nouvelles stratégies de commandes robustes combinant des approches linéaires et par mode glissant.

Mots clés : : Modes glissant d'ordre un, modes glissants d'ordre deux, modes glissants d'ordre supérieur, système électropneumatique, système éolien.

Résumé : Ce travail de thèse porte sur la conception des lois de commande pour des systèmes non linéaires, incertains et perturbés; ces lois de commande sont basées à la fois sur des approches par mode glissant, et sur des techniques linéaires. Les commandes par mode glissant (notamment d'ordre supérieur) sont connues pour leur robustesse face aux perturbations et incertitudes ainsi que pour leurs performances en terme de précision. Cependant, elles sont énergivores. Le retour d'état linéaire est connu pour être une commande lisse et à faible consommation d'énergie, mais il est très sensible aux perturbations et incertitudes. Le premier objectif de cette thèse est le développement de lois de commande présentant les avantages à la fois de la commande par mode glissant (robustesse et précision) et du retour d'état linéaire (faible consommation d'énergie). Le deuxième objectif est de montrer l'applicabilité des méthodes proposées aux systèmes physiques réels, notamment le banc électropneumatique de LS2N. Des applications sont également effectuées sur un système éolien.

Title: New robust control schemes linking linear and sliding mode approaches.

Keywords : First order sliding mode, Second order sliding mode, higher order sliding mode, electropneumatic system, wind system.

Abstract : This work deals with the design of control laws for nonlinear, uncertain and perturbed systems based on sliding mode control and linear state feedback. Sliding mode control is known for its robustness versus perturbations and uncertainties as well as high accuracy tracking; however, it is high energy consuming. The linear state feedback is known to be a smooth control and low energy consuming, but it is highly sensitive to perturbations and uncertainties. The first objective of this thesis is the development of control laws that have the advantages of both sliding mode control (robustness and accuracy) and linear state feedback (low energy consumption). The second objective is to show the applicability of the proposed methods to real physical systems, notably the LS2N electropneumatic bench. Applications are also made on a wind system physical systems, notably the LS2N electropneumatic bench. Applications are also made on a wind system.